Report of the GEWEX-GPCP Workshop on Precipitation Analysis March 11-13, 2003

European Center for Medium Range Weather Forecast
Shinfield Park, Reading, Berkshire RG2 9AX
United Kingdom

Masao Kanamitsu (Co-chairman)
Climate Research Division
Scripps Institution of Oceanography
University of California, San Diego

and

Arnold Gruber (Co-chairman)
NOAA's National Environmental Satellite Data and Information Service
Washington D.C.
&
Cooperative Institute for Climate Studies
Earth System Science Interdisciplinary Center
University of Maryland, College Park, MD 20742

Sponsored by:

Global Energy and Water Cycle
Global Precipitation Climatology Project
European Center for Medium Range Weather Forecasts

TABLE OF CONTENTS

1. SUMMARY OF THE WORKSHOP

The Workshop on the Objective Analysis of Precipitation sponsored by the Global Energy and Water Cycle Experiment, Global Precipitation Climatology Project (GPCP) and the European Center for Medium Range Weather Forecasts was held during March 11 – 13, 2000 at the European Center in Shinfield Park, Reading, United Kingdom. The workshop was organized and chaired jointly by Masao Kanamitsu of Scripps Institution of Oceanography and Arnold Gruber of NESIS.

The primary goals of the workshop were:

? To improve our understanding of the issues involved in the objective analysis of precipitation using the many sources of information available (e.g., gauges, satellite-derived estimates, radar observations, and model output data).

? To make recommendations for GPCP to advance its efforts to provide global analyses of precipitation.

The focus of the workshop was to exchange ideas and opinions concerning those goals with data assimilation experts. The location of the workshop was chosen for this purpose.

Twenty six participants from academia and government agencies from seven different nations presented their latest work on analysis procedures, data assimilation, and observational error characteristics. GPCP, Climate Prediction Center Merged Analysis of Precipitation (CMAP), data assimilation and other precipitation analysis methods were reviewed. The participants and their affiliations are shown in Appendix II. The focus of the presentations varied somewhat between the observation only analysis, and data assimilation analysis groups. In the former, center of attention was on the problem of precipitation observation, bias corrections, and merging of different types of observations. In the latter group, the use of the observations was limited to the Tropical Rainfall Measurement Mission (TRMM) and radar/rain gauge measurements, while the emphasis was on precipitation observation utilization methodology in the data assimilation system. This difference clearly contrasted the major interests of the two groups; one is more concerned with the precipitation observations themselves, while the other is concerned with the utilization methods. However, there are many common subjects between the activities of the two groups which resulted in valuable working group recommendations, described in more detail below. The quality control of precipitation observations, precipitation characteristics observed from TRMM, and monitoring of the precipitation in polar region were also presented. These talks emphasized importance of further research on data sampling and analysis methods, observed characteristics of precipitation (convective vs. stratus and liquid vs. solid), and verification/validation. A consensus regarding the necessity to enhance international collaboration on precipitation concluded the presentations. Extended abstracts of the presentations are included in Section 4. Deliberations by the working groups on observation only analysis, data assimilation, and quality control produced the key recommendations described in Section 3.

2. WORKSHOP BACKGROUND

The Global Precipitation Climatology Project has been producing monthly averaged precipitation analysis based on rain gauges, infra-red, and microwave radiometer measurements for quite some time (Huffman et al. 1997a,b, Adler et al. 2003). The method of analysis is a sequential merging of various gauge and satellite estimates by removing the bias estimated from reference observations (such as the rain gauge). There are many difficult aspects of these procedures, which are described in more detail by Huffman in this report. CPC Merged Analysis of Precipitation (CMAP) is another separate effort to obtain monthly averaged precipitation, that also utilizes satellite infra-red, microwave and gauge data, with differences in the bias corrections and analysis methods (Xie et al. 2003). These analyses have been used extensively for model verifications and climate research, and have been proven to be an invaluable source of data. These analyses will be referred to as "observation only analysis" in this report. There are other observation only precipitation analyses using neural network, and analyses based on rain gauge only. The success of the GPCP project is now leading the effort to refine the product to produce precipitation analysis in finer spatial and temporal scales (Huffman et al. 2001). Such a product requires a new approach to the analysis that is different from the monthly average precipitation analysis.

The utility of the observation only GPCP precipitation analysis is demonstrated in Figure 14 though 17, taken from Gruber et al. (2000). These figures compare GPCP, CMAP, AMIP and NCEP/NCAR reanalysis.

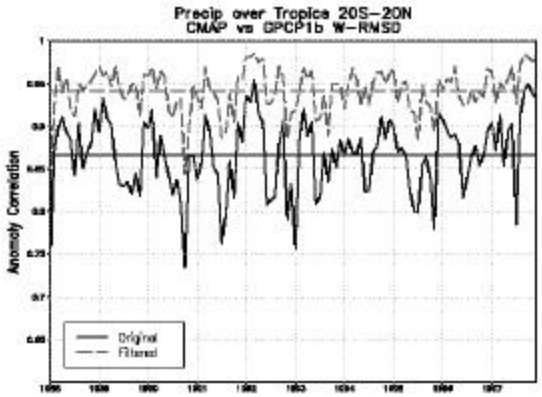

FIG. 14. Anomaly correlation coefficient between the CMAP and GPCP analyses over the Tropics (20°N–20°S). Solid line corresponds to AC with the original analyses and dashed line to the filtered analyses. Solid and dashed straight lines indicate average AC for the 1988–97 period.

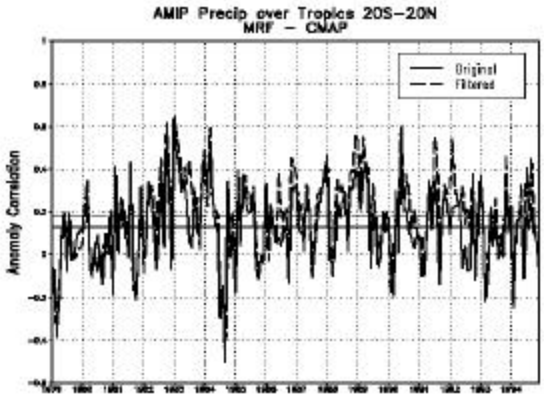

FIG. 15. Tropical (20°N–20°S) anomaly correlation coefficients of the MRF GCM simulations against the CMAP analysis. Solid line corresponds to AC between the original analysis and simulation and the dashed line to that of the filtered analysis and simulation. Solid and dashed straight lines indicate average AC for the 1979–94 period.

The anomaly correlation between the CMAP and GPCP is of the order of 0.9 (higher when spatially smoothed) over the tropics, indicating the degree of similarity between the two independent analyses (note that there are many observations common to both). The comparison of the model AMIP runs (in which the atmosphere is forced by observed SST) shows that the correlation is much lower (for both NCEP and ECHAM models). The NCEP/NCAR reanalysis precipitation, which is a model generated precipitation with atmospheric variables but without precipitation assimilation, has higher correlation than the AMIP runs, but still of the order of 0.5. Because of the low correlation with model precipitation, the observation only analysis is an important reference analysis against which the model precipitation can be verified.

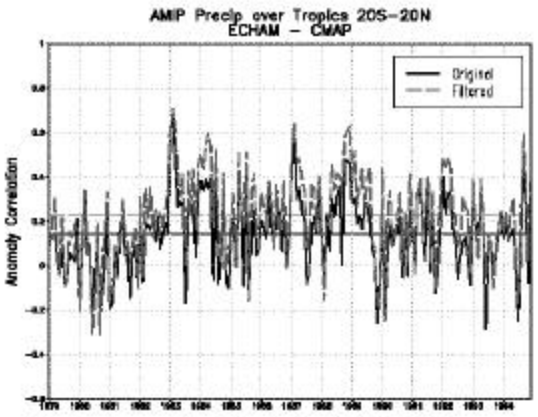

FIG. 16. Same as Fig. 15 but for the ECHAM GCM.

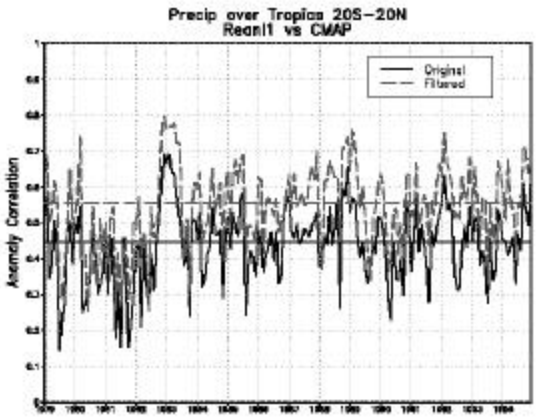

FIG. 17. Same as Fig. 15 but for reanalysis vs CMAP.

In contrast to the observation only precipitation analysis, operational numerical forecast centers around the world have been working on objective atmospheric analysis methods for the initial conditions of atmospheric models. Recent developments in variational data assimilation methods significantly improved analyses, particularly in its use of satellite observations. The method is capable of incorporating "retrievals" into the analysis scheme, allowing the direct use of satellite radiance observations. Although data assimilation methods are designed to provide the best initial conditions that produce the best forecasts, the improvement in forecast model and analysis procedures made the analysis suitable for more general use. The various reanalysis efforts that utilize data assimilation methodology to produce long series of atmospheric data for study of the climate and other applications are good examples. The application of 3- and 4-dimensional data assimilation made it possible, for the first time, to use a variety of observations. More recently, precipitation observations have been used in the data assimilation with some success. Such developments have the potential to provide a useful precipitation analysis comparable to the observation only analysis. The greatest advantage of the assimilation analysis is that the final analyses of the atmospheric and land surface parameters are in dynamical, thermodynamical and hydrological balance, which is required for understanding the global energy and water cycle. Unfortunately, observation only analyses are not capable of providing a complete picture of the atmospheric and land states. Data assimilation methods are always aimed at providing an analysis at synoptic times for weather forecasts. The instantaneous precipitation intensity data is preferred for input, and the resulting analysis of precipitation will be in the form of accumulation during the short model integration. In this sense, the objectives of observation only and assimilation analysis are getting closer to each other.

The existence of these two nearly independent analysis efforts prompted us to create an opportunity for these two groups to meet, discuss and learn from each other.

2.1 DISCUSSION POINTS FOR OBSERVATION ONLY ANALYSIS

The merging method and bias corrections applied in the current precipitation analysis lacks the strict concept of error minimization. Whether we need such a concept should be addressed, but removing empiricism is an important improvement. Discussion with the data assimilation group is valuable since their method is entirely dependent on this concept. The use of forecast model guess has been debated for a long time. The "model dependency" of analysis should not necessarily be avoided, if it is properly justified through proper verification. The model guess should be considered as a time extrapolation, and its use should be encouraged. Generating consistent analysis between precipitation and other variables, such as cloudiness and radiation fluxes needs to be considered. The data assimilation analysis automatically produces consistent analysis of all these variables. However, lack of the assimilation of these quantities makes the "analysis" move away from observations. Whether we wait for the improvement of the data assimilation, or consider other ways, needs to be discussed. (Is it worthwhile to consolidate observation only analysis to include other precipitation related variables, such as cloudiness, radiation fluxes and soil moisture?

2.2 DISCUSSION POINTS FOR DATA ASSIMILATION ANALYSIS

Currently, data assimilation limits the use of observed precipitation to Special Sensor Microwave Imager (SSM/I) and TRMM estimates, and radar calibrated by rain gauges. This is due to the requirement of the assimilation system that calls for specific knowledge of the character of the observation. Expansion of the observational data base to a variety of data sources is desirable, but the characterization of the observation for use in data assimilation is lacking. Mutual discussion and collaboration with the observation only analysis group may lead to better use of data as well as better understanding of the error characteristics of the GPCP precipitation analysis.

The geographical distribution of precipitation is strongly affected by orography, land/ocean distribution and subtle difference in land surface characteristics. The diurnal variation of precipitation is also known to be a significant part of precipitation variability, particularly in the tropics. The phase and amplitude of the diurnal variation is a strong function of surface conditions as well as geographical features. Incorporation of these inhomogeneous distribution characteristics into the data assimilation is a very difficult task. Again, the collaboration with other precipitation analysis experts is desirable.

The difficulties associated with the collaboration between the observation only analysis group and the data assimilation analysis group lies in communication with each other, since both groups tend to speak different "languages". This difficulty should be resolved by identifying common problems and interests. As discussed earlier, there are many common subjects regarding which collaboration will provide benefit to both groups.

2.3 REFERENCES

Adler, R.F., G.J. Huffman, A. Chang, R. Ferraro, P. Xie, J. Janowiak, B. Rudolf6, U. Schneider, S. Curtis, D. Bolvin, A. Gruber, J. Susskind, and P. Arkin, 2003: The Version 2 Global Precipitation Climatology Project (GPCP) Monthly Precipitation Analysis (1979-Present). *J. Hdrometeor.*, submitted.

Gruber, A., X. Su, M. Kanamitsu and J. Schemm, 2000: The comparison of two merged Rain gauge-Satellite precipitation datasets. *Bull. Amer. Met. Soc.*, **81**, 2631-2644.

Huffman, G.J., R.F. Adler, P. Arkin, A. Chang, R. Ferraro, A. Gruber, J. Janowiak, A. McNab, B. Rudolf, U. Schneider, 1997: The Global Precipitation Climatology Project (GPCP) Combined Precipitation Data Set. *Bull. Amer. Meteor. Soc.*, **78**(1), 5-20 (incl. cover).

Huffman, G.J., R.F. Adler, M. Morrissey, D.T. Bolvin, S. Curtis, R. Joyce, B McGavock, J. Susskind, 2001: Global Precipitation at One-Degree Daily Resolution from Multi-Satellite Observations. *J. Hydrometeor.*, **2**(1), 36-50.

Xie, P., J.E. Janowiak, P.A. Arkin, R.F. Adler, A. Gruber, R. Ferraro, G.J. Huffman, and S. Curtis, 2003: GPCP Pentad precipitation Analyses: An Experimental Data Set Based On Gauge Observations And Satellite Estimates. *J. Climate*, to appear.

3. WORKSHOP RECOMMENDATIONS

1. The observation only analysis needs to continue. The precipitation analysis from advanced data assimilation is still not sufficiently accurate, and observation only analysis needs to be used as a baseline. The quality of the observation only product should continue to improve. Various analysis issues, including data collection, bias correction and merge procedure should also be studied further. The requirements from NWP community were sub-divided into the validation of the global model (analysis and forecast), climate (monthly data), the use of precipitation observations for data assimilation (6 hourly), and the validation of extreme event forecasts (hourly). It was stressed that all data levels should be made available to allow the wide range of applications of precipitation information in NWP. This includes level-1b (calibrated, navigated raw instantaneous observations), 2 (first-order products; instantaneous), 3 (merged, accumulated products; gridded) data of rainfall, rainfall frequency of occurrence, and associated errors. It was pointed out that for the optimum utilization of precipitation data in NWP data assimilation systems, a very close collaboration between algorithm/product developers and modelers is needed.

2. It is clearly recognized that there is a need for providing error statistics more useable for data assimilation. This includes error statistics of individual observations, rather than the merged products, of each component of errors, namely, the errors associated with a) instruments, b) physical retrieval, c) assumptions on spatial representativeness and d) assumptions on temporal representativeness. It is also desirable to provide spatial and temporal correlations of observational error, error in precipitation detection and uncertainties in the bias.

3. Active collaboration between modelling/observation/validation groups is needed for a complete description of the analysis errors: biases (their uncertainties), error covariances, their state dependence, and methodologies for the description of their dependence on space and time scales and synoptic conditions. The GPCP analysis project can provide additional valuable information to the NWP community, but more communication between the two groups is needed. This can be achieved through GPCP, GRP and International Precipitation Working Group.

4. As to the future analysis method for GPCP, the data assimilation group believes that pursuing the assimilation method is not recommended and some other more nonlinear methods (such as Krieging method) suitable for analysis of precipitation should be developed. Such work will also complement the data assimilation analysis.

5. There is an indication that precipitation from the data assimilation system can be more accurate than satellite estimates over some areas, particularly in higher latitudes, orographic areas, rain over snow covered areas and during snowfall. Addition of data assimilation precipitation analysis into the observation only analysis should be considered for providing more accurate, fully global precipitation analysis to general users. In this regard, the exa mination of the accuracy of data assimilation precipitation needs was encouraged.

6. For the observation only analysis, it was recommended that research be pursued on the determination of frozen/snow precipitation in complex terrain and the use of new satellite observations. Also data products on smaller space and time scales need to be developed because data assimilation methods will increasingly focus on more regional applications.

7. It was recommended to continue developing high-quality, unbiased reference sites across the range of climate regimes for validation of precipitation analyses. There is also a need for research on radar precipitation estimates, which are increasingly used by regional data assimilation analyses.

8. Research on analysis methods of temporally and spatially discrete observation should be pursued. The diurnal variation of precipitation, rapid propagation of precipitation systems and satellite observations made from once/twice a day passage of the area may severely alias the real space and time scales. This also relates to the definition of space and time characteristics of the observational error.

10. Research on precipitation types and their spatial and temporal characteristics is encouraged. Such study is essential for determining the observational error characteristics of precipitation phenomena. The use of TRMM observation is ideal for such studies.

Finally, data assimilation methods holds the key to the future of precipitation analyses, since its greatest advantage is that it can provide the analysis of observed and derived meteorological variables (together with precipitation) in a dynamically, physically, and hydrologically consistent manner. However, it will take several more years before such analysis becomes as accurate as currently available observation only analyses. The GPCP collaboration will certainly accelerate this important development.

The Current Approach to GPCP Monthly And Daily Precipitation Estimates

G.J. Huffman[1,2] and R.F. Adler[1]

1: NASA Goddard Space Flight Center, Greenbelt, MD
2: Science Systems and Applications, Inc., Lanham, MD

1. INTRODUCTION

The Global Precipitation Climatology Project (GPCP) currently produces three precipitation analyses: The Version 2 Satellite-Gauge (SG) combination, the pentad product, and the One-Degree Daily (1DD) product. Most of the work is done with precipitation estimates as the input variable, rather than the sensor's native parameter(s). Where appropriate, we take the "best" estimators of precipitation to provide the underlying statistics for calibrating other estimators, which are frequently better in spatial or temporal coverage. We compute the calibrations by month to assure stability. In the course of developing the various algorithms we chose to build algorithms that only needed the parameters already available in the input data sets. Finally, we have emphasized producing random error estimates for each input data set (Huffman 1997).

2. AVAILABLE DATA SETS

One challenge for developing the GPCP algorithms was developing the list of input data sets that are quasi-global, have a long record, and have acceptable statistical characteristics. The current list is:

- Raingauge analyses (1979-present),
- Special Sensor Microwave Imager (SSM/I) passive microwave estimates (mid-1987-present),
- Geosynchronous Earth orbit infrared (geo-IR) and low Earth orbit infrared (leo-IR; both 1986-present),
- Television-Infrared Operational Satellite (TIROS) Operational Vertical Sounder (TOVS; 1979-present), and
- Outgoing Longwave Radiation (OLR) Precipitation Index (OPI; 1979-present).

In the first three types of data there are multiple algorithms with various periods of record based on the availability of the underlying data. In particular, the IR becomes easily available at finer scale starting in late 1996 (as the result of action by the GPCP), which enabled the start of the 1DD, even as the monthly and daily dataset production continued.

3. CURRENT ALGORITHMS

3.1 Version 2 SG Monthly

The Version 2 SG is a monthly estimate of precipitation and corresponding random error on a 2.5°x2.5° latitude/longitude grid. Besides these two final fields, there are more than a dozen intermediate fields available (with the exact number depending on the input data). See Adler et al. (2003) or the on-line documentation at the GPCP web site for details.

We consider the SSM/I era (July 1987 to the present) to be most accurate. This is due to the availability of passive microwave data, which has a much more direct physical connection to precipitation than the other satellite data we use. During this period we apply a third generation of the Satellite-Gauge-Model approach first described by Huffman et al. (1995) and updated in Huffman et al. (1997). Despite the name, note that no model data is used in the current system. The processing sequence is as follows:

- An SSM/I-TOVS composite is produced by taking the SSM/I in the band 40°N-S, then transitioning to TOVS adjusted by zonal-average gauge at 70°N and S, and using the adjusted TOVS to the poles.
- The Geosynchronous Operational Environmental Satellite (GOES) Precipitation Index (GPI) values computed from geo- and leo-IR are separately calibrated to the SSM/I using a month of approximately coincident data, resulting in the Adjusted GPI (AGPI).
- A multi-satellite (MS) field is created, consisting of the AGPI, where available, in the band 40°N-S and the SSM/I-TOVS composite elsewhere.
- The final SG is the result of bias-adjusting the MS to the gauges, where feasible, then combining the two using inverse error variance weighting.

In the years before the IR are available, a calibrated OPI is used as the MS and combined with the gauge as above. The OPI calibration is a monthly, climatological adjustment to the SG for 1988-1996.

During 1986-mid-1987 the IR are available, but not the SSM/I. There, the calibrated OPI stand in for the SSM/I-TOVS composite and the analysis proceeds as described.

In general, the Version 2 SG has proved to be useful for a wide variety of studies. The data boundaries at the beginning of 1986, in mid-1987, and at 40° N and S are known issues for which users should specifically check. As one example, the full time series of the GPCP global-average precipitation is shown in Fig. 1. The major dips in the smoothed land average have a high negative correlation with El Niño events; there is a slight positive correlation

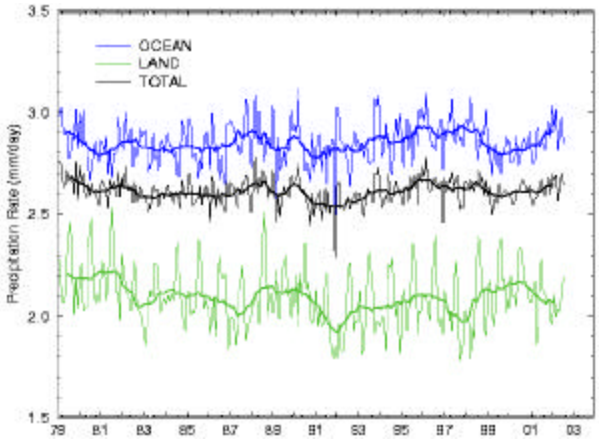

Figure 1. Time series of GPCP Version 2 global-average precipitation for ocean (upper curve), land (lower curve), and grand total. The heavy lines are 12-month running means, while the thin lines trace the individual monthly values.

in the ocean values and a near-zero correlation in the total field. Note the slow multi-year variations, but the lack of any obvious trend over the period as a whole. These last comments are quite preliminary due to the inhomogeneities in our data record.

3.2 Pentad

The pentad precipitation product is available on a global, pentad (5-day interval), 2.5°x2.5° grid for 1979 to the (delayed) present. It is essentially a data-driven disaggregation of the

Version 2 SG. There are 73 pentads in a year, and Leap Day is included in the pentad that spans the February-March month boundary. The interval is chosen because it is the interval of the underlying OLR dataset.

The OPI computed on pentads is approximately summed to months, calibrated against the corresponding month of SG, and the calibration is then applied to the individual pentad values. As with the SG calibrations, these OPI calibrations vary spatially, as well as by month. See Xie et al. (2003) for more details.

3.3 1DD Daily

The 1DD precipitation is available on a global, daily, 1°x1° grid for the period October 1996 to the (delayed) present. See Huffman et al. (2001) or the on-line documentation at the GPCP web site for details.

In the band 40°N-S the 1DD is built from the Threshold Matched Precipitation Index, a microwave-calibrated IR technique:

- Each month, coincident SSM/I-based fractional occurrence of precipitation and IR brightness temperature histograms are used to establish a spatially varying field of rain-no rain threshold, then
- the full IR fractional occurrence and the Version 2 SG are used to establish a spatially varying field of conditional rainrate – the single rate at which all "raining" IR pixels are assumed to rain.

Outside the band 40°N-S the 1DD is built from rescaled daily TOVS estimates. Taken over a month the (1996) TOVS estimates that we use have too high a fractional coverage and correspondingly low rainrates. In response, we

- reduce the local number of TOVS rain days by the ratio of average TMPI and TOVS rain days at 40°, applied separately in the northern and southern hemispheres, and
- rescale the remaining TOVS rain days to start at zero and sum over the month to the local Version 2 SG value.

Despite the data boundary at 40°N and S, the global patterns have strong spatial and temporal continuity across the boundary. Nonetheless, tt is important to note that the day-to-day occurrence of precipitation is driven by IR data at lower latitudes and TOVS data elsewhere, both of which primarily respond to clouds, not precipitation.

Comparison with other data sets shows reasonable qualitative agreement in the day-to-day variation of precipitation, although the scatter diagrams comparing individual grid box values to gauges show significant scatter, as expected. It does appear that the statistical properties of the 1DD, such as fraction of rainy days and daily rainrate distribution are robust. Thus, the 1DD will be more useful for applications that are more sensitive to the overall statistics of the daily rain, rather than to the detailed sequence of precipitation.

Figure 2 provides an example of the use of the 1DD, namely the construction of a Hovmoller diagram around the Equator that covers the period of the 1997-1998 El Niño. The peak of the El Niño is November 1997 to May 1998, but the precipitation in the eastern Pacific Ocean (right center of the horizontal axis) is anomalously high as early as February 1997.

4. CONCLUDING QUESTIONS

Work with the current GPCP products and coping with the limitations of the input products motivates the following questions:

- What improvements are possible in the recent/future era of plentiful satellite data (see companion talk)?

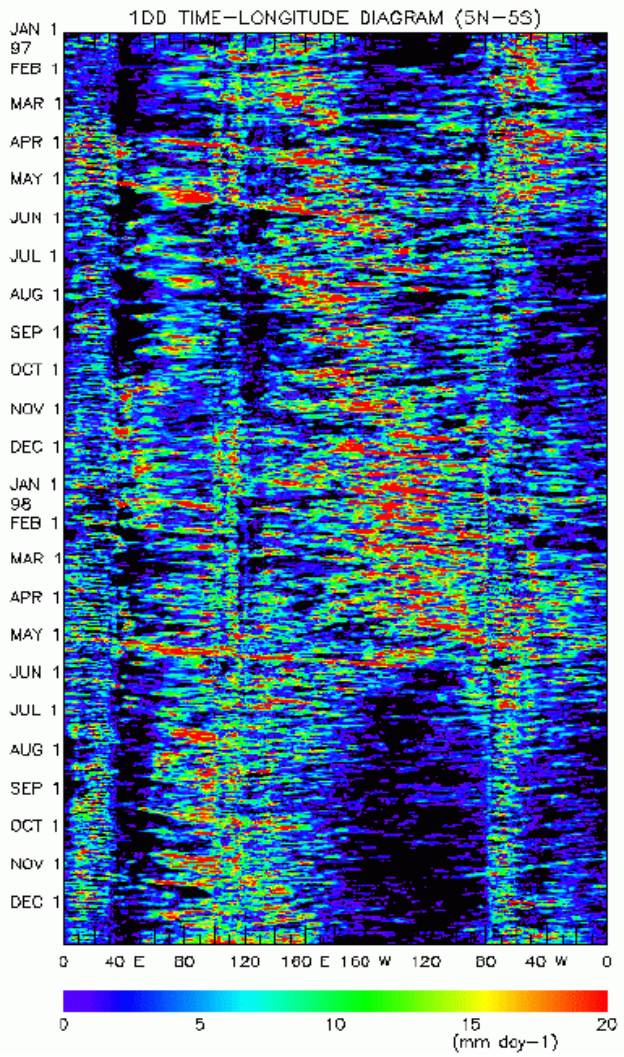

Figure 2. Hovmoller diagram of 1DD precipitation along the Equator (5°N-S) for the period 1997-1998.

- What can/must be done in the earlier era of limited satellite data?
  - What is the right trade-off of accuracy, fine scale, and length of record?
  - Can we get more-detailed data from the earlier era, either by recovering higher-resolution versions of currently available summaries (such as IR), or by re-examining some of the earlier data sets and estimates?
- What is the role of model-based estimates, given the earlier user opposition to any use of model data?
- What is the right interval for calibrating IR brightness temperatures by other precipitation estimates? Operational schemes run from monthly to complete recomputations for each SSM/I overpass.

REFERENCES

Adler, R.F., G.J. Huffman, A. Chang, R. Ferraro, P. Xie, J. Janowiak, B. Rudolf6, U. Schneider, S. Curtis, D. Bolvin, A. Gruber, J. Susskind, and P. Arkin, 2003: The Version 2 Global Precipitation Climatology Project (GPCP) Monthly Precipitation Analysis (1979-Present). *J. Hdrometeor.*, submitted.

Huffman, G.J., 1997: Estimates of Root-Mean-Square Random Error for Finite Samples of Estimated Precipitation. *J. Appl. Meteor.*, **36**(9), 1191-1201.

Huffman, G.J., R.F. Adler, P. Arkin, A. Chang, R. Ferraro, A. Gruber, J. Janowiak, A. McNab, B. Rudolf, U. Schneider, 1997: The Global Precipitation Climatology Project (GPCP) Combined Precipitation Data Set. *Bull. Amer. Meteor. Soc.*, **78**(1), 5-20 (incl. cover).

Huffman, G.J., R.F. Adler, M. Morrissey, D.T. Bolvin, S. Curtis, R. Joyce, B McGavock, J. Susskind, 2001: Global Precipitation at One-Degree Daily Resolution from Multi-Satellite Observations. *J. Hydrometeor.*, **2**(1), 36-50.

Huffman, G.J., R.F. Adler, B. Rudolf, U. Schneider, P.R. Keehn, 1995: A Technique for Combining Satellite Data, Raingauge Analysis and Model Precipitation Information into Global Precipitation Estimates. *J. Climate*, **8**(5), 1284-1295.

Xie, P., J.E. Janowiak, P.A. Arkin, R.F. Adler, A. Gruber, R. Ferraro, G.J. Huffman, and S. Curtis, 2003: GPCP Pentad precipitation Analyses: An Experimental Data Set Based On Gauge Observations And Satellite Estimates. *J. Climate*, to appear.

WEB SITES

http://precip.gsfc.nasa.gov/
http://www.ncdc.noaa.gov/wdcamet.html#GPCP

Huffman, G.J., and R.F. Adler, 2003: The Multi-satellite Precipitation Analysis (MPA) in Real and Post-Real Time. *GEWEX-GPCP Workshop on Precipitation Analysis*, 11-13 March 2003, Reading, U.K., to appear.

The Multi-satellite Precipitation Analysis (MPA) in Real and Post-Real Time

G.J. Huffman[1,2] and R.F. Adler[1]

1: NASA Goddard Space Flight Center, Greenbelt, MD
2: Science Systems and Applications, Inc., Lanham, MD

1. INTRODUCTION

Satellite data form the core of the information available for estimating precipitation on a global basis. While it is possible to create such estimates solely from one sensor, researchers have increasingly moved to using combinations of sensors in an attempt to improve accuracy, coverage, and resolution. The Multi-satellite Precipitation Analysis (MPA) reported in this presentation provides 3-hourly, 0.25°x0.25° lat./long. gridded precipitation estimates that are being computed for the Tropical Rainfall Measuring Mission (TRMM). Additional details are provided on the TRMM web site.

2. THE MPA ALGGORITHM

The MPA is the latest fine-scale, quasi-global estimate of precipitation developed in the authors' research group. The infrared (IR) approach traces back to schemes variously referred to as "3-hourly," "VARR," and "TMPI." The first MPA release was an experimental real-time (RT) system, starting in February 2002. Major upgrades occurred in March 2002 and February 2003. The latency of this product is about 6 hours after real time. A second release is planned as the Version 6 TRMM product 3B42, replacing the current product and moving it from 1°x1° daily in the band 40°N-S to 0.25°x0.25° 3-hourly in the band 50°N-S. Reprocessing to effect this transition should commence in June 2003 and take 9-12 months. At the same time that reprocessing starts, subsequent months of new data will also be processed with the new Version 6 algorithms. At that point, the RT will be considered a first look, to be replaced by the higher-quality after-real-time produce as each month of that becomes available.

2.1 Input Data

The majority of the input data is based on two different sets of sensors. First, microwave data are being collected by a variety of low-Earth-orbit (leo) satellites, including the TRMM Microwave Imager (TMI) on TRMM, the Special Sensor Microwave Sensor (SSM/I) on Defense Satellite Meteorology Program (DMSP), the Advanced Microwave Scanning Radiometer for the Earth Observing System (AMSR-E) on Aqua and the Advanced Earth Observation Satellite II (AdEOS-II), and Advanced Microwave Sounding Unit (AMSU) on the National Oceanic and Atmospheric Administration (NOAA) satellite series. These data have a strong physical connection to the hydrometeors that result in surface precipitation, but each individual satellite provides a very sparse sampling of the time-space occurrence of precipitation. Even taken together, there are significant gaps in the current coverage by microwave estimates.

In contrast, the IR data that are being collected by the international constellation of geosynchronous-Earth-orbit (geo) satellites provide excellent time-space coverage. Recently, access to these data has been greatly facilitated by the Climate Prediction Center (CPC) of the National Weather Service/NOAA, which is merging the geo-IR data into half-hourly 4x4-km-equivalent lat./long. grids. The IR brightness temperatures (T_b) are corrected for

zenith-angle viewing effects and inter-satellite calibration.

For post-real-time estimates before the start of the CPC data in early 1999, we use a GPCP data set that provides 24-class T_b histograms of geo-IR data on a 3-hourly, 1°x1° lat./long. grid covering the latitude band 40°N-S. We zenith-angle-correct the data, convert them to box-average T_b, and bilinearly interpolate them to the 0.25° grid. This data set also provides grid-box-average Geosynchronous Operational Environmental Satellite (GOES) Precipitation Index (GPI; Arkin and Meisner 1987) estimates computed from leo-IR data recorded by the NOAA satellite series. These data are used to fill holes in the GEO-IR coverage, most notably in the Indian Ocean sector before Meteorological Satellite 5 (METEOSAT-5) began providing observations there in June 1998.

The drawback to all IR-based precipitation estimates is that the T_b's sense cloud-top temperature, and implicitly cloud height. Arkin and Meisner (1987) showed that such information is poorly correlated to precipitation at the fine scales, but relatively well-correlated at scales larger that about 1 day and 2.5°x2.5°.

The project also makes use of the TRMM Combined Instrument (TCI) product, which is a multi-sensor estimate based on TMI and TRMM Precipitation Radar data. Finally, two sources of monthly rain gauge analyses are used, the GPCP analysis developed by the Global Precipitation Climatology Centre (GPCC), and the Climate Assessment and Monitoring System (CAMS) analysis developed by CPC.

In the course of developing the MPA, the authors realized that they could obtain (restricted) access to the requisite microwave and IR data within a few hours of observation time. Knowing that "real-time" (or more strictly, near-real-time) production could make the estimates useful to several new classes of users, a two-track approach was developed. The real-time and post-real-time approaches are sufficiently similar that a single description is given in the next section, with differences pointed out as needed.

2.2 Estimation Algorithm

The MPA produced in three stages; (1) the microwave estimates are combined, (2) infrared estimates are created with microwave calibration, and (3) the microwave and IR are combined. Each MPA data field is intended to represent the precipitation rate at the nominal observation time.

2.2.1 High Quality (HQ) Microwave Estimates

All of the available microwave data are converted to precipitation estimates. At the present this is achieved by applying the Goddard Profiling Algorithm (GPROF; Kummerow et al. 1996) to TMI, SSM/I, and AMSR-E (real-time only) pixel data, and averaging each to the 0.25° resolution over the time range ±90 minutes from the nominal observation time. All of these estimates are adjusted to a "best" estimate using probability matching of rain rate histograms assembled from coincident data. In the post-real-time system the calibrating data source is the TCI, while for the real-time system it is the TMI, since the TCI are unavailable in real time.

For the post-real-time estimates, the calibration month is a calendar month, and the resulting adjustment is applied to all of the microwave data for the same calendar month. This is not possible in the real-time system, so the calibration month is a trailing accumulation of 6 pentads, updated at the end of each pentad. A pentad is a 5-day period, except when Leap Day is included in the pentad that encompasses it; there are 73 pentads in each year.

2.2.2 Variable Rain Rate (VAR) IR Estimates

The CPC Merged IR data are averaged to 0.25° resolution and combined into hourly files

as ±30 minutes from the nominal time. The amount of imagery delivered to CPC varies by satellite operator, but international agreements mandate that full coverage is provided for the 3-hourly synoptic times (00Z, 03Z, …, 21Z). Histograms of time-space matched HQ rain rates and IR T_b's, each represented on the same 3-hourly 0.25° grid, are accumulated for a month, and then used to create calibration coefficients for IR precipitation rate that vary in space. By design, there is no rain when the T_b is greater than a threshold value that matches the frequency of precipitation in the IR to that of the microwave, and increasingly colder T_b's have increasingly large rain rates. The calibration coefficients are then applied to the entire hourly IR data set.

As with the HQ, the post-real-time calibration month is a calendar month, and the resulting coefficients are applied to the same calendar month of all IR data. In the real-time system the calibration month is a trailing accumulation of 6 pentads, updated at the end of each pentad.

2.2.3 Combined HQ+VAR Estimates

As a first step, we currently combine the HQ and VAR estimates with the simplest possible scheme, namely the physically-based HQ estimates are taken "as is" where available, and the remaining grid boxes are filled with VAR estimates. This scheme provides the "best" local estimate in each grid box, at the expense of a time series with heterogeneous statistics. If homogeneous statistics are important to the user, either the HQ or VAR estimates may be accessed, depending on the application.

It is highly advantageous to include rain gauge data in combination data sets (Huffman et al. 1997, among others). However, experience shows that on any time scale shorter than a month there is not sufficient gauge data available and reported on consistent observation intervals to warrant direct inclusion in a global algorithm. We solved this issue in the 1DD by scaling the short-period estimates to sum to a monthly estimate that includes monthly gauge data. Here, we take a similar approach with the post-real-time estimates. All available 3-hourly HQ+VAR estimates are summed over a calendar month to create a monthly multi-satellite (MS) product. The MS and gauge are combined as in Huffman et al. (1997) to create a post-real-time monthly SG, which is a TRMM product in its own right. Then the field of SG/MS ratios is computed (with controls) and applied to scale each 3-hourly field in the month. Of course, such a gauge adjustment is not possible for the real-time system.

3. EXAMPLES

Figure 1 provides a snapshot of the merged microwave (HQ, top), microwave-calibrated IR (VAR, middle), and combined (HQ+VAR, bottom) precipitation estimates for 18Z on 24 September 2002 from the real-time MPA algorithm. The corresponding product identifiers are 3B40RT, 3B41RT, and 3B42RT. The HQ panel shows a typical amount of coverage by the F13, F14, and F15 SSM/I's and the TMI; AMSR-E was not yet available and AMSU was not yet incorporated. In contrast, the IR coverage is essentially complete for this particular observation time. Visual inspection of the two images shows general agreement in the location of major precipitation features, even though there is considerable variation in the small-scale details. Note the rain systems associated with hurricanes Isadore (in the Gulf of Mexico) and Lili (in the eastern Caribbean Sea). A mid-latitude low-pressure center and trailing front are located north of Hawaii, and late-afternoon convection is taking place in central Africa.

Comparing, the convective systems, such as the African thunderstorms and hurricanes tend to show local differences, most likely due to the delay in time between the occurrence of precipitation and the growth of cirrus at the top

of the storm. The mid-latitude system shows a larger-scale offset, which is believed to result from the frontal-scale offset between high-level cirrus ahead of the system and precipitation, which is located closer to the low-pressure center and frontal zone. Some of the offsets shown in the difference field could also be due to the 3-hour window for HQ data.

The individual 3-hourly VAR fields show large RMS differences from corresponding HQ fields, but they are designed to reproduce the monthly histograms of HQ rain rates. Thus, at least in a probabilistic sense the time series of precipitation is representative. The advantage of the 3-hourly 0.25° detail is that users are free to tailor averages or composites of the data to their own needs.

The results of the MPA are best viewed as movie loops, which are beyond the scope of this preprint. Readers are urged to visit http://trmm.gsfc.nasa.gov and click on the button labeled "See More Images, Movies, & Accumulation Maps". A variety of instantaneous and cumulative images and movies are available for viewing and downloading, with larger movies available in lower resolution for users with limited-bandwidth network connections.

4. FUTURE DEVELOPMENT

4.1 MPA

As a work in progress, the MPA has a long list of issues that the authors would like to address. We will characterize the performance of this approach and explore differences between the real-time and post-real-time results. At the same time, we expect to start integrating AMSU precipitation estimates into the HQ product. Thereafter, we will extend the estimates to the poles by incorporating fully global precipitation estimates based on Television Infrared Operational Satellite (TIROS) Operational Vertical Sounder (TOVS) and Advanced Infrared Sounder (AIRS) data. The best approach to combining the HQ and VAR estimates is also a topic for future research. It would be helpful to develop a better IR-based algorithm so that the combination would not have to reconcile the strong fine-scale differences that currently exist between HQ and VAR. Finally, the study of precipitation in general needs a succinct statistical description of how fine-scale precipitation estimates perform over the range of scales up to global/monthly.

On the instrumentation side there is a concerted effort to provide complete 3-hourly microwave data. Most of this effort is focused on the National Aeronautics and Space Administration's proposed Global Precipitation Measurement (GPM) Mission. Besides simply increasing the frequency of coverage, it is planned to provide a TRMM-like "core" satellite to calibrate all the passive microwave estimates on an on-going basis. We expect a permanent role for the geo-IR in filling the inevitable gaps in microwave coverage, as well as enabling sub-3-hourly precipitation estimates at fine spatial scales.

4.2 GPCP Version 3

As in the present Version 2, the next version of GPCP will continue to need a diversity of approaches to provide the longest possible record of global precipitation. In the recent (and future) era of plentiful satellite data the trend seems to be to make satellite precipitation estimates at the finest possible time/space scales and average them up to coarser scales as needed. This is certainly feasible back to the start of the 1°x1° 3-hourly IR data in October 1996; further extension would depend on either ISCCP DX data or a new compilation of global IR data. At a minimum, it should be possible to process the entire GPCP IR record back to 1986 at pentad temporal resolution.

In the earliest, sparse-data era of 1979-1985, there are two issues. First, it would be helpful to have finer-scale or even full-resolution data sets for the known sensors, including IR, MSU, and TOVS. Second, modern insights should be applied to developing algorithms for these early data sets with an eye to ensuring consistency with the later data. Such "archaeology" is critical for developing the best input to studies of possible time trends in the global hydrologic cycle.

4.3 Critical Issues

To close, we raise three unsolved problems in creating combinations. All three are specific to the highly non-normal, non-negative statistical properties of precipitation. First, suppose two different satellite algorithms estimate similar rain events at a grid box, but at different times.

How should these be combined? Any linear combination will damage the statistics, with too high a fractional coverage and too low a peak rain rate.

Second, suppose the actual event is similar to the two satellite estimates, but at a third time, closer to Satellite 1's estimated time than to Satellite 2's. What is the appropriate validation statistic? By eye, one would say that 1 is better than 2, but the usual root-mean-square error score would be equally bad for both. Some averaging would help, but what's the right amount?

Third, the estimation of error for instantaneous precipitation estimates is quite primitive, particularly in gauging what the error might be for grid boxes with an estimated precipitation amount of zero. What additional information can be used to help improve our error estimates?

REFERENCES

Arkin, P.A., and B.N. Meisner, 1987: The Relationship Between Large-Scale Convective Rainfall And Cold Cloud Over The Western Hemisphere During 1982-1984. *Mon. Wea. Rev.*, **115**, 51-74.

Huffman, G.J., R.F. Adler, P. Arkin, A. Chang, R. Ferraro, A. Gruber, J. Janowiak, A. McNab, B. Rudolf, and U. Schneider, 1997: The Global Precipitation Climatology Project (GPCP) Combined Precipitation Data Set. *Bull. Amer. Meteor. Soc.*, **78**, 5-20.

Huffman, G.J., R.F. Adler, M. Morrissey, D.T. Bolvin, S. Curtis, R. Joyce, B. McGavock, J. Susskind, 2001: Global Precipitation at One-Degree Daily Resolution from Multi-Satellite Observations. *J. Hydrometeor.*, **2**, 36-50.

Kummerow, C., W.S. Olsen, and L. Giglio, 1996: A simplified scheme for obtaining precipitation and vertical hydrometeor profiles from passive microwave sensors. *IEEE Trans. Geosci. Remote Sens.*, **34**, 1213-1232.

Xie, P., J.E. Janowiak, P.A. Arkin, R.F. Adler, A. Gruber, R. Ferraro, G.J. Huffman, and S. Curtis, 2003: GPCP Pentad precipitation Analyses: An Experimental Data Set Based On Gauge Observations And Satellite Estimates. *J. Climate*, in revision.

WEB SITES

ftp://aeolus. nascom.nasa.gov
http://precip.gsfc.nasa.gov
http://trmm.gsfc.nasa.gov

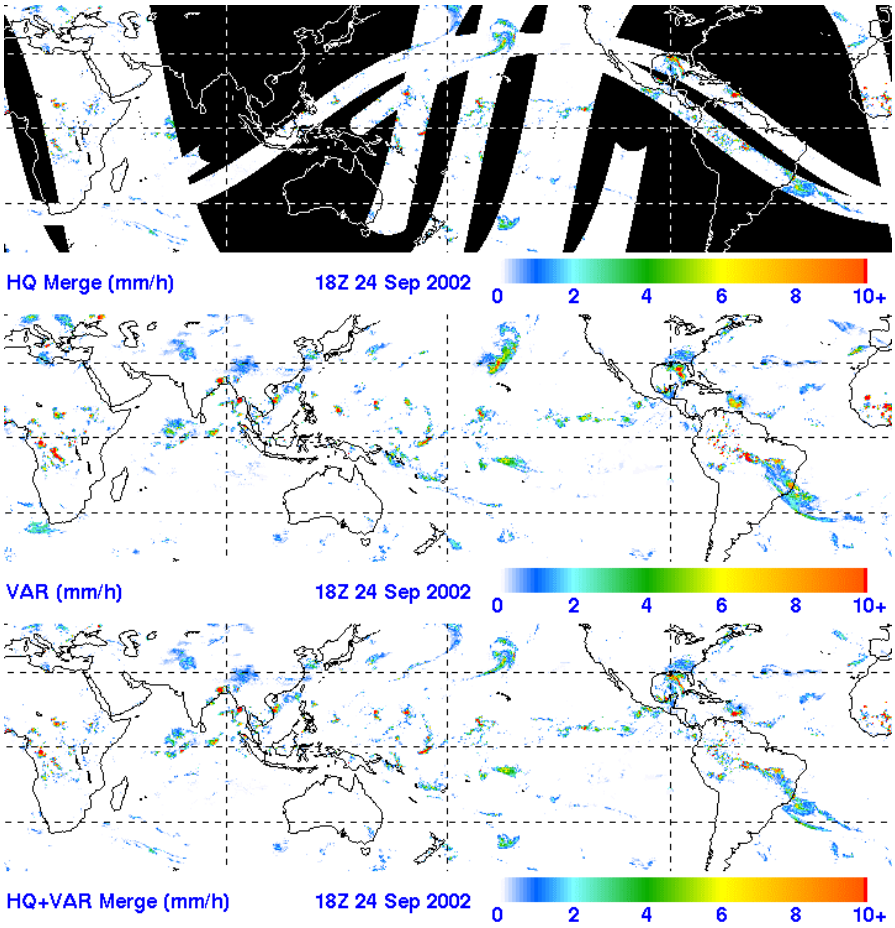

Figure 1. Example real-time MPA fields for 18Z on 24 September 2002, showing the merged microwave estimates (HQ, or 3B40RT; top), the microwave-calibrated IR (VAR, or 3B41RT; middle), and the combination (HQ+VAR, or 3B42RT; bottom).

Techniques Used to Create CMAP and Their Potential Improvements

Pingping Xie [1)], Yelena Yarosh [1)], Mingyue Chen [1)],
John E. Janowiak [1)], and Phillip A. Arkin [2)]

[1)] NOAA/NWS/NCEP/Climate Prediction Center
5200 Auth Road
Camp Springs, MD 20746, USA
[2)] The Earth System Interdisciplinary Center (ESSIC)
University of Maryland,
College Park, MD 20742, USA

1. Introduction

The objective of this article is to describe the objective techniques used to create the CPC Merged Analysis of Precipitation (CMAP, Xie and Arkin 1996)and to discuss the problems in the current version of the technique. The authors expect that comments and advice from the workshop attendees will help the future improvements of the CMAP.

2. The CMAP Algorithm

The CPC Merged Analysis of Precipitation (CMAP, Xie and Arkin 1996, 1997a, 1997b) is defined by merging seven kinds of individual input data sources. These input data sets include the gauge data (the GPCC gauge-based analyses of Rudolf et al. 1994 over land and the atoll gauge data of Morrissey et al. 1995 over ocean),5 sets of satellite estimates derived from 1) the IR-based GPI (Arkin and Meisner 1987), 2) OLR-based Precipitation Index (OPI, Xie and Arkin 1998), 3) SSM/I scattering-based estimates of Ferraro and mark (1995), 4) SSM/I emission-based estimates of Wilheit et al. (1993), and 5)MSU-based estimates of Spencer (1993). Precipitation fields generated by the NCEP/NCAR reanalysis (Kalney et al. 1996) are also utilized as an additional source.

The merging of the individual input data sources is conducted in two steps. First, to reduce the random error, satellite estimates and reanalysis precipitation fields are combined linearly through the Maximum Likelihood Estimation method, in which the linear combination coefficients are inversely proportional to the squares of local random error of the individual data sources. Over global land areas, the individual random error is defined for each grid and for each time step (month/pentad) by comparing the data sources with the concurrent gauge-based analysis over the surrounding areas. Over global oceanic areas, it is defined by comparison with atoll gauge data (Morrissey et al. 1995) over tropics and by subjective assumptions regarding the error structures over the extra-tropics (Xie and Arkin 1997a).

Since the output of the first step contains bias passed through from the individual input data sources, a second step is included to remove it. For that purpose, the gauge-based analyses are combined with the output of the first step. Over land areas, the gauge data and the output of the first step are blended through the method of Reynolds (1988), in which the first-step-output and the gauge data are used to define the relative distribution (or "shape") and the magnitude of the precipitation fields, respectively. Over the oceans, the bias in the first-step-output is ?removed? by comparison with the atoll gauge data over the tropics and by subjective assumptions regarding the bias structures over the extra-tropics.

The techniques described above have been applied to construct analyses of monthly and pentad precipitation on a 2.5o lat/lon grid over the globe for a 24-year period from 1979 to the present. Called the monthly and pentad CMAP (Xie and Arkin, 1997a and b), these analyses have been used widely for climate analysis, model verifications and other applications.

The CMAP techniques were designed and developed almost 10 years ago to ensure that analyses of precipitation are created with complete spatial coverage and reasonable accuracy by merging individual inputs with spatial resolution, availability and quality of 1993/1994:

- Multiple satellite estimates are combined linearly to achieve maximum spatial/temporal coverage with reduced random error;

- Gauge observations were used over both land and ocean to assure stability in the magnitude of the final merged analyses throughout the data period;

- Precipitation fields generated by the NCEP/NCAR reanalysis were included to ensure complete global coverage and to complement the reduced quality of satellite estimates over mid- and hi-latitudes;

3. Problems and Potential Improvements

In recent years, several examinations and comparisons have been conducted for the CMAP datasets. While the data sets have proved to be useful for many applications in climate analysis and model verifications, several problems have been reported, most of which are due to the shortcomings of the objective techniques used to create the data sets.

3.1 Analyses over land

Over land areas, the precipitation distribution over regions subject to orographic effects is poorly represented in the current CMAP data sets, due to the sparse gauge networks there and lack of appropriate techniques to combine information from gauge observations, satellite observations and other sources.

Work is underway in NOAA/CPC to improve the quality of the merged analyses over the global land areas. As a first step, the optimal interpolation technique (OI, Gandin 1963) has been applied to create analyses of global monthly precipitation (Chen et al. 2002). In the OI-based precipitation analyses, the climatology of monthly precipitation is first defined for over 17,000 stations using the gauge observations of Global Historical Climatology Network (GHCN, NOAA/NCDC) for a 40-year period from1951-1990. Gridded analyses of monthly climatology are then defined for the 12 calendar months by interpolating the station climatology and used as the first guess fields in the OI. Monthly precipitation at a grid point is finally defined by adding increments determined from nearby gauge observations to the first guess.

Several tests have been conducted to examine the quality and robustness of the OI technique. Figure 1shows the sensitivity test performed for the OI and the interpolation algorithm of Shepard (1968) over the African continent for a 21-year period from 1950 to 1970 during which station observations are available from relatively dense gauge networks over the target domain. The Shepard (1968) technique is used to define the gauge-based analyses of GPCC, which determine the magnitude of the CMAP analyses over the land areas.

4 sets of monthly precipitation analyses were constructed by interpolating all and a subset of the GHCN gauge data using the OI and the Shepard (1968)techniques. Presented in figure 1 are comparison results for the 21-year mean precipitation distribution among the4 sets of analyses. Fig.1 1950-1970 mean precipitation differences between analyses defined by interpolating all and a subset of the available gauge data using the OI and the Shepard techniques.

It is clear from the above figure that small differences are observed between the analyses created by the OI and the Shepard (1968) when gauge observations from all stations are used (left-top panel), indicating that the analysis is NOT sensitive to the interpolation algorithm used when the gauge network is dense. The 21-year mean precipitation in the OI-based analyses using fewer gauges is almost the same as that in the OI analyses using all gauges (left-bottom panel). Substantial differences, however, are observed when the analyses are generated from fewer gauges using the interpolation technique of Shepard (1968) (right panels). These preliminary results show that by making use of the climatology defined from dense gauge network, the OI is capable of representing the overall magnitude of precipitation fields better than a simple interpolation algorithm like Shepard (1968) in which only station observations available for the target month are used.

Further work is underway to develop an OI-based technique to combine the gauge observations with various satellite estimates.

3.2 Analyses over ocean

Over oceanic areas, uncertainty exists in the magnitude of the CMAP precipitation fields. The current CMAP techniques rely too much on the atoll gauge data. In particular, the CMAP procedures that use the atoll gauge data to adjust the oceanic bias may add noise to the combined satellite estimates and alias the global oceanic mean precipitation by assuming that the relative bias is identical over the entire tropical oceans and decreases gradually toward high latitudes. A comprehensive examination may be needed to check the bias structure for satellite estimates. Comparison with water budget calculation from reliable models may give us hints on the overall magnitude of precipitation, especially over mid- and high latitudes. New techniques need to be developed to ensure stable magnitude for the oceanic precipitation analyses.

3.3 Analyses over the high latitudes

Over high latitudes (polar caps), the CMAP analyses are basically defined as the same as the precipitation fields generated by the NCEP/NCAR reanalysis. While the circulation fields are reasonably well produced in the current version of the reanalysis, the precipitation fields are not represented as well. While collection of precipitation

observations from more gauge stations will help improve the quality of the merged analysis, the final solution to the problem may lie in the development of completely new objective analysis techniques that combines the circulation fields from models with observations from gauges and satellites. Comments and advices from experts on this topics are highly appreciated.

References:

Arkin, P.A., and B.N. Meisner, 1987: The relationship between large-scale convective rainfall and cold cloud over the western hemisphere during 1982 -84. Mon. Wea. Rev., 115, 51 - 74.

Chen, M., P. Xie, J.E. Janowiak, P.A. Arkin, 2002: Global Land Precipitation: A 50-yr Monthly Analysis Based on Gauge Observations. Journal of Hydrometeorology: 3, pp. 249??266.

Ferraro, R.R., and G.F. Marks, 1995: The development of SSM/I rain rate retrieval algorithms using ground-based radar measurements. J. Atmos. Oceanic Technol., 12, 755 - 770.

Gandin, L. S., 1963: Objective analysis of meteorological fields. Gidrometeor. Isdaty., Leningrad. [Israel Program for Scientific Translations, Jerusalem,1965, 242 pp.]

Kalnay, E., M. Kanamitsu, R. Kistler, W. Collins, D. Deaven, L. Gandin, M. Iredell, S. Saha, G. White, J. Woollen, Y. Zhu, M. Chelliah, W. Ebisuzaki, W. Higgins, J. Janowiak, K. C. Mo, C. Ropelewski, J. Wang, A. Leetmaa, R. Reynolds, Roy Jenne, and Dennis Joseph,1996: The NMC/NCAR 40-Year Reanalysis Project. Bull. Amer. Meteor. Soc., 77, 437 -471.

Morrissey, M.L., M.A. Shafer, S.E. Postawko, and B. Gibson, 1995: Pacific rain gauge data. Water Resources Research, 31, 2111-2113.

Reynolds, R.W., 1988: A real-time global sea surface temperature analysis. J. Clim., 1, 75 - 86.

Rudolf, B., H. Hauschild, W. Rueth, and U. Sdchneider,1994: Terrestrial precipitation analysis: Operational method and required density of point measurements. NATO ASI Ser., 126, 173-186.

Shepard, D., 1968: A two -dimensional interpolation function for irregularly spaced data. 23rdNatl. Conf. Of Amer. Computing Machinery, Princeton, N.J.

Spencer, R.W., 1993: Global oceanic precipitation from MSU during 1979 - 91 and comparisons to other climatologies. J. Clim., 6, 1301 - 1326.

Wilheit, T., A.T.C. Chang, and L.S. Chiu, 1991: Retrieval of monthly rainfall indices from microwave radiometric measurements using probability distribution functions. J. Atmos. Oceanic Technol., 8, 118 -136.

Xie, P., and P.A. Arkin, 1996: Analyses of global monthly precipitation using gauge observations, satellite estimates, and numerical model precipitations. J. Clim., 9,840 - 858.

Xie, P., and P.A. Arkin, 1997a: Global Precipitation: A17-year monthly analysis based on gauge observations, satellite estimates and numerical model outputs. Bull. Amer. Meteor. Soc.,78,2539 - 2558.

Xie, P., and P.A. Arkin, 1997b: Global pentad precipitation analysis based on gauge observations, satellite estimates and model outputs. Amer. Geophys. Union 1997 Fall Meeting, December 8-12, 1997, San Francisco, CA, USA.

Xie, P., and P.A. Arkin, 1998: Global monthly precipitation estimates from satellite-observed outgoing longwave radiation. J. Clim., 11, 137- 164.

Precipitation assimilation at ECMWF

Philippe Lopez, Emmanuel Moreau, Peter Bauer, Frédéric Chevallier,
Adrian Tompkins and Marta Janisková, ECMWF

GEWEX Workshop on Objective Analysis of Precipitation
ECMWF, 11-13 March 2003

1 Introduction

The assimilation of observations related to cloud and precipitation has become a very important issue for most operational weather services including ECMWF. Marécal and Mahfouf (2000) developed a 1D-Var method for correcting individual profiles of the model's control variables in order to decrease the discrepancies that may exist between the simulated surface rainfall rates and corresponding retrievals from the Tropical Rainfall Measuring Mission Microwave Imager (TRMM/TMI) or from the Special Sensor Microwave/Imager (SSM/I).

Marécal and Mahfouf (2002) also found that an indirect "1D-Var + 4D-Var" assimilation of TMI derived rainfall rates could improve the quality of humidity, temperature and wind forecasts in the Tropics. In this approach, the background-observation departures on surface rainfall rates are first converted into total column water vapore (TCWV) increments thanks to the 1D-Var, and the corresponding TCWV pseudo-observations are then assimilated in the 4D-Var system. They also showed that this indirect method is more robust than a direct 4D-Var assimilation of the TMI rainfall rates, because of some inconsistencies between the inner and outer loops of 4D-Var. The "1D-Var + 4D-Var" technique therefore seems more appropriate for performing the future assimilation of such data, as long as these inconsistencies are not removed.

Instead of performing the 1D-Var on surface rainfall rates that are derived from multi-channel microwave brightness temperatures (BTs) thanks to various algorithms, the 1D-Var calculations could also very well be applied to the BTs directly. The multiple sensitivities of the BTs to the vertically integrated amounts of rain water and cloud water should provide a stronger constraint on the 1D-Var minimization. Another advantage of this method could result from the better knowledge of observation errors on BTs than on derived rainfall rates.

The potential of applying 1D-Var directly to TMI and SSM/I microwave brightness temperatures has been investigated and its results have been compared with the 1D-Var on derived rainfall rates. The two methods will be referred to as 1D/BT and 1D/RR hereafter. In addition, "1D-Var + 4D-Var" assimilation experiments have been run with the most up-to-date version of ECMWF's forecasting system in order to assess the impact of TMI or SSM/I observations in precipitation areas on 4D-Var analyses and on subsequent forecasts.

2 Modifications of ECMWF's operational convection scheme

Prior to all experiments, some modifications were made to ECMWF's parameterizations of convection and large-scale condensational processes. These changes were expected to increase the level of physical realism of the parameterizations with respect to the very simplified ones used in current 4D-Var. At the same time, the modified schemes were designed such as to behave more linearly when compared to the highly non-linear operational schemes originally designed by Tiedtke (1989, 1993).

The modified convection scheme is still based on the mass-flux approach, but it now features uncoupled equations for the mass-flux and for the updraft characteristics. The total entrainment rate (turbulent and organized) is expressed as $1/(2z)$, where z denotes the height above the updraft starting level, according to Siebesma and Jakob's recent ideas (personal communication). Detrainment is assumed to be equal to the entrainment rate, except close to cloud top where an enhanced constant value is applied. The vertical evolution of the updraft vertical velocity is parameterized as in Simpson and Wiggert (1969), and the closure of the scheme is based on the relaxation of convective available potential energy for all types of convection.

Tompkins and Janisková (personal communication) have recently developed a new simplified statistical diagnostic cloud-scheme that includes precipitation generation according to Sundqvist (1989) and a new formulation of precipitation evaporation based on the subgrid scale distribution of total water.

3 1D-Var experiments on TMI and SSM/I observations

3.1 Description of the 1D-Var method

The purpose of the unidimensional variational method (1D-Var) is to determine increments that need to be added to the model's control variables so that the difference between a selected output quantity of the model and its observed equivalent becomes minimal in a least-square sense. In the present study, two control variables are considered in the model: temperature and specific humidity.

The selected output quantity to be optimized is either the surface rainfall rate (like in Marécal and Mahfouf 2000) or the multi-channel microwave brightness temperatures. Surface rainfall rate is an output from the model convective and large-scale condensation parameterizations and can also be derived from observed microwave brightness temperatures thanks to a proper retrieval algorithm (see section 2). On the other hand, brightness temperatures can be simulated applying first the parameterizations of moist processes to the model's control variables and then a microwave radiative transfer model.

The 1D-Var method searches for the model's state vector **x** that minimizes the following functional:

$$J(\mathbf{x}) = \frac{1}{2}(\mathbf{x}-\mathbf{x_b})^T \mathbf{B}^{-1}(\mathbf{x}-\mathbf{x_b}) + \frac{1}{2}\left[\frac{H(\mathbf{x})-Y_{obs}}{\sigma_{obs}}\right]^2$$

where $\mathbf{x_b}$ is the background model state, and $H(\mathbf{x})$ is the non-linear observation operator which permits to convert the model's variables into either surface rainfall rates or microwave brightness temperatures. Y_{obs} denotes the corresponding observed quantity and σ_{obs} is the standard deviation of the observation errors. Matrix **B** contains the model's background error covariances. The result of the 1D-Var is therefore a linear combination of the background term and of the observation term, weighted by the inverse of their respective error statistics.

The minimization of $J(\mathbf{x})$ is performed thanks to the quasi-Newton descent algorithm (M1QN3) developed by Gilbert and Lemaréchal (1989). It involves the jacobian matrix of the nonlinear observation operator $H(\mathbf{x})$ which consists of the modified parameterizations of convection and of large-scale condensation described in section 2. In the case of 1D/BT, the minimization also involves the forward non-linear version and the adjoint version of the radiative transfer model designed by Bauer (2002) and Moreau *et al.* (2002), which takes into account the diffusion of microwave radiation by precipitation.

3.2 Set-up of the 1D-Var experiments

1D-Var experiments have been run on three recent meteorological events: Super-typhoon MITAG near the Philippines at 1200 UTC 5 March 2002, tropical cyclone ZOE close to the Fiji Islands at 1200 UTC 26 December 2002, and an extra-tropical front in the North Atlantic at 1200 UTC 9 January 2002. TMI observations have been used for MITAG and ZOE, SSM/I ones in the mid-latitude frontal case.

In 1D/RR, various algorithms have been tested for retrieving surface rainfall amounts from the multi-channel microwave brightness temperatures observed by either TMI or SSM/I: 2A12-v5 (Kummerow *et al.* 1996), PATER (Bauer 2002), Ferraro (1996) and Bauer-Schluessel (1993). The rainfall retrievals at instrument resolution were then averaged onto the Gaussian grid of the ECMWF model which corresponds to a T511 spectral truncation (grid point resolution of about 40 km), so that observation and model points became co-located. The retrieval errors for PATER have been estimated as in Bauer *et al.* (2002), while the errors derived by L'Ecuyer and Stephens (2002) have been applied to 2A12-v5 retrievals. For the two other algorithms, a constant error of 50% of the rainfall rate has been assumed.

In 1D/BT on TMI observations, the minimization has been applied to seven channels: 10 GHz (V/H), 19 GHz (V/H), 22 GHz (V) and 37 GHz (V/H), where V and H denote the vertical and horizontal polarizations. With SSM/I data, only the 19 GHz (V/H), 22 GHz (V) and 37 GHz (V/H) channels are available. Increasing the number of microwave channels used in the 1D-Var is expected to be beneficial because of their differing sensitivities to temperature, water vapour, cloud water and precipitation. The observed BT at each model grid point has been set equal to its value at the closest TMI pixel, in each microwave channel. For BTs, σ_{obs} has been set to 3 K (resp. 6 K) for the vertically (resp. horizontally) polarized channels. This is assumed to account for both the instrumental errors and the errors of the radiative transfer model.

The model's background fields that enter the 1D-Var have been obtained from 12-hour T511 forecasts with the ECMWF model. The covariance matrix of background errors **B** used in the 1D-Var is taken from the operational ECMWF 4D-Var system (Rabier *et al.* 1997). The temperature and specific humidity errors are assumed to be uncorrelated.

3.3 Summary of the 1D-Var results

As an illustration, Fig.1 displays the results of the 1D-Var calculations on super-typhoon MITAG: the model's background surface rainfall rates are shown in panel (a). The observed rainfall rates as retrieved with the 2A12-v5 algorithm from the TMI BTs appear in panel (b). "Analysed" surface rainfall rates can be simulated using the parameterizations of moist processes after adding the 1D-Var increments to the model's background profiles of temperature and specific humidity. These analysed rainfall rates are shown in panel (c) for 1D/BT and (d) for 1D/RR. Fig. 2 shows the TCWV background field and the corresponding increments from 1D/RR on PATER observations and from 1D/BT.

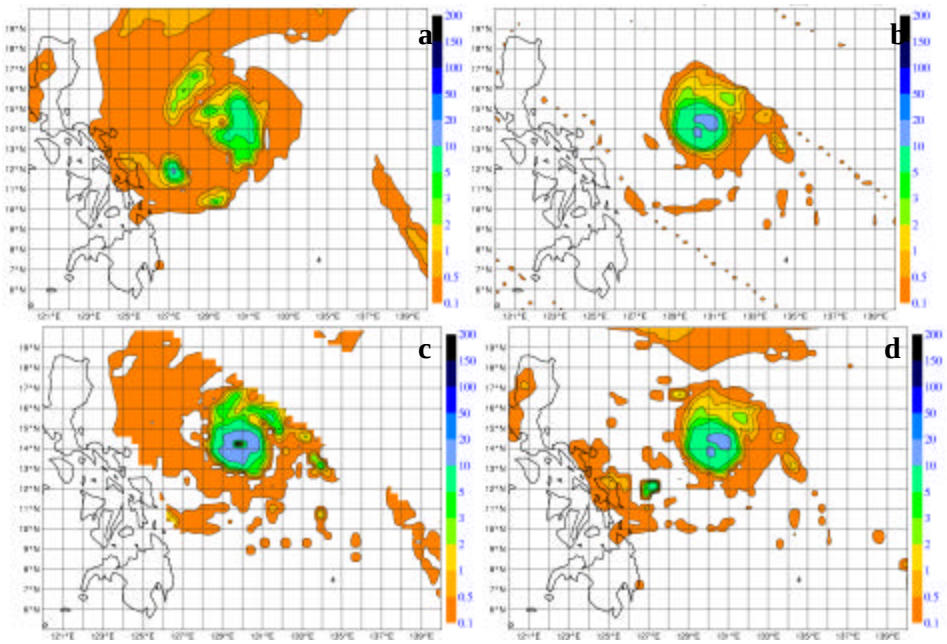

Fig.1. Surface rain rates from model background (a) for the case of super-typhoon MITAG at 1200 UTC 5 March 2002. Corresponding TMI observations from the PATER algorithm (b), and corresponding analysed rainfall rates from 1D/BT (c) and from 1D/RR (d). Units are in mm h^{-1}.

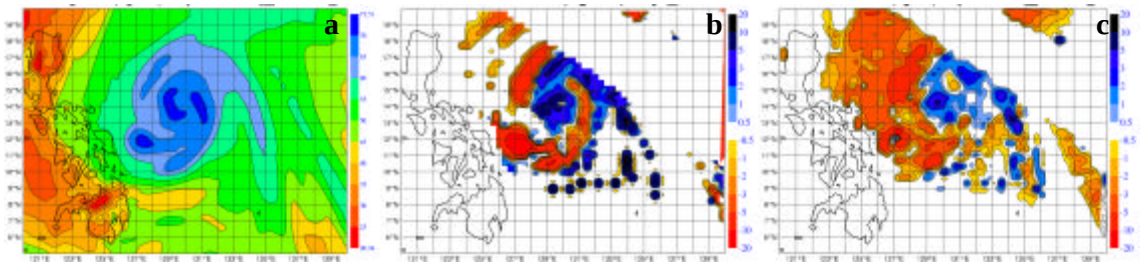

Fig.2. Background TCWV (a) for the case of super-typhoon MITAG at 1200 UTC 5 March 2002. TCWV increments from 1D/BT (b) and from 1D/RR on PATER surface rainfall rates (c). Units are in kg m^{-2}.

Fig.1 clearly demonstrates that both 1D/RR and 1D/BT are able to correct the initial temperature and specific humidity profiles in such way that the model gets closer to the observations. It is noteworthy that in the case of 1D/BT the agreement is all the more remarkable as the PATER rainfall rates provide an *independent* source of validation. The tighter initial screening of points applied in 1D/BT to save computational time explains why the light rain area around the storm is not modified in Fig.1.c. It should also be recalled here that 1D/RR only works at points where the jacobian matrix **R** is non-zero, that is only at rainy points of the model's background. Fig.2 points out the similarity between the patterns of the TCWV increments obtained with the two 1D-Var methods. However, 1D/BT systematically produces increments with a stronger magnitude than 1D/RR, as a result of the multiple sensitivities of microwave brightness temperatures to precipitation but also to cloud condensate and water vapour. All these findings have been confirmed in the two other studied cases (not shown), as well as for the different rainfall rate retrieval algorithms tested.

By looking at the other cases, it has also been evidenced that 1D/RR performs better at points where the background precipitation originates from the large-scale condensation scheme and not from the convective parameterization which involves more non-linearities. This was clearly seen in the case of tropical cyclone ZOE for which 1D/BT was more successful than 1D/RR in the presence of intense deep convection in the model.

A statistical cross-comparison of 1D/RR with 1D/BT has pointed out that the reduction of the model-observation errors on BTs with 1D/RR is more systematic than the reduction of the model-observation errors on rainfall rates with 1D/BT. Furthermore, the 1D-Var outputs have been validated against independent measurements from the TRMM precipitation radar (both in terms of rainfall rates and reflectivities) and from the NOAA AMSU-B instrument.

4 "1D-Var + 4D-Var" assimilation of TMI observations in rainy areas

After running 1D/RR and 1D/BT on TMI observations over the region of tropical cyclone ZOE, pseudo-observations of TCWV have been obtained by vertical integration of the 1D-Var increments of specific humidity and adding the result to the background TCWV. These TCWV pseudo-observations have been assimilated inside ECMWF's 4D-Var in order to study their impact on 4D-Var analyses and on subsequent forecasts. Three experiments have been run: a "control" 4D-Var assimilation of all available routinely used observations, a 4D-Var assimilation of the same data plus the 1D/RR TCWV pseudo-observations, and a similar experiment with 1D/BT TCWV pseudo-observations.

These tests have permitted to find 1) that 4D-Var can properly handle the 1D-Var/TMI TCWV pseudo-observations, 2) that significant increments can be seen on the humidity field but also on the dynamics in the vicinity of the storm, and 3) that the amplitude of these increments remain significant in the forecasts started from the new analyses. These findings confirm earlier results from Marécal and Mahfouf (2000) obtained with an older set-up of ECMWF's model.

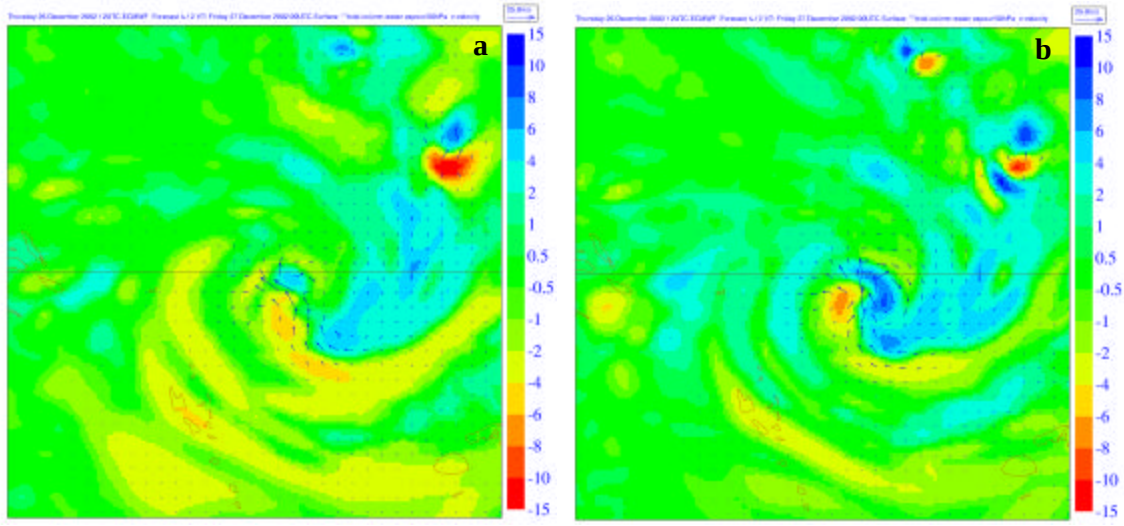

Fig.3. Differences between 12-hour forecasts started from the 4D-Var analysis with TMI observations and from the control 4D-Var analysis, when using 1D/RR (a) and 1D/BT (b). Differences of TCWV are displayed in colors and differences of 850 hPa winds are plotted as arrows. At this time (0000 UTC 27 December 2002), tropical cyclone ZOE is centered at the middle of the plotted domain. Units for TCWV are in kg m^{-2}, while for wind differences the longest arrow corresponds to 25 m s^{-1}.

As an illustration, Fig.3 displays differences of TCWV and 850 hPa winds between 12-hour forecasts issued from the new analysis and from the control analysis, when using 1D/RR (a) and 1D/BT (b) TCWV pseudo-observations.

In both cases, the impact on the TCWV and wind fields is still large after 12-hours, but is even stronger when using 1D/BT, despite a smaller number of TCWV observations because of differences in the 1D-Var screening. This is due to the fact that the 4D-Var analysis increments (not shown) are already larger when using 1D/BT.

In addition, Fig. 4 illustrates the clear improvement of the track forecast for tropical cyclone ZOE in the "1D/RR+4D-Var" and "1D/BT +4D-Var" experiments compared to the control experiment and to observations.

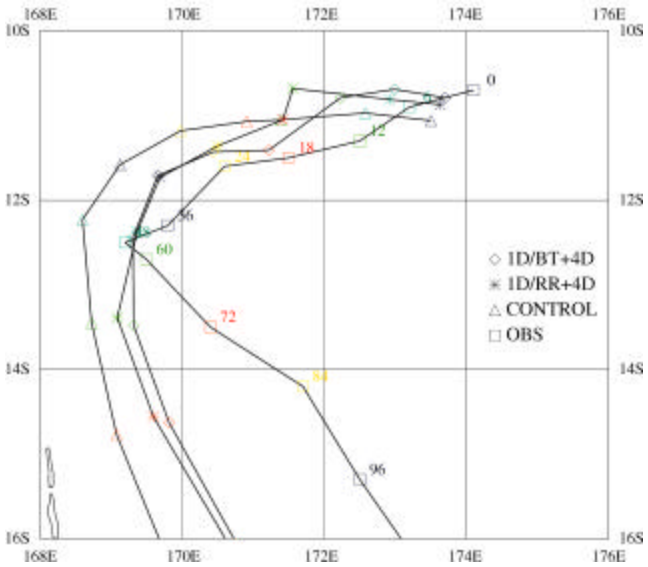

Fig.4. Comparison of the tracks of tropical cyclone ZOE as from observations (squares), from control 4D-Var (triangles), from '1D/TMI-RR + 4D-Var' (stars), and from '1D/TMI-BT + 4D-Var' (diamonds). Forecast times in hours are indicated along the observed track, and similar colors correspond to similar forecast times in the experiments. Time 0 corresponds to the analysis.

5 Conclusions

1D-Var experiments based on retrieved surface rainfall rates as observed from TMI and SSM/I have been compared to 1D-Var experiments directly performed on the TMI and SSM/I brightness temperatures, for three tropical and mid-latitude cases. These runs include simplified versions of ECMWF's operational parameterizations of moist processes. Both 1D-Var methods are successful in producing reasonable and consistent temperature and specific humidity increments that permit to correct either the model's surface rainfall rates or the simulated BTs towards their observed equivalents. Besides, specific humidity increments dominate and are generally larger with 1D/BT than with 1D/RR.

The 1D-Var on rainfall rates has the main advantage of being computationally cheaper than the 1D-Var on BTs. The two major drawbacks of the former lies in its total inefficiency wherever the background rainfall rate is zero and in the necessity of choosing the proper retrieval algorithm for converting microwave BTs into surface rainfall rates. On the other hand, two advantages of the brightness temperature approach can be listed: firstly, the error statistics are better known for BTs than for derived surface rain rates that depend on the retrieval algorithm used. Secondly, the fact that microwave BTs are sensitive not only to precipitation but also to water vapour and cloud water, make it possible to correct the model's control variables outside non-rainy areas of the background.

Preliminary 4D-Var assimilation of pseudo-observations of TCWV obtained from the 1D-Var on TMI rainfall rates or BTs in rainy areas around tropical cyclone ZOE have shown that these extra observations can lead to significant thermodynamic and dynamical changes in the 4D-Var analyses and the subsequent forecasts. The changes in 4D-Var obtained with 1D/BT TCWV observations are clearly larger than with 1D/RR. A clear improvement is also found in the track forecast of the studied storm.

Global monthly experiments currently in progress will help determine whether the assimilation of TMI and SSM/I observations can lead to a systematic improvement of both analyses and forecast scores.

References

Bauer, P., and P. Schluessel, 1993: Rainfall, total water, ice water, and water vapour over sea from polarized microwave simulations and special sensor microwave/imager data. *J. Geophys. Res.*, **98**, 20737-20759.

Bauer, P., 2002: Microwave radiative transfer modelling in clouds and precipitation. Part I: Model description. *Satellite Application Facility for Numerical Weather Prediction*, NWPSAF-EC-TR-005, version 1.0.

Bauer, P., J.-F. Mahfouf, W.S. Olson, F.S. Marzano, S. Di Michele, A. Tassa and A. Mugnai, 2002: Error analysis of TMI rainfall estimates over ocean for variational data assimilation. *Q. J. R. Meteorol. Soc.*, **128**, 2129-2144.

Ferraro, R.R., F. Weng, N.C. Grody, and A. Basist, 1996: An eight-year (1987-1994) time series of rainfall, clouds, water vapour, snow cover, and sea ice derived from SSM/I measurements. *Bull. Am. Meteorol. Soc.*, **77**, 891-905.

Gilbert, J.-C. and Lemaréchal, C., 1989: some numerical experiments with variable-storage quasi-Newton algorithms. *Math. Programming*, **45**, 407-435.

Kummerow, C.D., Olson W.S. and L. Giglio, 1996: A simplified scheme for obtaining precipitation and vertical hydrometeor profiles from passive microwave sensors. *IEEE Trans. Geosci. Remote Sensing*, **34**, 1213-1232.

L'Ecuyer, T. S. and G. L. Stephens, 2002: An Uncertainty Model for Bayesian Monte Carlo Retrieval Algorithms: Application to the TRMM Observing System. *Q. J. R. Meteorol. Soc*., **128**, 1713-1738.

Marécal, V. and J.-F. Mahfouf, 2000: Variational retrieval of temperature and humidity profiles from TRMM precipitation data. *Mon. Weather Rev*., **128**, 3853-3866.

Marécal, V. and J.-F. Mahfouf, 2002: Four-dimensional variational assimilation of total column water vapour in rainy areas. *Mon. Weather Rev.*, **130**, 43-58.

Marécal, V., J.-F. Mahfouf and P. Bauer, 2002: Comparison of TMI rainfall estimates and their impact on 4D-Var assimilation. *Q. J. R. Meteorol. Soc*, **128**, 2737-2758.

Moreau, E., P. Bauer and F. Chevallier, 2002: Microwave radiative transfer modelling in clouds and precipitation. Part II: Model evaluation. *Satellite Application Facility for Numerical Weather Prediction*, NWPSAF-EC-TR-005, version 1.0.

Rabier, F., A. McNally, E. Andersson, P. Courtier, P. Unden, J. Eyre, A. Hollingsworth and F. Bouttier, 1997: The ECMWF implementation of the three dimensional variational assimilation (3D-Var). Part II: Structure functions. *Q. J. R. Meteorol. Soc*., **124**, 1809-1829. 27

Simpson, J. and V. Wiggert, 1969: Models of precipitating cumulus towers, *Mon. Weather Rev*., **97**, 471-489.

Sundqvist, H., E. Berge, and J.E. Kristjánsson, 1989: Condensation and Cloud Parameterization Studies with a Mesoscale Numerical Weather Prediction Model, *Mon. Weather Rev*., **117**, 1641-1657.

Tiedtke, M., 1989: A comprehensive mass flux scheme for cumulus parametrization in large-scale models. *Mon. Weather Rev.*, **117**, 1779-1800.

Tiedtke, M., 1993: Representation of Clouds in Large-Scale Models. *Mon. Weather Rev.*, **121**, 3040-3061.

Precipitation Assimilation Research at NASA Goddard

Arthur Y. Hou, Sara Zhang, Jiu-Lin Li

NASA Goddard Space Flight Center, Greenbelt, Maryland 20771
E-mail: Arthur.Y.Hou@nasa.gov

GEWEX Workshop on Objective Analysis of Precipitation, ECMWF,11-13 March 2003

1. Introduction

Precipitation estimates produced by global data assimilation systems without rainfall data differ significantly from each other and from observational estimates such as the combined satellite-gauge rainfall from the Global Precipitation Climatology Project (GPCP, Huffman et al. 1997). The discrepancies are especially pronounced in the Tropics, where conventional observations are sparse and analyses are strongly influenced by parameterized diabatic processes in global models (Trenberth and Olson 1988). In terms of monthly-mean spatially-averaged rain rates at 2.5^o x 2.5^o horizontal resolution, estimates from global re-analyses can deviate locally from GPCP rain rates by more than 10 mm day^{-1}, much greater than the estimated uncertainty of 10-20% in GPCP analyses. Since 1 mm day^{-1} of rain rate is associated with a latent heating flux of roughly 30 W m^{-2}, uncertainties on the order of 10 mm day^{-1} are too large to be useful in closing the global energy budget (For comparison, the accuracy goal set by the GEWEX radiation panel for the monthly-mean net radiative fluxes is ~ 5 W m^{-2} at 200 km resolution by 2010). Assimilation of precipitation observations is one way to improve the utility of global analyses for understanding the water and energy cycle.

Current operational global weather forecast systems typically assimilate observations using a multi-dimensional variational scheme to optimize the initial condition at the beginning of an analysis window. Such schemes assume that forecast errors arise from uncertainties in the initial condition rather than deficiencies in the forecast model. For precipitation assimilation, this assumption needs to be re-examined since rainfall in global models is derived from parameterized moist processes with simplifying approximations, which can have significant systematic errors (Randall et al. 2003). As model biases can lead to poor forecasts even with perfect initial conditions, the influence of systematic model errors needs to be considered in assimilating precipitation information effectively in the presence of model biases. Additionally, one must also consider such issues as the temporal, spatial, and physical compatibility between the model-predicted rain from parameterized physics with implicit quasi-equilibrium assumptions and the nearly instantaneous satellite measurements.

2. Variational continuous assimilation of precipitation information

At NASA Goddard, we have been exploring rainfall assimilation using prognostic tendency corrections as a control variable within the framework of variational continuous assimilation (VCA, Derber 1989) to compensate for model deficiencies. Since the model-predicted precipitation is diagnostically linked to latent heating and moisture tendencies, a VCA-type of approach offers a natural framework for assimilating rainfall information using moisture/temperature tendency corrections. As a test of the effectiveness of such a strategy, we developed a "1+1" dimensional (1+1D) variational algorithm to assimilate 6-h accumulated TMI and SSM/I surface rain rates in the Goddard Earth Observing System (GEOS) global data assimilation system (DAS). The scheme minimizes the functional:

$$\boldsymbol{J}(\boldsymbol{x}) = (\boldsymbol{x})^{\mathrm{T}}\, \mathbf{Q}^{-1}\, (\boldsymbol{x}) + \{\, \boldsymbol{H}(\boldsymbol{x}) - \boldsymbol{y}^{\boldsymbol{o}} \,\}^{\mathrm{T}}\, \mathbf{R}^{-1}\, \{\, \boldsymbol{H}(\boldsymbol{x}) - \boldsymbol{y}^{\boldsymbol{o}} \,\} \qquad (1)$$

where $\boldsymbol{y}^{\boldsymbol{o}}$ and $\boldsymbol{H(x)}$ are logarithms of the observed and model rainfall, respectively (the logarithmic singularity is removed with a rain threshold of 0.01 mm day^{-1}), $\boldsymbol{x}$ is the temperature/moisture tendency correction within a 6-h assimilation window. $\mathbf{Q}$ is the error covariance for a prior estimate of the tendency error, $\boldsymbol{x}$, which is not known *a priori*. The working assumption is that $\mathbf{Q}$ closely follows the error covariance of the background pseudo-relative humidity, which is temperature-dependent through the saturation humidity. $\mathbf{R}$ is the "observation" error covariance parameterized in terms of variance of *relative* observation errors in TMI rainrate retrievals. Based on the work of Bauer et al. (2002) and Bell et al. (1990), the standard deviation for relative errors is taken to be 15-30% for 6-h rain averaged to 1^o x 1^o model resolution. The observation operator, $\boldsymbol{H(x)}$, is based on a 6-h integration of a column model of the GEOS moist physics with large-scale forcing estimated from a 3-h assimilation of the full GEOS DAS, as described in Hou et al. (2000). The minimization is obtained using a quasi-Newton method, with the gradient of $\boldsymbol{J}$ updated at each iteration. See Hou et al. (2003) for further details.

The 1+1D VCA scheme differs from nudging or physical initialization in that it is a statistical analysis within the optimal estimation framework. The VCA scheme as implemented in the GEOS DAS effectively operates as an online forecast bias estimation and correction for precipitation and moisture every 6 hours. In its generalization to four dimensions, the VCA scheme is similar to 4DVAR schemes with the forecast model as a weak constraint (Zupanski et al. 2002). However, as a technique for precipitation estimation, the VCA scheme differs from others in one important aspect: *The VCA-based precipitation estimate is not a forecast product but is determined by the 6-h rain accumulation from a continuous 4D data assimilation constrained by precipitation observations.*

3. Impact on GEOS analysis and forecast

Results from GEOS DAS experiments show that assimilating TMI and SSM/I surface rainrates using the 1+1D VCA scheme improves not only precipitation and moisture fields in the analysis but also related climate parameters such as clouds and atmospheric radiation fluxes, as verified against the top-of-the-atmosphere radiation measurements from Clouds and the Earth's Radiation Energy System (CERES) sensors and brightness temperatures for moisture-sensitive channels of High-resolution Infrared Radiation Sounder (HIRS). Model forecast experiments show that the improved analyses also lead to better 5-day track forecasts and quantitative precipitation forecast (QPF) threat scores in eight case studies of Hurricane Bonnie and Hurricane Floyd, as illustrated in Figure 1. Despite the limited number of forecasts, these results have been shown to be robust by varying the weights assigned to TMI and SSM/I rain rates in the analysis used to initialize the forecasts. As more rainfall information is retained in the analysis, there is a systematic increase in forecast skills, confirming that the improvements seen in Fig. 1 reflect the use of rainfall data in the initial condition.

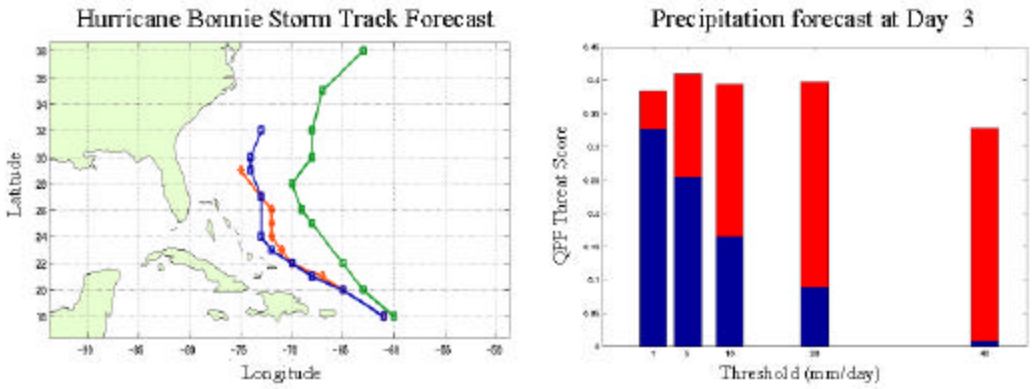

Figure 1. Improved storm track prediction and QPF Equitable Threat Scores for a 5-day forecast of Hurricane Bonnie initialized at 12:00 on 20 August 1998. Left panel: Red is the best track analysis from NOAA. Green is the control forecast from 1^{o} x 1^{o} GEOS analysis without rainfall data. Blue is the forecast from GEOS analysis with TMI and SSM/I surface rain rates. Right panel: QPF threat scores for the control experiment (blue) and for the rainfall assimilation experiment (red).

Currently, we are exploring ways to assimilate TMI-retrieved convective and stratiform latent heating profiles to seek further improvements. One scheme under testing is to assimilate the latent heating profiles by optimizing selected parameters in moist physics schemes within the general framework of model parameter estimation. Preliminary experiments show that this approach leads to comparable improvements in surface rain analyses as well as improved vertical latent heating and moistening profiles.

4. Prospects and recommendations

Our study suggests that precipitation assimilation can significantly improve the quality of global analyses. In the coming years, more satellite rain products will become available from operational and research satellites, culminating to a constellation of 8 or more satellites with the proposed Global Precipitation Measurement (GPM) mission in 2007. Realizing the full potential of these observations in data assimilation will require continued advances in satellite algorithms, error characterization, model physics, and assimilation techniques. As we continue to advance in

these areas, precipitation assimilation provides the means by which we can ultimately obtain an optimal, dynamically consistent precipitation analysis. In a wide range of applications and physical process studies, an assimilated global analysis that replicates the observed space-time variability in precipitation and its coupling to other physical components is essential for understanding the role of water in the climate and climate feedback processes. The GPCP community with experts in rainfall observations and analyses can play an important role in rainfall validation and error estimation. We recommend that GPCP extend its focus beyond observation-based precipitation analyses to support the goal of producing physically consistent precipitation analyses using both observations and model information.

5. References

Bauer, P., J.-F. Mahfouf, W. S. Olson, F. S. Marzano, S. di Michele, A. Tassa, and A. Mugnai, 2002: Error analysis of TMI rainfall estimates over ocean for variational data assimilation. *Q. J. Roy. Meteoro. Soc.*, **128**, 2129-2144.

Bell, T. L., A. Abdullah, R. L. Martin, and G. North, 1990: Sampling erro rs for satellite-derived tropical rainfall: Monte Carlo study using a space-time stochastic model. *J. Geophs. Res.*, **95**, 2195-2205.

Derber, J.C., 1989: A variational continuous assimilation technique. *Mon. Wea. Rev.*, **117**, 2437-2446.

Hou, A.Y., D. Ledvina, A. da Silva, S. Zhang, J. Joiner, R. Atlas, G. Huffman, and C. Kummerow, 2000: Assimilation of SSM/I-derived surface rainfall and total precipitable water for improving the GEOS analysis for climate studies. *Mon. Wea. Rev.*, **128**, 509-537.

Hou, A.Y., S. Zhang, O. Reale, 2003: Variational continuous assimilation of TMI and SSM/I rainrates: Impact on GEOS3 hurricane analyses and forecasts. *Mon. Wea. Rev.*, submitted.

Huffman, G. J., R. F. Adler, P. Arkin, A. Chang, R. Ferraro, A. Gruber, J. Janowiak, A. Mcnab, B. Rudolf, and U. Schneider, 1997: The global precipitation climatology project (GPCP) combined precipitation data set. *Bull. Amer. Meteor. Soc.*, 78, 5-20.

http://www.nhc.noaa.gov/1999floyd.html].Randall, D., S. Krueger, C. Bretherton, J. Curry, P. Duynkerke, M. Moncrieff, B. Ryan, D. Starr, M. Miller, W. Rossow, G. Tselioudis, B. Wielicki, 2003: Confronting models with data: The GEWEX Cloud Systems Study. *Bull. Amer. Meteor. Soc.*, in press.

Trenberth, KE., and J.G. Olson, 1988: An evaluation and intercomparison of global analyses from the National Meteorological Center and the European Center for Medium Range Weather Forecasts. *Bull. Amer. Meteor. Soc.*, 69, 1047-1057.

Zupanski, M., D. Zupanski, D. Parrish, E, Rogers, and G. DiMego, 2002: Four-dimensional Variational data assimilation for the blizzard of 2000. *Mon. Wea. Rev.*, **130**, 1967-1988.

Precipitation Assimilation at the Met Office (UK) & COST-717 collaboration within Europe

by

Bruce Macpherson

NWP, The Met Office, Bracknell, Berkshire RG12 2SZ, UK.

1. Rainfall Assimilation in the Mesoscale Model

The Met Office introduced the assimilation of radar-derived rainfall data into its operational mesoscale model (MES) in April 1996. The model currently has a grid-length of approximately 12km and 38 vertical levels. The assimilation technique used is known as Latent Heat Nudging (Jones and Macpherson, 1997). The basic idea behind LHN is that since relatively little moisture is stored in clouds, the precipitation rate is proportional to the vertically integrated condensation (latent heating) rate. Also, latent heating is important for the development and forcing of precipitating systems, so if the correct latent heating can be supplied to the model, the forecast will improve. Latent heating acts as a source term in the thermodynamic equation influencing the adjustment of the vertical velocity. If we know (or can specify) the vertical structure of latent heating, then we can scale its vertical integral by the ratio of observed precipitation rate to model precipitation rate, and then add a temperature increment to the model consistent with this scaling. One can also add moisture increments to try and produce saturation in raining areas.

For the moisture component of LHN, we apply the Moisture Observation Pre-processing System (MOPS), which blends satellite imagery and surface cloud reports with radar imagery to produce a 3-dimensional cloud analysis for assimilation by the MES (Macpherson et al., 1996). The cloud fraction data are converted into humidity increments through a relationship derived from the model cloud scheme.

The surface precipitation rate estimates are supplied by the radar analysis step of the 'Nimrod' nowcasting system (Golding, 1998). The data have been through anaprop removal, bright band correction, orographic enhancement and the system incorporates weekly calibration against rain gauges. The rainfall data are prepared on a 5km grid, then averaged to 15km and interpolated to the model's 12km grid. At each model timestep, the observed rain rate and the latest model forecast rain rate are combined to derive a target analysed rain rate, towards which the model is nudged.

In the LHN algorithm, the vertical structure of latent heating rates is taken from the model's latest estimated heating distribution, and the scaling by precipitation rates is applied, as described above. If the model is producing no rain where rain is observed, then a search is conducted around that grid-point to find a point where the model is raining, and the heating profile from that point is used to calculate increments at the point where it is desired to introduce rain. As reported by Jones and Macpherson (1997), LHN was found on average to improve precipitation forecasts in the first 6-9 hours of the forecast, with little impact beyond that time. Frontal cases showed more beneficial impact than convective cases.

2. Impact Studies and later developments

In 1997, more extended impact studies of the LHN technique were conducted. These experiments revealed that on a monthly timescale, impact from LHN can be detected objectively up to t+12 in some months, with a very marked benefit in the first 6 hours, while in other months LHN may give only a neutral signal. Figure 1 shows results for a period in July/August 1997 when LHN of radar data gave significant benefit. The improvements in ETS are appreciable relative to those noted in annual means for this score. By contrast, results for a period covering June 1997 (not shown) were close to neutral. The study also revealed an example of a longer lasting forecast impact from LHN (Figure 2), this time at t+15 hours. The situation involved a rainband which formed near the south of the model domain and moved slowly northwards as it developed, so the signal from initial conditions was not swept out of the domain as quickly as with a more rapidly moving system in a westerly flow.

The next development in the rainfall assimilation system, introduced in 1999, was an increase in the frequency of radar data assimilated from 3-hourly to hourly. The benefit of this enhancement was mainly seen in the first 6 hours of the forecast, in situations where the rainfall field was evolving more rapidly. For more details, see Macpherson (2001).

The initial treatment of the error characteristics of radar based surface precipitation rate estimates was very simple. Relative to the model, we assumed the radar data to be of high quality within 100km of the nearest radar and of diminishing quality out to maximum range around 200km. However, more fundamentally, surface precipitation rate estimates are found to be less accurate when the radar beam is above the freezing level. This is primarily due to the difficulty in extrapolating the observed reflectivity above the freezing level to the reflectivity that would be observed at ground level, which in turn is used to determine the precipitation rate at the ground. Therefore, it is desirable to have a quality measure which takes account of radar beam geometry and freezing level height. This has now been developed within the radar analysis step of the Nimrod nowcasting system, as reported by Gibson et al.(2000).

Figure 1: Impact of assimilating radar rainfall data, averaged over 25 cases of widespread rain in July and August 1997. Results give Equitable Threat Score, ETS (%) for mesoscale model forecasts of 3-hour precipitation accumulation up to the forecast time shown. The model is verified against 3-hour accumulations derived from the UK radar network, for thresholds of 0.1, 0.5 and 1.0mm in 3 hours. Solid line is for forecasts including assimilation of radar data, dashed line for forecasts without radar data.

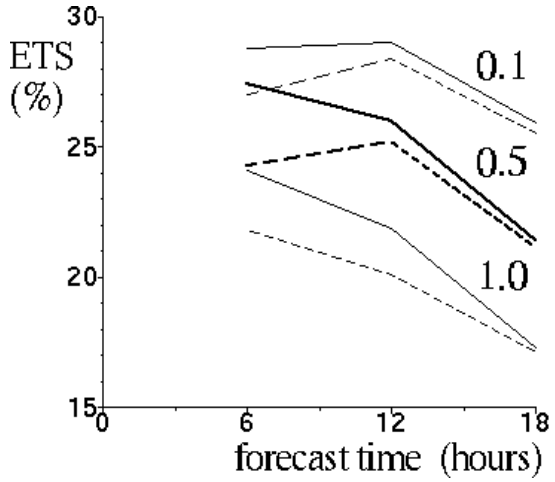

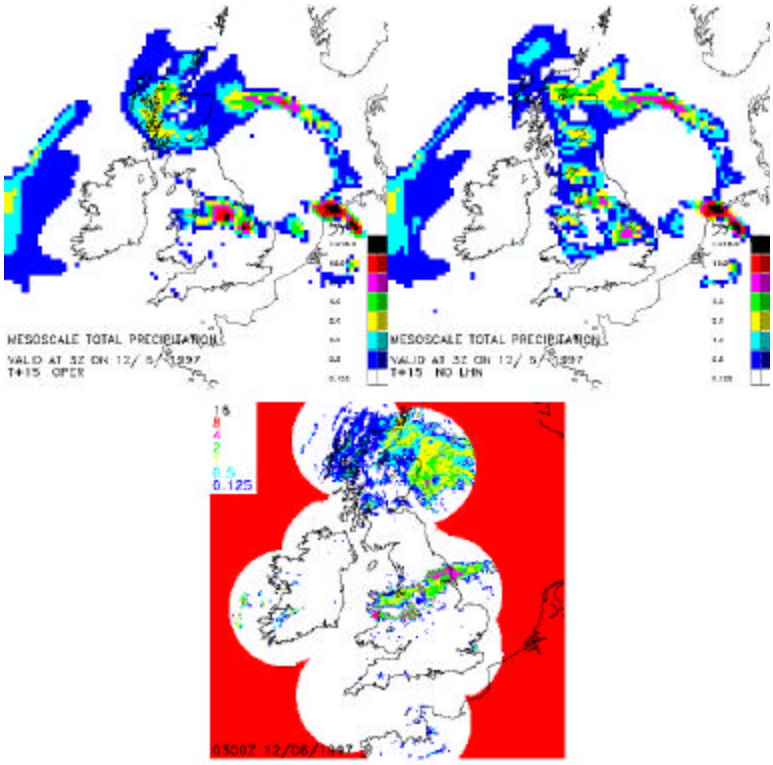

Figure 2: An unusually long lasting forecast impact of radar rain rate assimilation in the Met Office mesoscale model. Bottom frame shows radar picture for 03 UTC on 12th June 1997, with northward moving rainband over central England. Top left frame shows operational precipitation rate forecast at t+15 hours. Top right frame is from a run with NO assimilation of radar data.

Examples of significant impact such as Figure 2 provided encouragement to extend the coverage of radar data, especially to the south. In summer 1998, the model southern boundary was extended to ~44°N and in late 1999 work began on integrating radar data from other European nations into the UK radar composite for mesoscale data assimilation. Early in 2003, the coverage achieved is as shown in Figure 3.

Future plans are to develop a 4-dimensional variational assimilation of rainfall data to replace the latent heat nudging scheme.

3. COST-717 collaboration within Europe

The above work has been stimulated by collaboration within the COST-717 Action entitled: 'Use of Radar Observations in Hydrological and NWP Models' (Rossa, 2000), especially Working Group 3 (Macpherson, 2000) with its focus on assimilation of radar data into NWP models. Other working groups are focused on use in hydrological models, and on applications of radar data to model validation and verification, so aiding parametrization development. The action's web site with reports and documentation is at: www.smhi.se/cost717

Several European nations are now testing precipitation assimilation in high resolution models, and COST-717 is working to help define the quality requirements on radar data for that purpose. It is collaborating with the OPERA group on operational exchange of radar data within Europe, seeking to raise awareness that the NWP community is destined to be a primary customer for quantitative real-time precipitation data from radar networks.

Figure 3: Operational coverage of radar data assimilated by the Met Office mesoscale model in spring 2003.

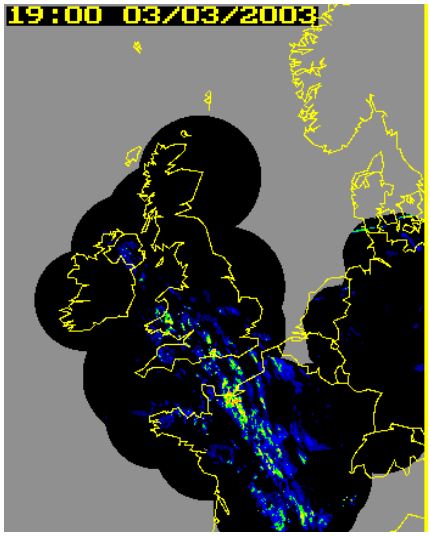

References

Gibson, M., Harrison, D.L., Macpherson, B., 2000: Recent Developments in Assimilation of Radar Data at the Met Office. Physics and Chemistry of the Earth, Part B, **25**, 1229-1231.

Golding, B. W., 1998: Nimrod: A system for generating automated very short range forecasts. Meteorological Applications, **5**, 1-16.

Jones, C. D., Macpherson, B., 1997: A latent heat nudging scheme for the assimilation of precipitation data into an operational mesoscale model. Meteorological Applications, **4**, 269-277.

Macpherson, B., 2000: Radar Data in NWP models, an Outline of COST-717 Working Group 3. Physics and Chemistry of the Earth, Part B, **25**, 1225-1227.

Macpherson, B., 2001: Operational Experience with Assimilation of Rainfall Data in the Met. Office Mesoscale Model. Meteorol. Atmos. Phys, **76**, 3-8.

Macpherson, B., Wright, B. J., Hand, W. H., Maycock, A. J., 1996: The impact of MOPS moisture data in the UK Meteorological Office mesoscale data assimilation system. Mon. Wea. Rev., 122, 341-365.

Rossa, A., 2000: COST-717: Use of Radar Observations in Hydrological and NWP Models. Physics and Chemistry of the Earth, Part B, **25**, 1221-1224.

Estimation of Rainfall and its Error Characteristics from Satellite Observations

Peter Bauer, ECMWF
Jean-François Mahfouf, Meteorological Service of Canada
GEWEX Workshop on Objective Analysis of Precipitation, ECMWF, 11-13 March 2003

Introduction

Currently, rainfall retrieval over ocean from passive microwave satellite observations represents the best compromise between estimation accuracy and spatial data coverage. Infrared data is available with higher temporal frequency from geostationary satellites but the link of top-of-the-atmosphere infrared emission to near-surface rainfall is very indirect. Therefore, all algorithms have to exploit the space-time relation between cloud cover / cloud top height and areal mean rainfall. With TRMM[1] the first spaceborne precipitation radar became available and provides the most detailed information on precipitation vertical structure and quantity over both land and ocean up to date.

The accuracy of precipitation estimates from satellite observations has been the target of numerous intercomparison studies (Ebert and Manton 1998, Smith et al. 1998, Adler et al. 2001) which were initiated to evaluate the large number of algorithms that had emerged with the availability of the operational SSM/I[2] series. As a consequence, permanent and globally coordinated activities have been founded such as the GPCP[3], the TRMM validation field campaigns, and the WMO-IPWG[4].

TRMM has also encouraged several data assimilation efforts (e.g. Marécal and Mahfouf 2002, Hou et al. 2002). In data assimilation, the proper definition of errors associated with the assimilated product is crucial because it determines the weight that is put on the observation in the analysis. Thus recent algorithm development efforts have made the error definition one of their key issues (Kummerow et al. 2001).

This paper presents two approaches for the estimation of rainfall retrieval errors as well as an example of the influence of data with different error characteristics on data assimilation. The latter is particularly important if, for example, data coverage has to be traded-off against data quality which becomes an issue in the preparation of GPM[5]. In this paper, retrieval errors are calculated using the definition of random errors inherent to the retrieval method itself and by the validation of retrieved profiles with independent data. Secondly, the issue of data quality/coverage in data assimilation is illustrated by comparing rainfall retrievals from TMI[6] vs. SSM/I data in an assimilation experiment over one month.

Retrieval algorithm

Methodology

Bayes' formulation of the 'a posteriori' probability, $P(\mathbf{x}|\mathbf{y})$, that state $\mathbf{x}$ occurs and observation $\mathbf{y}$ can be made for non-linear problem is:

$$-2\ln P(\mathbf{x}\mid\mathbf{y}) = \left[\mathbf{y}-\mathbf{F}(\mathbf{x})\right]^T \mathbf{S}_e^{-1}\left[\mathbf{y}-\mathbf{F}(\mathbf{x})\right] + \left[\mathbf{x}-\mathbf{x}_a\right]^T \mathbf{S}_a^{-1}\left[\mathbf{x}-\mathbf{x}_a\right] \quad (1)$$

---

[1] Tropical Rainfall Measuring Mission.

[2] Special Sensor Microwave / Imager.

[3] Global Precipitation Climatology Project.

[4] World Meteorological Organisation - International Precipitation Working Group.

[5] Global Precipitation Mission.

[6] TRMM Microwave Imager.

(e.g. Rodgers 2000). $\mathbf{F}(\mathbf{x})$ denotes the simulated observation with observation operator $\mathbf{F}$ applied to state $\mathbf{x}$, and $\mathbf{S}$ denotes the error covariance matrix of observation/simulation (index 'e') and 'a priori' state (index 'a'). Eq. (1) assumes that some 'a priori' knowledge exists and that the errors have Gaussian distributions. In the presence of clouds and precipitation the probability distribution $P(\mathbf{x}|\mathbf{y})$ is not very well described by a Gaussian distribution and the 'a priori' knowledge is difficult to obtain in a stand-alone algorithm so that the 'expected' value of $E(\mathbf{x})$ may be taken as a solution to the optimum estimate of $\mathbf{x}$ that is the mean state averaged over the probability distribution:

$$E(\mathbf{x}) = \int \ldots \int \mathbf{x} P(\mathbf{x} \mid \mathbf{y}) d\mathbf{x} \tag{2}$$

Using Eq. (1) and assuming that the two terms on the right hand side are uncorrelated:

$$E(\mathbf{x}) = \int \ldots \int \mathbf{x} \exp\left\{-\frac{1}{2}[\mathbf{y}-\mathbf{F}(\mathbf{x})]^T \mathbf{S}_e^{-1}[\mathbf{y}-\mathbf{F}(\mathbf{x})]\right\} P(\mathbf{x}) d\mathbf{x} \tag{3}$$

$P(\mathbf{x})$ is the known distribution of $\mathbf{x}$-$\mathbf{x}_a$. Assuming that a database - say from combined cloud-radiative transfer model simulations - exists that represents sufficiently well the true distribution of $\mathbf{x}$, the integral may be replaced by a summation over all $\mathbf{x}_i$ contained in the database:

$$E(\mathbf{x}) = A^{-1} \sum_i \mathbf{x}_i \exp\left\{-\frac{1}{2}[\mathbf{y}-\mathbf{F}(\mathbf{x}_i)]^T \mathbf{S}_e^{-1}[\mathbf{y}-\mathbf{F}(\mathbf{x}_i)]\right\} \tag{4}$$

with normalization factor:

$$A = \sum_i \exp\left\{-\frac{1}{2}[\mathbf{y}-\mathbf{F}(\mathbf{x}_i)]^T \mathbf{S}_e^{-1}[\mathbf{y}-\mathbf{F}(\mathbf{x}_i)]\right\} \tag{5}$$

This form is used in several algorithms for the retrieval of precipitation from passive microwave observations (e.g. Kummerow et al. 1996, Olson et al. 1996, Bauer et al. 2001).

Error estimation

In a similar way, the retrieval uncertainty can be estimated:

$$E(\mathbf{x}') = E\left\{[\mathbf{x}-E(\mathbf{x})][\mathbf{x}-E(\mathbf{x})]^T\right\} \tag{6}$$

Apart from numerous studies on algorithm validation by independent observations from rain gauges or surface radars, only a few have dealt with the error estimation from error modelling. Physical algorithm development usually involves the combined modelling of clouds, precipitation, and radiative transfer also accounting for effects such as radiometer viewing geometry and varying spatial resolution per channel. Therefore error modelling requires the estimation of individual error sources and their propagation through the entire modelling chain. At present, only this combined error has been analyzed in terms of contributions from signal ambiguity to the total error (Bauer 2001) or the insufficient representation of the natural variability in the retrieval database vs. modelling errors (L'Ecuyer and Stephens 2002).

Both Bauer et al. (2002) and L'Ecuyer and Stephens (2002) have quantified the gross functional dependence of rainfall retrieval errors as a function of rain rate on the basis of Eq. (6) and different datasets for algorithm training and application. Figure 1 shows this dependence for three different algorithms (PATER, BAMPR, 2A12 V5.1) which employ Eq. (4) but use different simulation databases and quality control checks. The solid lines represent the standard deviation between radiometer and precipitation radar (PR) estimates and the comparison suggests that the errors represented by Eq. (6) are quite realistic even though they only cover the random error component.

All algorithms have in common that the relative errors are fairly large at low rain rates (100-200%) because of the increasing noise contribution from surface emission and atmospheric/cloud background emission. In the region of highest sensitivity of microwave window channels with respect to precipitation (~1-20 mm/h), errors decrease to 50% or even less. Depending on whether the algorithm uses higher frequency channels (Figure 1b, c) and the representativeness of the database, relative errors may increase again for larger rain amounts.

Figure 1: Bayesian retrieval errors from as a function of rain rate at product resolution for PATER (a), BAMPR (b), and 2A12 V5.1 (c). Superimposed are lines denoting average differences between PATER and PR (a) and 2A12 V5.1 and PR (c) retrievals, respectively [for algorithm details see Bauer et al. (2002)].

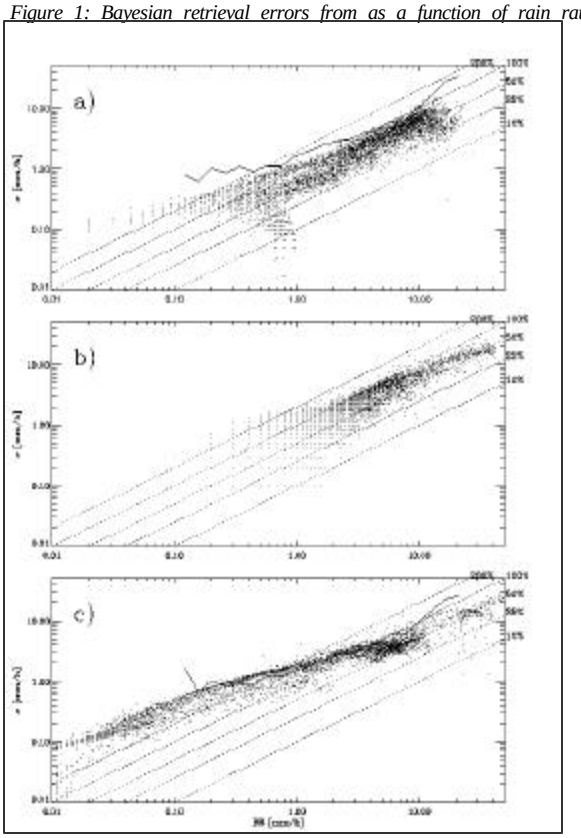

Application example

The retrieval algorithm [Eq. (4)] was implemented to demonstrate the potential of microwave temperature-sounding channels for precipitation profile retrieval. The algorithm uses a database from combined cloud-radiative transfer model simulations of hurricane Bonnie over the Western Carribean Sea. The cyclone was also well observed during the field campaign CAMEX-3[7] on August 26, 1998. The retrieval method was applied to airborne observations with the NAST-M[8] radiometer onboard the ER-2 aircraft. This radiometer has sounding channels in two oxygen absorption complexes near 50-57 GHz and 118.75 GHz (Blackwell et al. 2001). The channels in both bands are collocated in such a way that for a channel near 50 GHz there is a channel near 118 GHz with a similar clear-sky weighting function. Clouds and precipitation can be sensed by their differential absorption and scattering features in both bands. Once precipitation profiles are retrieved, radar reflectivities can be simulated and compared to EDOP[9] observations from the same aircraft. Therefore the retrieval accuracy can be estimated from the theoretical retrieval error given by Eq. (6) and by a comparison with radar reflectivities (Bauer and Mugnai 2003). The latter also leads to an estimate of systematic errors.

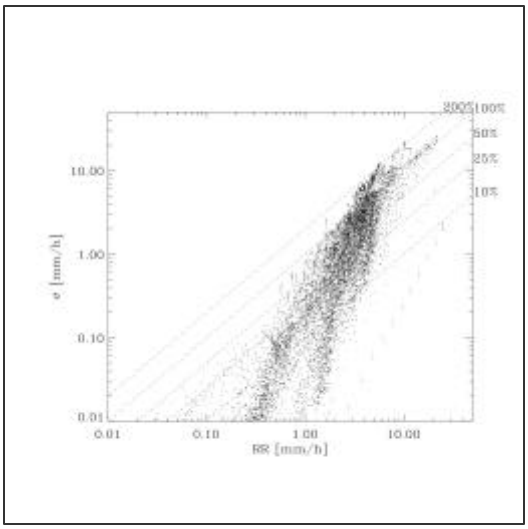

Several overpasses over hurricane Bonnie were carried out by the NASA ER-2 aircraft on August 26. The payload of the ER-2 aircraft also contained the ER-2 Doppler (EDOP) radar (Heymsfield et al. 1996). The EDOP radar is a two-antenna 9.6 GHz Doppler radar with one antenna pointing in nadir direction and the other pointing forward. In this study only the reflectivities from the nadir beam are used for validating the retrievals from NAST-M nadir observations.

Figure 2: Retrieval errors as a function of rain rates from aircraft data (> 200 000 data points).

A graph similar to Figure 1 was produced from the aircraft retrievals (Figure 2). While for rain rates > 5 mm/h, the errors match those from the satellite retrievals fairly well, the errors are much smaller below 5 mm/h. A possible explanation is the difference of spatial resolutions. This is because the aircraft data resolves details at 2 km scales while the satellite retrievals suffer

[7] Convection and Moisture Experiment.

[8] National Polar-Orbiting Operational Environmental Satellite System (NPOESS) Aircraft Sounder Testbed-Microwave (NAST-M).

[9] ER-2 Doppler radar

from beam-filling errors that is the mismatch between spatially averaged high-resolution retrievals and retrievals from spatially averaged observations.

The retrieved profiles are converted to synthetic radar reflectivity profiles to be compared to the observed profiles. The advantage of this approach over the comparison of rain rates is that the utilization of a radar retrieval algorithm with different assumptions on particle size distributions and optical properties is avoided. The comparison of reflectivities employs the same radiative transfer model that was used for the generation of the retrieval database. Therefore, attenuated reflectivities at any given frequency can easily be calculated and compared to the observations. The microwave retrievals were carried out for 2, 8, and 16 channels (at 50-57 and at 118 GHz) to test the contribution of channel combinations to retrieval accuracy, respectively.

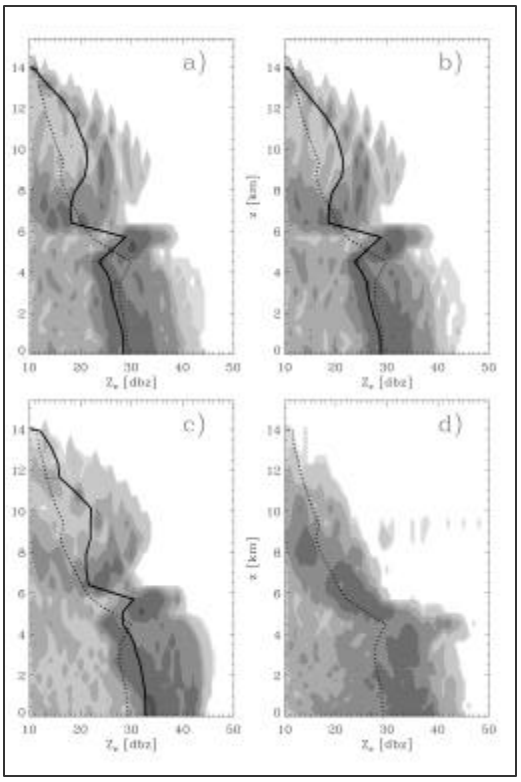

The reflectivity statistics over all 929 profiles are summarized in Figure 3. The shading indicates the histograms of reflectivities vs. altitude and the solid lines represent the average profiles to be compared to the averaged observations given by the dashed line. The main observations are that both 16-channel and 8-channel retrievals work well and produce almost identical results. In the rain layer, average reflectivities agree within 1 dBZ (15-20% of rainrate).

Figure 3: Modelled EDOP reflectivity from NAST-M retrievals using 16 channels (a), 8 channels (b), 2 channels (c) as well as observed reflectivities (d).

Near the freezing level, differences occur for two reasons: (1) the observed freezing level height is near 5-5.5 km and the maximum of the bright band is at 4.5 km. The retrievals show a little more intense peak and a higher frequency of occurrence as well as a freezing level at 6.5 km.

This difference in altitude is explained by a temperature bias that was identified comparing (1) the temperature profiles from the database with those from the ECMWF analysis on 26/08/1998 at 12 UTC; (2) the clear-sky TB's between observations and simulations. Even though the biases in TB's may be corrected, the database still contains biased temperature profiles. Another observation is that the simulated reflectivities above freezing level are considerably higher (up to 5 dBZ) than the observed ones. This can only be explained by rather large differences between simulated and observed snow/graupel contents. In any case, the retrieval of rain profiles is not drastically affected by this problem.

Data assimilation of satellite derived rain rates

Rain rate retrievals from the microwave radiometers SSM/I and TMI have been calculated at pixel resolution and calibrated with data from the precipitation radar (PR) for TMI and SSM/I (Bauer et al. 2001). Each rain rate R_i (actually a rain liquid water content) is provided along with its error estimate. Averaged rain rates have been obtained by binning each observation within model grid boxes to avoid a spatial interpolation of temperature and humidity profiles at observation locations (Marécal and Mahfouf 2000). The estimation of averaged rain rate errors needs depends on their spatial correlation within each model grid box. The standard deviation of the mean rain rate is defined by:

$$\sigma_{\overline{R}} = \frac{1}{N}\left[\sum_{i=1}^{N} C_{ij}\sigma_i\sigma_j\right]^{1/2} \qquad (7)$$

where C_{ij} is the spatial correlation of errors between two points i and j separated by a distance d_{ij}. Therefore, before computing rain rate averages and their associated errors, it is first necessary to use a sample of the raw satellite retrievals in order to compute C_{ij}.

On a model grid having a resolution of about 120 km, all pairs of rainy points within each model grid box where collected together with their associated errors. The use of a coarser grid than the actual model grid allows the computation of correlations over distances up to 120 km. The resolution of the TMI product is about 15 km with a sampling at ~10 km. Distances have been binned into 5 km intervals for TMI to compute spatial correlations. For SSM/I this distance is reduced to 25 km because this satellite has a coarser sampling. The polynomial fit used in Bauer et al. (2002) has been kept (with different coefficients):

$$C(r) = \sum_{k=0}^{2} a_k r^k \tag{7}$$

The curves C (r) are plotted in Figure 4 for TMI and SSM/I. The spatial correlations are very consistent between the two retrievals, since both TMI and SSM/I retrievals were calibrated with PR data. For a given 6-hour period (26 May 2002: 0300-0900 UTC) the TMI and SSM/I rain rates are plotted with their associated errors both at the pixel resolution (15 km for TMI and 25 km for SSM/I) and averaged to the model resolution (Figure 5).

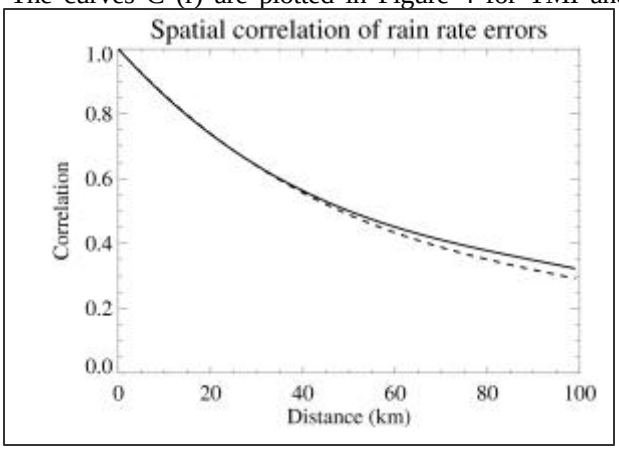

Figure 4: Spatial correlation of TMI (solid line) and SSM/I (dashed line) rainfall rate retrieval errors.

At pixel resolution, important differences are noticed between the products. First, the lack of the 10 GHz channel and also the larger pixels reduce the SSM/I rain rate intensities to maximum values around 15 mm/h. On the contrary, the TMI product shows significant amounts of rain rates above 10 mm/h. The averaging procedure reduces error by 20-50%.

Ambiguities in the retrieval database are illustrated by the fact that some rain rate values can be retrieved with a wide range of different accuracies. For SSM/I rain rates, the larger footprint reduces the differences between the scatter plots at pixel and model resolution. Rain rate errors are usually larger than with TMI and there is a non-negligible amount of very low rain rates (<0.01 mm/h) that may come from the different rejection criteria between the two products. However, it is unlikely that such small amounts could have a significant impact when assimilated due to the very large corresponding errors at model scale (>1000%). It is interesting to note that in the range 0.1 to 5 mm/h (peak of the model pdf) the errors between the two products are quite similar.

A series of three 4D-Var assimilation experiments starting on the 01 May 2001 over one month where performed using the ECMWF forecasting system. An ensemble of 10-day forecasts was also run from the 1200 UTC analyses. The assimilation system is an incremental 4D-Var where the minimisation in performed at a lower model resolution (horizontal grid about 120 km) and the assimilation window is 12 hours.

First, simplified 1D-Var assimilations of rain rates are performed every 6 hours using observations 3 hours before and after the analysis time to produce total column water vapour (TCWV) retrievals. Then these two batches of TCWV retrievals in rainy areas are introduced in 4D-Var as new observations. The first assimilation is a 'control' using the operational configuration of the forecasting system at the time, the second assimilation includes TMI PATER rain rates on top of all data from the control, while the third experiment is similar to TMI PATER but assimilates rain rates from SSM/I instead (two satellites are used: DMSP F-13 and F-14).

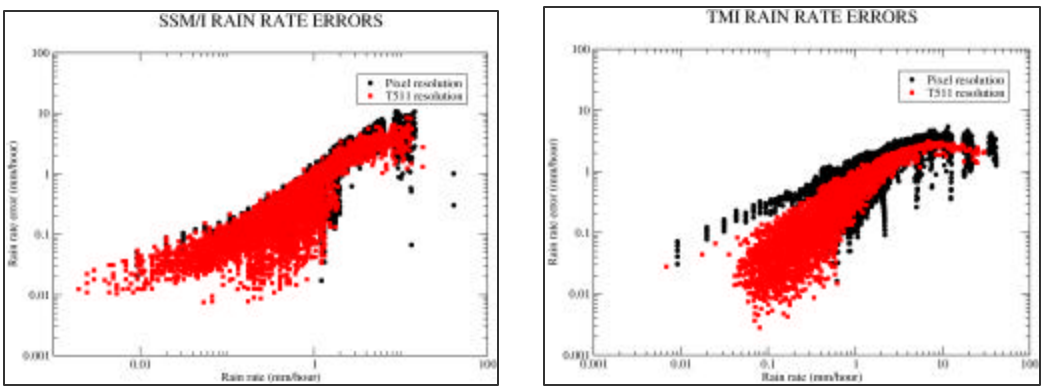

Figure 5: Errors as a function of rain rate at pixel resolution and model resolution (~40 km) for SSM/I products (left panel) and TMI products (right panel).

Time series of day-3 and day-5 forecasts for a 3-week period over the Northern American continent were examined for the geopotential at 500 hpa. For three forecasts starting on the 17, 18 and 19 May the root mean square errors (rmse) at day-5 are larger than 100m. The impact of TMI data is to improve significantly the forecast starting on 2002/05/18 (rmse around 60m) and also to have a positive (but weaker) impact on the two other poor forecasts. The impact in the medium range is also present at shorter ranges (over this period there is an almost systematic improvement at 72 h). The impact of SSM/I data is even more spectacular since the three poor forecasts are all improved with rmse's reduced by more than a factor of two.

To the question: Is it better to have a small number of accurate rain rate observations (i.e. from TMI) than to have more observations but with a reduced accuracy (i.e. from SSM/I)? The answer from the above example is that it seems more beneficial to increase the number of observations because: (1) The accuracy of SSM/I and TMI are similar in the range of 0.1 mm/h to 5 mm/h corresponding to the maximum of the rainfall distribution. (2) Rather accurate TMI high intensity rain rates (by using the 10 GHz channel) are probably not assimilated efficiently because the model physics at 40 km resolution can hardly produce instantaneous rain rates above 10 mm/h (therefore quality control will tend to reject such observations).

Conclusions

From the experience of ~20 years of rainfall retrieval algorithm development, the 'physical' approach that is the Bayesian retrieval methodology applied to pre-defined databases from combined cloud-radiative transfer modelling emerged as the most versatile technique. This is because it provides the largest detail on the microphysical precipitation structure and because it allows the calculation of theoretical retrieval errors. Comparing the errors obtained from different algorithms very similar features can be observed; however, there may be large differences comparing retrievals from spaceborne and airborne data due to beam-filling issues. In any case, systematic errors seem to be comparably small compared to random errors - this is a conclusion from the analysis of both airborne and spaceborne data.

Once rainfall observations are assimilated, the spatial error correlation has to be taken into account because the observations must be averaged to represent the spatial model resolution. Rainfall rate assimilation experiments with the ECMWF modelling system have shown that apart from the positive impact of the data on analyses and forecasts, the accuracy of the observations has to be traded off against the data coverage. Depending on the case, better coverage may compensate reduced accuracy. This will be an important research issue for future assimilation studies as well as algorithm design.

References

Adler, R.F., C. Kidd, G. Petty, M. Morrissey, and H.M. Goodman, 2001: Intercomparison of global precipitation products: The third Precipitation Intercomparison Project (PIP-3). *Bull. Amer. Met. Soc*., **82**, 1377-1396.

Bauer, P., 2001: Over-ocean rainfall retrieval from multi-sensor data of the Tropical Rainfall Measuring Mission (TRMM). Part I: Design and evaluation of inversion databases. *J. Atmos. Oceanic Technol.*, **18**, 1315-1330.

Bauer, P., P. Amayenc, C.D. Kummerow, and E.A. Smith, 2001: Over-ocean rainfall retrieval from multisensor data of the Tropical Rainfall Measuring Mission. Part II: Algorithm implementation. *J. Atmos. Oceanic Technol.*, **18**, 315-330.

Bauer, P., J.-F. Mahfouf, W.S. Olson, F.S. Marzano, S. Di Michele, A. Tassa, and A. Mugnai, 2002: Error analysis of TMI rainfall estimates over ocean for variational data assimilation. *Quart. J. Roy. Meteor. Soc.*, **128**, 2129-2144

Bauer, P. and A. Mugnai, 2003: Precipitation profile retrievals using temperature-sounding microwave observations. *J. Geophys. Res.*, submitted.

Blackwell, W.J., J.W. Barrett, F.W. Chen, R.V. Leslie, P.W. Rosenkranz, M.J. Schwartz, and D.H. Staelin, 2001: NPOESS Aircraft Sounder Testbed-Microwave (NAST-M): Instrument description and initial flight results. *IEEE Trans. Geosci. Remote Sens.*, **39**, 2444-2453.

Ebert, E. and M. Manton, 1998: Performance of satellite rainfall estimation algorithms during TOGA-COARE. *J. Atmos. Sci.*, **55**, 1537-1557.

Heymsfield, G.M., S. Bidwell, I.J. Caylor, S. Ameen, S. Nicholson, W. Boncyk, L. Miller, D. Vandemark, P.E. Racette, and L.R. Dod, 1996: The EDOP radar system on the high altitude NASA ER-2 aircraft. *J. Atmos. Oceanic Tech.*, **13**, 795-809.

Hou, A.Y., S. Zhang, and O. Reale, 2002: Variational continuous assimilation of TMI and SSM/I rain rates: Impact on GEOS-3 hurricane analyses and forecasts. *Mon. Wea. Rev*., submitted.

Kummerow, C.D., W.S. Olson, and L. Giglio, 1996: A simplified scheme for obtaining precipitation and vertical hydrometeor profiles from passive microwave sensors. *IEEE Trans. Geosci. Remote Sens.*, **34**, 1213-1232.

Kummerow, C.D., Y. Hong, W.S. Olson, S. Yang, R.F. Adler, J. McCollum, R.R. Ferraro, G.W. Petty, D.-B. Shin, and T.T. Wilheit, 2001: The evolution of the Goddard Profiling Algorithm (GPROF) for rainfall estimation from passive microwave sensors. *J. Appl. Meteor.*, **40**, 1801-1820.

L'Ecuyer, Y.S. and G.L. Stephens, 2002: An uncertainty model for Bayesian Monte-Carlo retrieval algorithms: Application to the TRMM observing system. *Q. J. R. Meteor. Soc*., **128**, 1713-1737.

Marécal V. and J.-F. Mahfouf, 2000: Variational retrieval of temperature and humidity profiles from TRMM precipitation data. *Mon. Wea. Rev*., **128**, 3853-3866

Marécal V. and J.-F. Mahfouf, 2002: Four-dimensional variational assimilation of total column water vapour in rainy areas. *Mon. Wea. Rev*, **130**, 43-58

Olson, W., C.D. Kummerow, G. Heymsfield, and L. Giglio, 1996: A method for combined passive-active microwave retrievals of cloud and precipitation profiles. *J. Appl. Meteor.*, **35**, 1763-1789.

Rodgers, C.D., 2000: Inverse methods for atmospheric sounding, Theory and Practice. Series on Atmospheric, Oceanic and Planetary Physics, Vol. 2. World Scientific, Singapore, New Jersey, London, Hong Kong, 238 pp.

Smith, E. and co-authors, 1998: Results of WetNet PIP-2 project. *J. Atmos. Sci.*, **55**, 1483-1536.

PRECIPITATION ASSIMILATION TO JMA MESOSCALE MODEL USING A FOUR-DIMENSIONAL VARIATIONAL METHOD

Ko KOIZUMI (JMA/NPD), Yoshihiro ISHIKAWA (NSSL),
Tadashi TSUYUKI, Shigenori MURAKAMI (JMA/MRI), Yoshiaki SATO(JMA/MSC)

1. INTRODUCTION

In March 2001 the Japan Meteorological Agency (JMA) started the operation of the mesoscale model (MSM) to produce 18 hour forecasts four times a day (00, 06, 12 and 18 UTC initial) to assist forecasters in issuing warnings (JMA, 2002). MSM is a hydrostatic spectral model with a horizontal resolution of 10 km and 40 vertical levels up to 10 hPa.

The initial condition of MSM was at first prepared by a 1-hour cycle analysis system with optimum interpolation and physical initialization to assimilate 1-hour accumulated precipitation data. This analysis system was executed for the 3-hour period just before the initial time with the first guess at the beginning of the period taken from the latest forecast of RSM. This analysis system is hereafter referred to as the pre-run system. The pre-run system was successfully replaced in March 2002 by a full forecast-analysis cycle with a 4-dimentional variational (4D-Var) method with 3-hour assimilation windows.

This paper describes the precipitation data assimilation to MSM by the mesoscale 4D-Var system and reports on the impacts of precipitation assimilation on the MSM precipitation forecasts.

2. PRECIPITATION NOWCASTING IN JMA

JMA has 20 operational C-band radars and about 1,300 automatic surface weather stations called AMeDAS. Using those observations, a precipitation nowcasting product is made as follows.

First, radar echo intensity is converted to precipitation rate using the relationship $Z = 200R^{1.6}$. Then, the estimated precipitation rate is averaged over eight observations during one hour to produce an estimate of one-hour precipitation amount. Finally, the estimated amounts are calibrated using rain gauges to provide one-hour precipitation amount distribution all over Japan and surrounding are with 2.5 km resolution (cf. Makihara, 2000).

This nowcasting product is called "radar-AMeDAS precipitation analysis" which is up-scaled to model grids and assimilated to MSM.

3. MESOSCALE 4D-VAR SYSTEM

The cost function of mesoscale 4D-Var system consists of a background term, observation terms, and a penalty term for reducing gravity wave noise. The control variables are the initial and boundary conditions of unbalanced wind, temperature, surface pressure, and specific humidity. The background error statistics are obtained by using the NMC method. The horizontal background error correlations are assumed to be homogeneous and Gaussian type to significantly reduce memory requirement.

An incremental method is taken for reducing computational time. The forward model in this system has the same architecture as the forecast model (viz. MSM) except that its horizontal resolution is reduced to 20km. The adjoint model has the same dynamical process as the forward model while its physical processes include moist processes, boundary layer processes, long-wave radiation and horizontal diffusion only.

Assimilated data are radiosonde, synop, ship, buoy, aircraft, wind-profiler and radar-AMeDAS precipitation data.

It is to be noted that most of precipitation in MSM comes from the grid-scale condensation although MSM contains a prognostic Arakawa-Schubert scheme to parameterize deep cumulus convection. Therefore, the absence of deep cumulus convection in the adjoint model may not cause a serious problem in the 4D-Var system.

4. OBSERVATIONAL COST FOR PRECIPITATION

Since the precipitation amount has quite different error probability distribution from other elements such as temperature or wind speed, the Gaussian type cost-function is not appropriate for precipitation. Fig.1(b) shows scatter diagram of first-guess values of precipitation and departures of observation from first-guess. It is not symmetrically distributed around zero departure as in the case of temperature at 500hPa (Fig.1 (a)).

Then we assume probability density distribution of precipitation as the exponential distribution which is suggested from Fig. 1(b).

According to the maximum likelihood method the cost function of precipitation becomes

$$J_{rain} = -\log(\ p(y \mid x)) = \log(\ x) + \frac{y}{x} \qquad (2)$$

However, this formulation is not appropriate to be used in minimization algorithms as it becomes singular around x=0. Moreover, it is more preferable that the cost function has a quadratic form for the stability of optimizing process. Therefore, the above function is expanded around its minimum point (x=y)

$$J_{rain} = 1 + \log(\ y) + \frac{1}{2y^2}(x-y)^2 + O((x-y)^3) \qquad (3)$$

If truncated at the second order of (x-y), the function becomes Gaussian type with the observation error equal to y.

On the other hand, the function (2) is not symmetric around its minimum point (fig. 2) which means that the observation error is assumed smaller in the case of x<y than in the case of x>y. This asymmetricity is seen from Fig. 1(b).

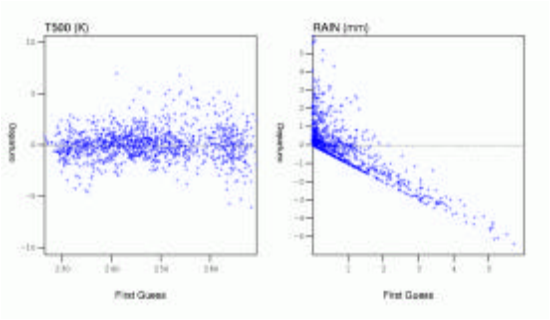

Fig. 1 scatter diagram of first-guess value and departure of observation from first-guess. (a) temperature at 500hPa, (b) one-hour precipitation amount.

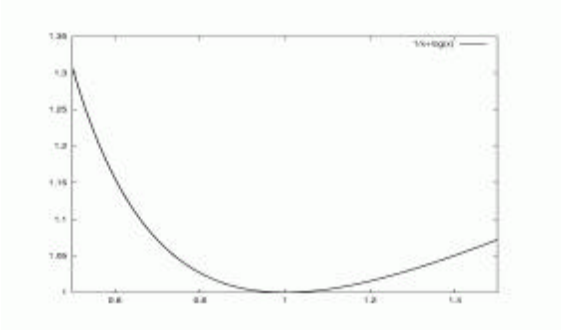

Fig. 2 Function (2) around its minimum point in the case of y=1

Considering these properties, we practically define the cost function as follows:

$$J_{rain}(x) = \frac{1}{2r^2}(x-y)^2, \qquad (4)$$

where

$$r = \begin{pmatrix} r_1 & (x \le y) \\ r_2 = 3r_1 & (x > y) \end{pmatrix}.$$

When y<1mm/h, r1 has a constant value which is the forecast error of precipitation for observed precipitation less than 1mm/h. Otherwise r1 is proportional to observed precipitation amount.

5. ASSIMILATION TEST

Figure 3 shows an example of precipitation assimilation. By assimilating one hour precipitation amounts during three hour assimilation window, precipitation distribution is well reproduced. The forecast starting from the initial condition to which precipitation data were assimilated also shows good agreement with observation (fig. 4).

6. IMPACTS ON FORECASTS

In order to evaluate the performance of 4D-Var and the impact of precipitation assimilation, several analysis-forecast cycle experiments were performed.

First, two sets of one-month experiments during June and September 2001 were made to compare the 4D-Var and pre-run systems. The result shows that the precipitation forecasts starting from 4D-Var are much better than those from the pre-run (figures not shown).

Second, an observation system experiment (OSE) for precipitation data was performed for June 2001 using the 4D-Var system. Threat scores (fig.5 left) show that the precipitation forecasts were improved by assimilating precipitation data especially for first few hours and bias scores (fig. 5 right) show that the spin-up problem of MSM is alleviated by precipitation assimilation.

However, the 4D-Var system sometimes failed to assimilate the precipitation data when the first guess was in a dry condition in spite of the fact that the full-physics nonlinear model is used as the inner-loop forward model. This is an inherent problem with 4D-Var assimilation of precipitation data using model physics that contain "on-off" switches. That problem may be ameliorated by assimilating moisture data.

Then the third experiment is an OSE for TMI (TRMM Microwave Imager) precipitable water data and combined use of TMI-PW and precipitable water data from ground-based GPS observation.

Figure 6 shows an example of first three hour forecasts. A spurious heavy rain area ("A" in fig. 6) produced by precipitation assimilation was reduced by using TMI-PW data though it was a little bit too much suppressed ("B"). Complemental use of TMI-PW (moisture information over sea) and GPS-PW (moisture information over land) gave the best result among them. Threat scores of 1mm per 3 hour precipitation (fig. 7) show that the combined use of TMI and GPS improves the precipitation forecasts all through the 18-hour forecast time.

7. CONCLUDING REMARKS

Precipitation forecasts of JMA mesoscale model are improved by assimilating precipitation data especially for first few hours of forecast time, that means that the NWP precipitation of first few hours may become more reliable by assimilating precipitation data. However, the 4D-Var is not always successful in assimilating precipitation as stated in the previous section, hence the assimilation of moisture data from GPS, satellite microwave observation and others is indispensable.

A negative aspect of the NWP precipitation is that it has considerable errors even for short forecast time and its probability density distribution is sometimes different from the nature (see fig. 1). Whether spatial or temporal averaging can alleviate the problem requires further investigation.

REFERENCES

JMA, 2002: *Outline of the Operational Numerical Weather Prediction at the Japan Meteorological Agency*, 158pp. Available from the Japan Meteorological Agency.

Makihara, Y., 2000: Algorithms for precipitation nowcasting focused on detailed analysis using radar and raingauge data. *Technical Reports of the Meteorological Research Institute* **39**, pp63-111.

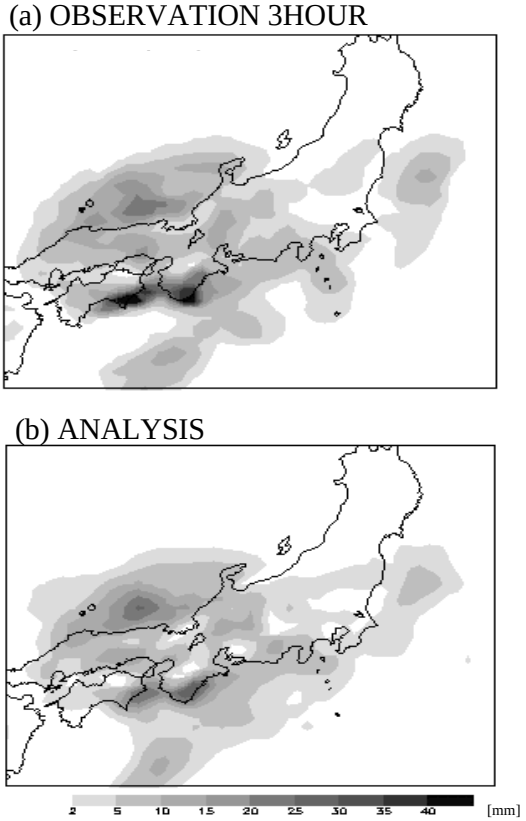

Fig.3 The 3-h precipitation accumulated over the assimilation window for (a)observation and (d)4D-Var analysis. The target analysis time is 00UTC 16 March 2000. The operational forecast with JMA regional spectral model from initial condition of 12UTC 15 March 2000 is used as the first guess.

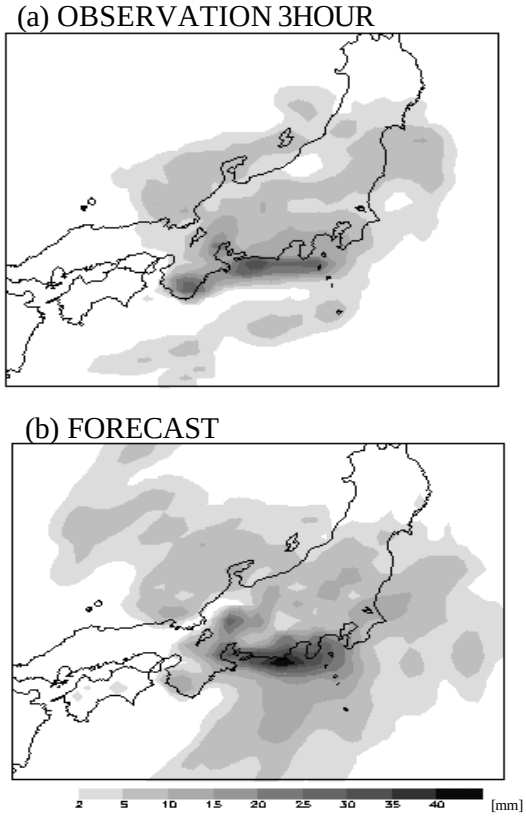

Fig.4 The 3-hour precipitation accumulated over 0-3hours for (a)observation and (d) forecast starting from the initial condition produced by precipitation assimilating 4D-Var.

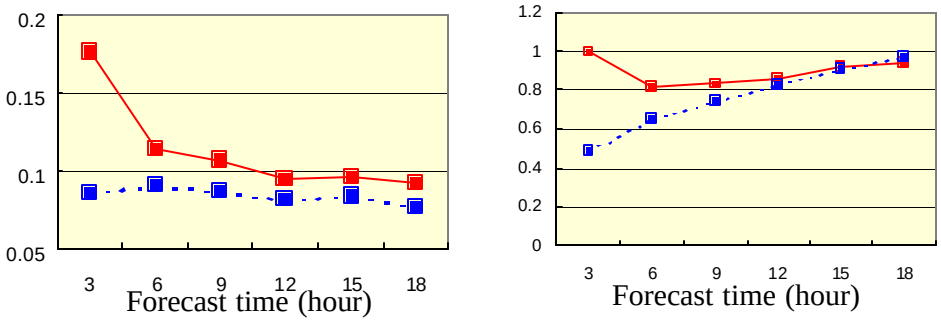

Fig. 5 Threat score (left) and bias score (right) of 3-hour accumulated precipitation over Japan plotted against forecast time for one month period of June 2001. Threshold value is 10 mm with a horizontal resolution of 10 km. Solid and dashed lines are with and without assimilating the precipitation data, respectively.

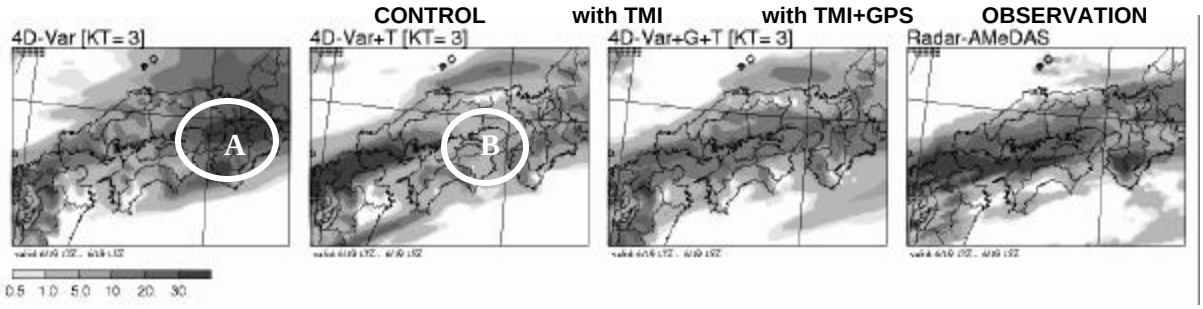

Fig.6 Three hour precipitation amount during 12 – 15 UTC 19th June 2001 of control run, TMI run, TMI+GPS run and observation from left to right respectively. Initial time of forecasts is 12 UTC 19th June 2001.

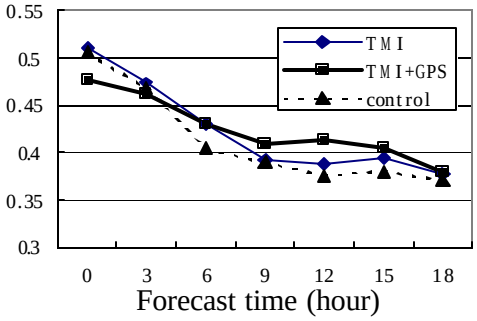

Fig. 7 Threat scores of forecast precipitation over 1 mm/3 hour. Forecast time is –3-0 (within assimilation window), 0-3, 3-6, 6-9, 9-12, 12-15 and 15-18 hour from left to right respectively. Solid bold line shows those of TMI+GPS run, solid thin line TMI run and dashed line control run. Scores are calculated for 15 cases during 18 UTC 18th June 2001 to 12 UTC 21st June 2001 against radar-AMeDAS precipitation analysis data which are interpolated to model grid.

The precipitation in ERA-40

GEWEX_GPCP Workshop on Precipitation Analysis
ECMWF March 11-13 2003

Per Kållberg, ECMWF

6 The ECMWF ERA-40 data assimilation system

The production phase of the second ECMWF reanalysis project, ERA-40, is just about to be finalized. ERA-40 is a project under the European Union Framework 5 programme, with further support from WCRP, Fujitsu Ltd. and ECMWF Member States, and it covers the period from August 1957 to March 2002. The basic idea of a reanalysis is to produce a consistent set of multi-annual global analyses with a frozen data-assimilation system as suggested by e.g. Bengtsson & Shukla in 1988. However, during the 45 ERA-40 years there have been many major changes in the global observing system; old observations may have been lost, there have been (political and budgetary) reductions in the amount of conventional observations ('weather ships'), new technologies have improved the accuracy of measurements, and above all, there are many new space-based observing systems. It is therefore unavoidable that there will still be interannual variations in the reanalyses from other reasons than real changes in the atmosphere's circulation.

The data assimilation system for ERA-40 is essentially the same as that used for operational forecasting at ECMWF in recent years, although with a lower horizontal resolution and a 3-dimensional (rather than the operational 4-dimensional) variational analysis. Ground- and air-based observations for the project were assembled from many sources, primarily NCAR/NCEP, COADS, US-Navy, JMA and the GTS. Space-based observations were also assembled from many sources, NASA, NOAA/NESDIS, Eumetsat, Wentz, ESA, LMD and the GTS.

The main characteristics of the ERA-40 data assimilation system are:

The ECMWF IFS (Integrated Forecasting System version Cy23r4) has a spectral resolution of TL159 - and a corresponding 'reduced' Gaussian grid of ~125*125km. There are 60 vertical hybrid levels with the top level at 0.1hPa (~64km) and with a high vertical resolution in the boundary layer. The 3-dimensional variational analysis is made intermittently every 6th hour, with the observations used at their appropriate time (within the hour). Satellite radiances - from the HIRS, MSU, SSU, SSM/I and VTPR instruments on the NOAA and DMSP spacecraft - are assimilated directly using a radiative transfer model (RTTOV). There is also an analysis of ozone from the satellite TOMS and SBUV data, and a wave height analysis based on altimeter data from ERS-1 & 2. Sea surface temperatures and sea ice limits come from the UKMO Hadley Centre monthly HadISST1 1957-1981 and from the NCEP weekly 2-D variational analyses 1982-2001. These, together with the IPCC trends for CO_2, are the external forcings of the reanalyses.

There is no analysis of precipitation in ERA-40. The model's diagnostic precipitation is produced and released by parameterized microphysical processes in clouds. Clouds are formed at supersaturation by two processes, convective and 'large-scale'.

In addition to the 6-hourly forecasts used for the data assimilation, 36-hour forecasts were run twice daily, from 00UTC and 12UTC. Accumulated precipitation is extracted from these short-range forecasts and averaged into monthly/daily means, at +6 hours and from the +12h to +24h accumulation.

The ERA-40 data assimilation system is described in the web documents for ERA-40 (http://www.ecmwf.int/research/era/DA-system/index.html)

7 Comparison with GPCP

Version 2 of the Global Precipitation Climatology Project monthly mean precipitation (http://precip.gsfc.nasa.gov/gpcp_v2_comb.html) estimates were downloaded and compared with ERA-40 for the 23-year period 1979-2001. The original ERA-40 Gaussian grid forecasts were interpolated (bi-linearly) to the 2.5°* 2.5° grid used for GPCP. Zonal means, separately for land and ocean areas, averaged over 23 years are seen in figure 1. The ERA-40 monthly mean precipitation is summed from the twice daily +12h to +24h forecasts (full red) in order to avoid the spin-down/spin-up in the 6-hour forecasts (dotted blue). At middle and high latitudes ERA-40 generally agrees very well with GPCP (black). The large differences at high southern latitude land areas are explained by the limitations of GPCP in steep orography (the Andes).

In the tropics, on the other hand, the ERA -40 precipitation is very large, peaking at 9.5 mm/day in the oceanic ITCZ compared with 6 mm/day in GPCP. That the reanalysis precipitation is 'excessive' is seen in the global hydrological balance, P-E (precipitation minus evaporation) extracted from the 24h forecasts. In the latter years, 1989-2001, when there was a dense coverage of humidity observations in the tropics, it rains more than it evaporates also over the sea. This is obviously unrealistic. In the early years when humidity observations in the tropics were very sparse or absent, P-E is in excellent balance.

+12h -> +24h	1958-1970	1989-2001
Land	+0.72	+0.86
Ocean	-0.25	+0.31
Globe	+0.03	+0.47

Table 1: Global hydrological balance (Precipitation - Evaporation in mm/day) in the +12h to +24h forecast range. 13 year averages from pre-satellite and satellite years.

Figure 1. Zonally averaged monthly mean precipitation, averaged from January 1979 to December 2001, separately for ocean (below) and land (above) areas. The full red line is the ERA-40 +12h to +24h accumulation, the dotted blue line the 00h to +06h accumulations and the black is GPCP.

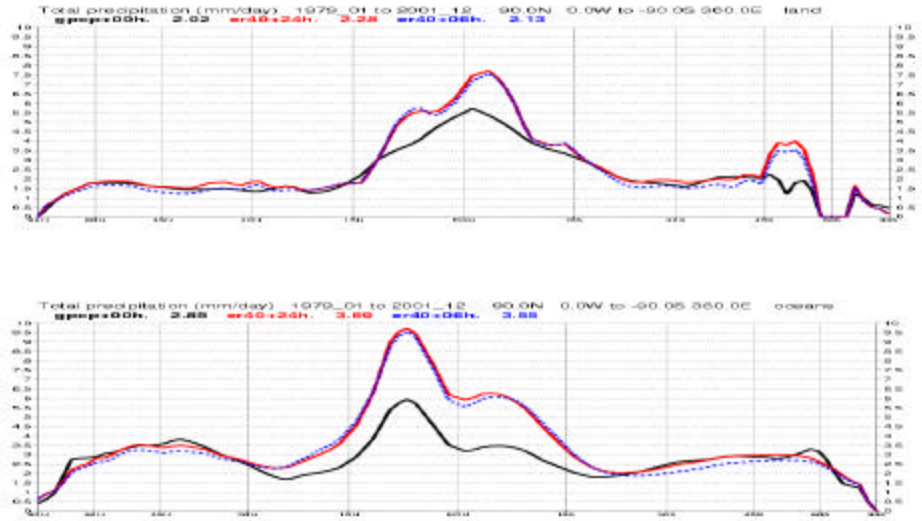

Month-by-month comparisons between ERA-40 and GPCP can be displayed as scatterograms. In the Asian monsoon land regions for instance, (not shown here), ERA-40 does indeed rain more than the GPCP estimate, but there is a quite high correlation (0.97) between them, indicating that the reanalysis describes the monsoon variability qualitatively well, if not quantitatively (the bias is +0.66mm/day). At higher latitude land areas in regions well covered by gauges, the agreement between the reanalysis and GPCP is quite good, e.g. over North America or the British Isles (figure 2).

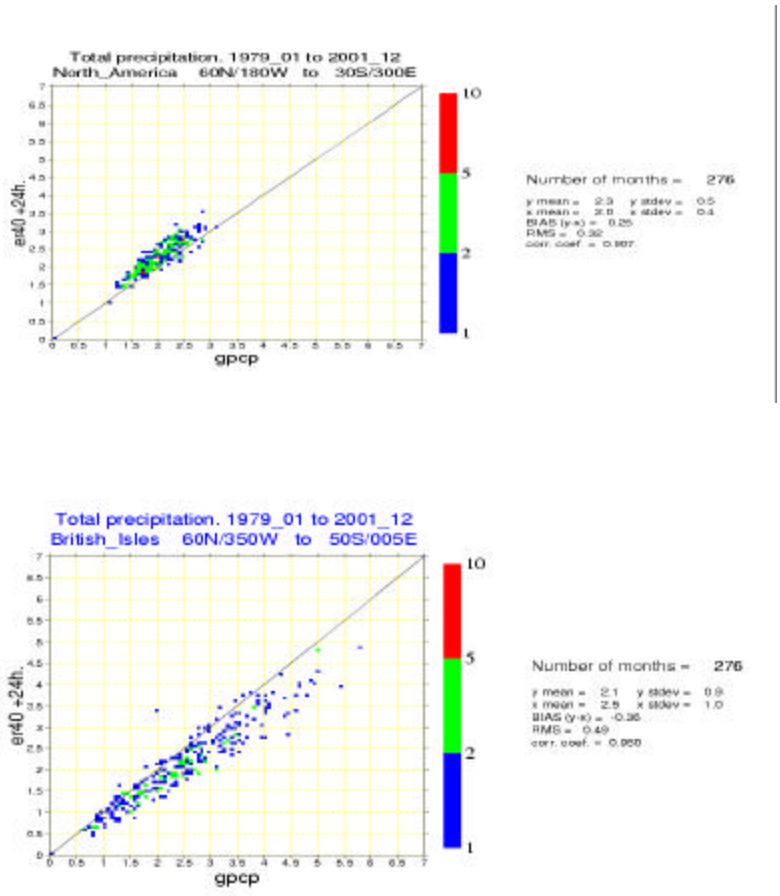

Figure 2. Scatterogram of 23 years of monthly mean precipitation estimates in land points in northern America (above) and the British Isles (below)

There have been several attempts to explain the unrealistically large precipitation in the tropics, particularly over the oceans. Among them volcanic aerosols ('Pinatubo' in 1991), ENSOs, biases in the SSMI data, uncertainties with bias corrections for the TOVS radiances (IR or □-wave) or even aliasing in the geographical distribution of used radiances. None of these have been found to be the root cause

Very recent developments at ECMWF are however now providing a plausible explanation (H^lm, pers. comm.). The control variable for humidity in the variational analysis is the specific humidity, q. With the assumption of Gaussian background error covariances, observations of high specific humidity near saturation can generate widespread saturation, leaving it for the forecast model to take care of the adjustment in the ensuing 6-hour forecast.

This suggestion is strongly supported by figure 3, which shows the spinup/spindown of the two precipitation components, convective and stratiform over the oceans. The global convective precipitation spins down from 1.77 mm/day during the initial +6h forecasts to 1.68 mm/day in the 12h to 24h interval. The spindown in the convection happens almost entirely in the ITCZ. Spindown of the tropical ocean convection has also been noted in the operational 4D-Var analyses. The stratiform precipitation on the other hand increases during the first day, globally from 1.78 mm/day to 2.01 mm/day, both in the ITCZ and in the mid latitudes. It can furthermore be noted by comparing with figure 1 that the convective spindown and the stratiform spinup in the tropics compensate each other almost perfectly.

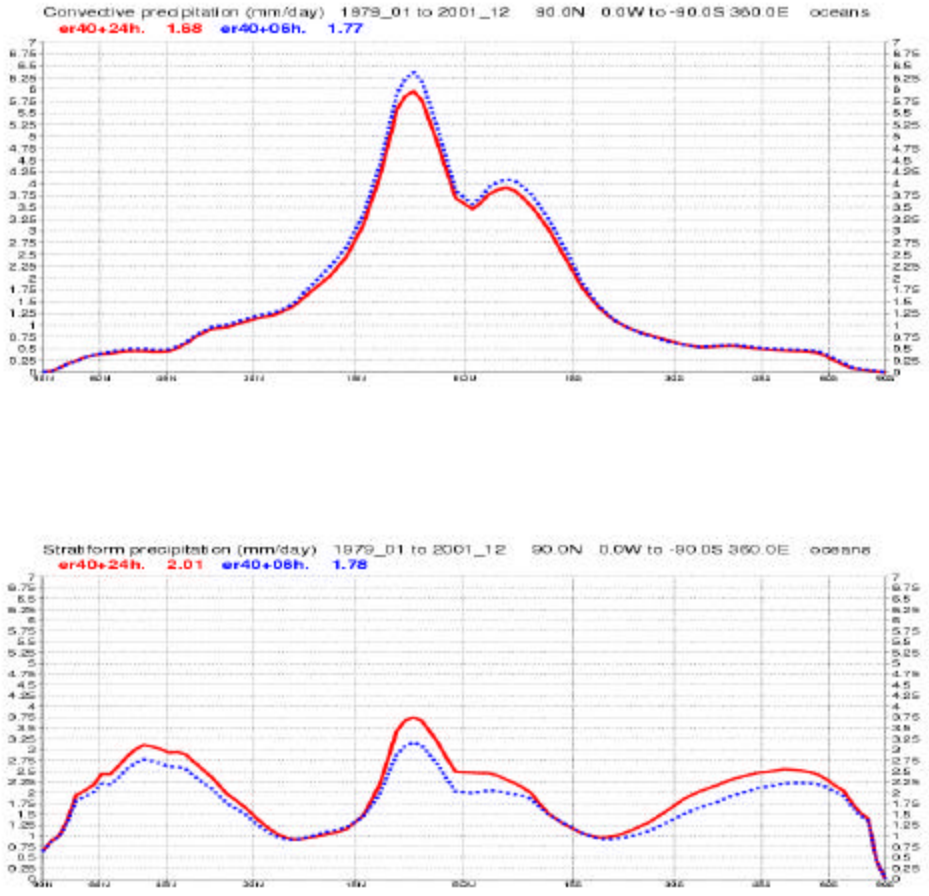

Figure 3. Spinup/spindown of the two precipitation components, convective (above) and stratiform (below). 23 years of monthly means 1979 to 2001 over the oceans.

8 Conclusions

The second ECMWF reanalysis is now finalized. Comparisons of the model diagnosed precipitation in ERA-40 with GPCP show good or excellent agreement with GPCP in mid- and high latitudes over the years 1979 to 2001. In the tropics on the other hand the ERA-40 system overestimates the precipitation, particularly in the oceanic ITCZ.

The explanation for the overestimate is believed to be a fundamental feature of the variational data assimilation assumptions, in that specific humidity is used as the control variable. With the Gaussian background error covariance model employed, there will be a bias towards saturation in the humidity increments. This 'extra water is only removed by convective scheme in the subsequent forecast steps. Release of 'extra' latent heat by the convection is enhancing the intensity of the ITCZ circulation, and leads to an increase in the tropical stratiform precipitation. In short, the combination of high density of (tropical) humidity observations from SSMI and TOVS and the choice of control variable and error covariance assumptions for humidity lead to an overestimation of tropical precipitation in ERA-40. However, since the 'extra' water is added in areas already close to saturation and with large specific humidities, it is likely that the reanalysis synoptics is structurally close to reality also here, albeit a bit too intense. We believe the ERA-40 analyses will be very useful also for studies of the tropical circulation (MJO, westerly bursts ...).

In the pre-satellite years 1958-1970 when there were very few upper air observations of humidity in the tropics, the hydrological cycle is in very good balance (Table 1).

Finally, there is also a noticeable spinup in midlatitude stratiform precipitation, and this is in both the satellite and the pre-satellite years. A likely cause here is the intermittent nature of the 3D-Var data assimilation. Developing baroclinic disturbances in the forecasts are damped at each analysis time by the vertically oriented analysis increments from the analysis. This deficiency can only be addressed with flow dependent model error covariances, as in the 4D-Var analysis method used operationally at ECMWF.

9 Acknowledgements

ERA-40 is a massive undertaking of the entire ECMWF. The responsibility for the production lay with core group lead by Adrian Simmons and Sakari Uppala and with the following present and past members: Ulf Andrae, Vanda da Costa Bechtold, Mike Fiorino, Angeles Hernandez, Per Källberg, Xu Li, Kazutoshi Onogi, Sami Saarinen and Niko Sokka.

Many other ECMWF staff members have been heavily involved in ERA-40, for development, tuning, running and monitoring.

Within the European Union Framework 5 programme several validation partners around Europe have been very helpful with early monitoring and validation of the analyses.

No reanalysis can be carried out without observations, and without the excellent cooperation with the data providers, in particular NCAR (Roy Jenne and his group) and NCEP (Jack Woollen), but also several satellite data producers and users, the ERA-40 project would have been impossible. A special mention must be made of Eumetsat, where cloud motion winds from Meteosat were re-processed for the years 1982 to 1988 for the benefit of ERA-40.

Gridding of Global Precipitation
from Asynoptic Satellite Measurements

Murry L. Salby
Program in Atmospheric and Oceanic Sciences
Campus Box 311
University of Colorado
Boulder, CO 80309

February 24, 2003

1. Introduction

Precipitation is observed from space through active and passive microwave techniques. Available from several orbiting platforms, those observations provide continuous global coverage. However, the information content of satellite observations, on which precipitation analysis rests, is limited by the sampling in space and time.

Satellites observe the global precipitation field *asynoptically*. Different sites are observed at different times. Observations are continuous along a satellite's track, but discrete between successive orbits. These features limit the space-time resolution of satellite data. For an individual platform, asynoptic sampling resolves about half a dozen zonal wavenumbers and frequencies less than 1 cpd. The precipitation field, on the other hand, involves variance on much shorter scales.

Variance at short space and time scales is undersampled in satellite data, lying beyond the Nyquist limits of asynoptic sampling. Such variance aliases behavior at longer scales which would otherwise be correctly represented in asynoptic data. This limitation complicates the gridding of data into synoptic maps of the instantaneous precipitation field. Through the diurnal cycle, undersampled variance also aliases the time-mean precipitation field.

2. Information Content of Asynoptic Data

Figure 1

Rooted in sampling considerations, these errors involve behavior that is misrepresented in asynoptic data. Figure 1 illustrates the sampling along an individual latitude circle from a single platform with about 14 orbits/day. Plotted is the sampling with a Narrow Field of View (NFOV), characteristic of an active instrument like the TRMM radar (solid/open circles). Analogous sampling applies to a Wide Field of View (WFOV), characteristic of a scanning radiometer (shaded). Although capturing instantaneous structure within 25° of longitude, the WFOV likewise leaves most of the precipitation field at that time unobserved.

For the NFOV, 28 longitudes are observed during one day: 14 from each side of the orbit. Were those longitudes observed simultaneously, this sampling would resolve 14 zonal wavenumbers. On the next day, 28 different longitudes are sampled. They are nested *nonuniformly* within the original 14 longitudes. Collected with those of the first day, they imply the resolution of 28 zonal wavenumbers. After several days, this nested sampling accumulates, yielding a dense mesh of longitudes that, although nonuniform, implies very fine spatial resolution.

The consideration which preventts this benefit is transience. The precipitation field evolves on time scales much shorter than the time for the globe to be covered. Hence, while precipitation is being observed at one site, it is changing at another.

When observations on the latitude circle are represented in extended longitude and time (Fig. 2), the {non-uniform} character of asynoptic sampling disappears. Observations from the NFOV then form a uniform grid along two ``asynoptic coordinates":} s and r (Salby, 1982): Each is a mixture of space and time. Much the same picture holds for the WFOV (shaded). Despite high spatial resolution within the instantaneous field of view, the WFOV likewise leaves large gaps in space and time between successive orbits. Small-scale structure within the instantaneous WFOV is incoherent between adjacent orbits (e.g., Lait and Stanford, 1988). Consequently, it does not lend itself to interpolation into a continuous description of the global precipitation field.

Figure 2:

Figure 3:

Figure 4:

The uniform sampling along asynoptic coordinates establishes the resolution in space and time. It, in turn, defines the information content of satellite data. Illustrated in Fig. 3 in terms of zonal wavenumber and frequency, the information content corresponds to a rectangle oriented along two ``asynoptic wavenumbers'': k_s and k_r. Analogous to their counterparts in phhysical space, k_s and k_r are mixtures of synoptic wavenumber and frequency. The boundaries of this rectangle represent the Nyquist limits of asynoptic sampling. Resolved are about 7 zonal wavenumbers and frequencies out to about 1 cpd (0.5 cpd if asymmetry inherent to asynoptic sampling is not accounted for; Salby, 1989). The information content is comparable to that of synoptic sampling, with 14 longitudes observed simultaneously twice per day.

Variance outside this rectangle is undersampled. In the asynoptic data, it is {indistinguishable} from variance inside the rectangle. An example is illustrated by the two solid circles in Fig. 3: They describe a high-wavenumber stationary component and a low-wavenumber transient component. In a continuous representation along the asynoptic coordinate s (equivalent to time in a reference frame moving with the satellite), those components are mutually distinct (Fig. 4). In the discrete asynoptic data, however, the two components are identical.

Variance outside the Nyquist limits is undersampled. It is therefore misrepresented in the asynoptic data as variance inside the Nyquist limits. Undersampled variance folds back onto behavior at longer (resolvable) scales, which would otherwise be correctly represented.

These sampling considerations are violated by two important classes of variability: (1) Broad-band variance is widely distributed over wavenumber and frequency, spilling beyond the Nyquist limits of asynoptic sampling. (2) Diurnal variations involve harmonics of a day, which lie at and beyond the Nyquist limits. Those harmonics alias zero frequency, introducing a bias into the time-mean distribution. These classes of variability challenge the information content of asynoptic data. They also represent the two major elements of the precipitation field.

3. High-Resolution Description of Convection

Figure 5:

The impact of undersampled variance has been studied in high-resolution Global Cloud Imagery (GCI), which has been constructed from 6 satellites simultaneously monitoring the earth (Salby et al., 1991). Illustrated in Fig. 5, each image represents a nearly instantaneous snapshot of the global convective pattern. With horizontal resolution of 0.5º and temporal resolution of 3 hrs, the GCI resolves the dominant scales of organized convection.

Cold cloud fraction η_c provides a proxy for areal-averaged rainfall (e.g., Richards and Arkin, 1981), serving as a cornerstone even in diverse analyses like GPCP that include ground-based measurements (Huffman et al., 1997). Through η_c, the GCI has been married with monthly-mean precipitation in GPCP to map the global distribution of rainfall at horizontal resolution of 2.5° and temporal resolution of 3 hrs. In the sampling experiments below, we rely on the raw imagery of η_c in the GCI. Available at increments of 0.5° and 3 hrs, it provides short-scale behavior that approaches the granularity of the actual precipitation field. The GCI then provides a litmus test of asynoptic sampling.

Figure 6 plots the frequency spectrum of cold cloud, over tropical Africa. The spectrum at individual sites (dotted) is broad band, punctuated by pronounced spikes at harmonics of the diurnal cycle. Those harmonics reflect brief but heavy rainfall at preferred local times, which contributes disproportionately to the daily accumulation (Janowiak et al., 1994). More sobering is what happens if cold cloud is averaged spatially over the convective center. The spectrum (solid) is then dominated by diurnal variance. Unlike other fluctuations, the diurnal variation is spatially coherent across the region of convection (Bergman, 1996; Bergman and Salby, 1996). Consequently, it is not removed by spatial averaging. It is, in fact, the large-scale coherent component that is important for climate studies and for refining models.

4. Aliasing by the Diurnal Cycle

Figure 6:

We turn now to what undersampled variance implies for deriving the time-mean distribution. To cope with diurnal variance, satellites are flown in a precessing orbit: Observations on a latitude circle then drift through local time, eventually sampling all phases of the diurnal cycle. However, even this sampling is limited by two practical considerations: (1) The precession period is long, typically a month or longer. (2) The diurnal variation is not steady, but random. It varies from one day to the next according to the presence of convection. These considerations require *a population of observations*, several at each local time, to composite the mean diurnal variation. Only in a large enough population is the mean diurnal variation truly separated from the time mean.

To evaluate the systematic error from diurnal aliasing, the GCI has been sampled asynoptically from a single platform with specified orbital and viewing geometries. The resulting time-mean distribution is then compared against the true time mean in the GCI. Figure 7 plots the relative error recovered from a WFOV, with a precession period of about a month. After 1 month

of averaging, the bias from undersampled diurnal variance exceeds 50° over regions of tropical convection. Even after 3 months of averaging (not shown), the systematic error still exceeds 30%.

Figure 7:

Figure 8:

Figure 8 plots the same information, but for a NFOV. The systematic error is noticeably greater. After 1 month of averaging, it approaches 80% in regions of tropical convection. Even after 3 months of averaging (not shown), the bias exceeds 40%.

The different systematic errors produced by these viewing geometries follows from how often individual sites are sampled (Salby and Callaghan, 1997). During one month, a 2.5° cell is sampled by the NFOV instrument 50--100 times. This yields only 2–4 observations per hour of local time for each 2.5° cell. In contrast, the same cell is sampled by the WFOV instrument an order of magnitude more frequently. The larger population better separates the mean diurnal variation from the time mean, which then contains a smaller bias.

5. Synoptic Mapping of Large-Scale Structure

We turn next to undersampled small-scale variance and its implications for synoptic maps of global structure. Constructing synoptic maps is more ambitious than the time-mean distribution. However, two features work in its favor: (1) Small undersampled scales are not of primary interest in climate applications. Rather, it is their organization by large scales that is most important. (2) Aliases of those undersampled scales are random.

A technique has been developed to reject undersampled incoherent variance, leaving a more accurate representation of large-scale coherent variance (Salby and Sassi, 2001), As before, the GCI is sampled asynoptically from a single orbiting platform. Figure 9a plots, from the raw sampled data, the spectrum over asynoptic wavenumber k_s. (It is equivalent to the spectrum over frequency in a frame moving with the satellite.) Broadly distributed over wavenumber, the spectrum is statistically white. It can be shown that only variance within a neighborhood of integer k_s lies within the asynoptic rectangle of Fig. 3. Variance removed from integer k_s, which dominates the spectrum in Fig. 9a, is then undersampled. Figure 9b plots the same information, but after the technique has been applieed to the raw asynoptic data. Variance is now concentrated about integer k_s. Variability has therefore been discriminated to those space and time scales that are resolved in the asynoptic data.

Figure 9:

This technique has been applied to data sampled asynoptically from the GCI to produce daily synoptic maps over a 1-month period. The results are then compared against the true synoptic behavior in the GCI. When synoptic maps are produced from the raw asynoptic data, the error at large scales is as great as the large-scale signal present. However, when the asynoptic data are processed via this technique,
the error variance is reduced to 10% or less.

Figure 10:

Figure 11:

Figure 10 illustrates the synoptically-mapped evolution over the equatorial central Pacific. The period shown includes an amplification of the Madden-Julian oscillation (MJO), which organizes tropical convection. In the synoptically-mapped evolution (dashed), cold cloud is magnified during the first week, when convection in the MJO crosses the dateline. Cold cloud then decreases sharply, as convection migrates eastward and leaves the region. The mapped evolution faithfully tracks the true large-scale evolution in the GCI (solid). So does the global structure in synoptic maps (ibid.).

6. Representation of Convection in Models

Analyzed precipitation, derived through a model, must contend with the misrepresentation of scales in asynoptic data. A precipitation analysis also relies on the model's representation of precipitation. It competes with observed precipitation where measurements are available, but serves in place of them where they are not.
In general, cumulus convection is poorly represented in models, as is its diurnal variation. Although details of its simulation vary with model and convective parameterization, certain forms of pathological behavior are common to many GCMs. Figure 11 plots, from the BMRC model, the forecast distribution of cloud brightness temperature for the same time as in Fig. 5. Comparison shows that the model reproduces observed structure remarkably well at middle and high latitudes, where cloud is organized by sloping convection. In the tropics, however, where cloud is organized by cumulus convection, the simulation is less successful. Not only does the instantaneous structure differ, but so does the evolution.

The simulation in the tropics deviates from observed behavior on the time scale of days and, most conspicuously, in relation to the diurnal cycle. This form of pathological behavior is not unique to the BMRC model. In fact, it is intrinsic to many GCMs, including the COLA model and the NCAR CCM (Ricciardulli and Garcia, 2000). Figure 12 compares the power spectrum of areal-averaged precipitation over the equatorial Pacific (inside the window shown in Figs. 5 and 11) represented in the GCI vs that simulated during the same period by the COLA model. The observed behavior (Fig. 12a) involves a red spectrum, in which variance is distributed broadly out to 1 cpd. The diurnal cycle, although present, is comparatively minor because the region considered is principally maritime. In the simulated behavior (Fig. 12b), however, power is sharply concentrated at low frequency and at the diurnal cycle. At intermediate scales, where convection is organized through interaction with the circulation, power is virtually absent. Analogous behavior is evident in other models (ibid.). Depending on the convective parameterization, the diurnal cycle can be even stronger, dominating the organization of tropical convection.

Figure 12:

7. Implications

Aliasing by undersampled diurnal variance is significant over much of the tropics. This is especially true near land, where convection undergoes a pronounced diurnal variation. The time-mean precipitation field can therefore be determined only as accurately as can the mean diurnal variation. This systematic error requires data from a single platform to be averaged over several months -- even if that platform is in a precessing orbit.

The random component of sampling error can be sharply reduced by rejecting incoherent variance. Large-scale coherent structure, describing the organization of precipitation, can then be mapped synoptically on individual days. This opens the door to a wide range of scientific applications, including issues surrounding how precipitation interacts with the general circulation.

The foregoing limitations stem from sampling error, which leads to a misrepresentation of scales in asynoptic data. Once the precipitation field has been undersampled, aliased behaviorr is difficult to distinguish from behavior that is genuinely present. This feature is an important consideration for assimilating satellite measurements into a forecast model. Beyond incorporating observed behavior, the model generates precipitation at other locations and times, for which observations are absent. The characteristic scales of precipitation are much shorter than space-time gaps in asynoptic data from a single platform. For this reason, only the large-scale organization and statistics of observed precipitation can be interpolated reliably into a continuous description of the global precipitation field. An accurate analysis of global precipitation will require (1) the input data to be properly interpreted and (2) statistical properties and the organization of precipitation in the model, inclusive of the diurnal cycle, to faithfully represent counterpart behavior in the atmosphere.

The ultimate solution to these limitations is more frequent sampling in space and time. This feature is provided by *multiple orbiting platforms*. If details of the combined sampling are accounted for, such precipitation measurements make possible accurate monthly-mean structure, as well as synoptic maps with enhanced frequency and horizontal resolution.

References

Bergman, J. and M. Salby, 1996: Diurnal variations of cloud cover and their relationship to climatological conditions. *J. Climate* **9**, 2802-2820.

Bergman, J., 1996: A numerical investigation of cloud diurnal variations. *J. Climate* **10**, 2330-2350.

Huffman, G., Adler, R., Arkin, P., Chaing, A., Ferraro, R., Gruber, A., Janowiak, J., McNab, A., Rudolf, B., and U. Schneider, 1997: The Global Precipitation Climatology Project (GPCP) combined precipitation data set. *Bull. Amer. Meteorol. Soc*., **78**, 5--20.

Janowiak, J., Arkin, P., and M. Morris sey, 1994: An examination of the diurnal cycle in oceanic tropical rainfall using satellite and in situ data. *Mon. Wea. Rev*., **122**, 2296-2311.

Lait, L. and J. Stanford, 1988: Applications of asynoptic space-time Fourier transform methods to scanning satellite measurements. *J. Atmos. Sci*., 4**5**, 3784-3799.

Ricciardiulli, and R. R. Garcia, 2000: The excitation of equatorial waves by deep convection in the NCAR community climate model (CCM3) *J. Atmos. Sci* **57**, 3461-3487.

Richards, F., and P. Arkin, 1981: On the relationship between satellite-observed cloud cover and precipitation, *Mon. Wea. Rev*. **109**, 1081--1093.

Salby, M. L., 1982: Sampling theory for asynoptic satellite observations. *J. Atmos. Sci*., **39**, 2577--2600.

Salby, M., 1989: Climate monitoring from space: Asynoptic sampling considerations *J. Climate,* **2**, 1091-1105.

Salby, M. L., H. Hendon, K. Woodberry, and K. Tanaka, 1991: Analysis of global cloud imagery from multiple satellites. *Bull. Am. Meteor. Soc.*, **72**, 467--480.

Salby, M. and P. Callaghan, 1997: Sampling error in climate properties derived from satellite measurements: Consequences of undersampled diurnal variability. *J. Climate,* **10**, 18-36.

Salby, M. and F. Sassi, 2001: Synoptic mapping of convective structure from undersampled satellite observations. *J. Climate*, **15**, 2281-2295.

FIGURE CAPTIONS

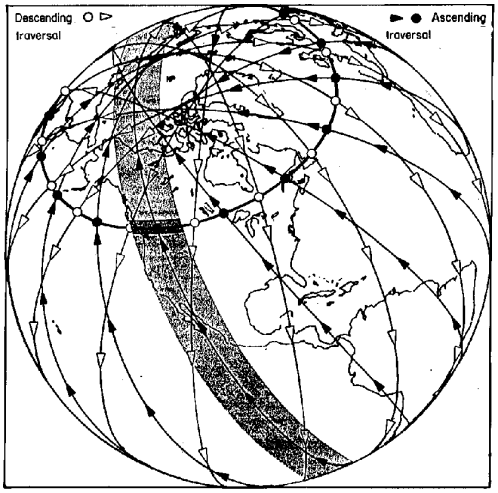

Figure 1: Asynoptic sampling along a latitude circle from a single orbiting platform with a narrow field of view (solid/open circles) and a wide field of view (shading).

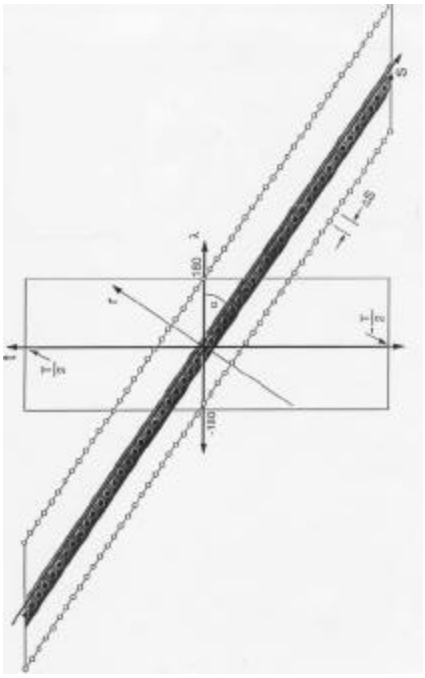

Figure 2: Sampling along the latitude circle, as function of extended longitude ? and time *t*.

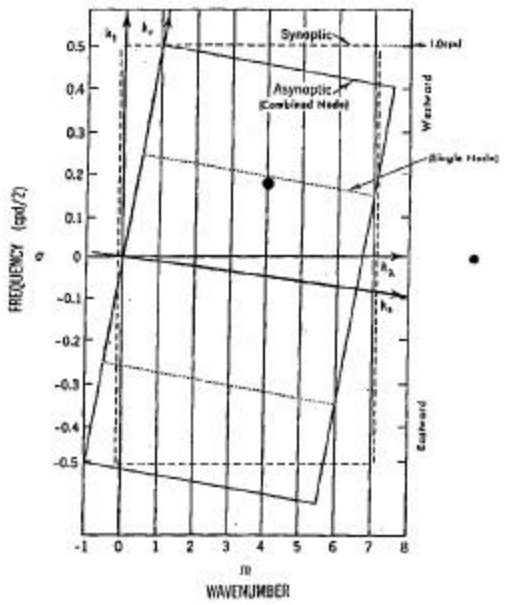

Figure 3: Information Content of asynoptic data from a single platform,as function of zonal wavenumber k_λ and frequency k_t

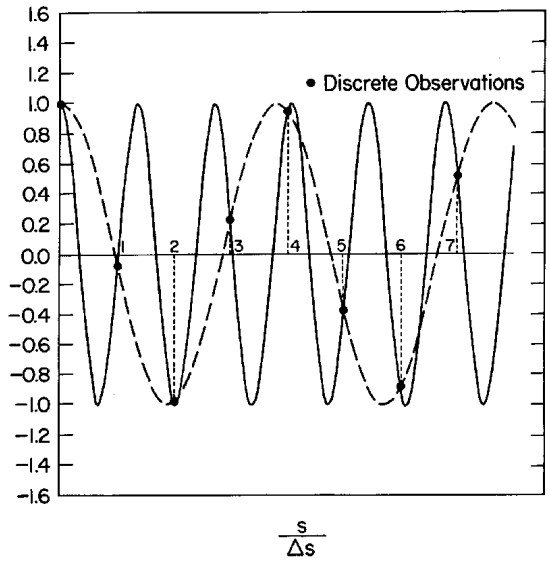

Figure 4: Behavior along asynoptic coordinate s of a high-wavenumber stationary component and a low-wavenumber transient component (solid circles in Fig. 3), which form an alias pair. Values actually sampled by satellite indicated in solid circles.

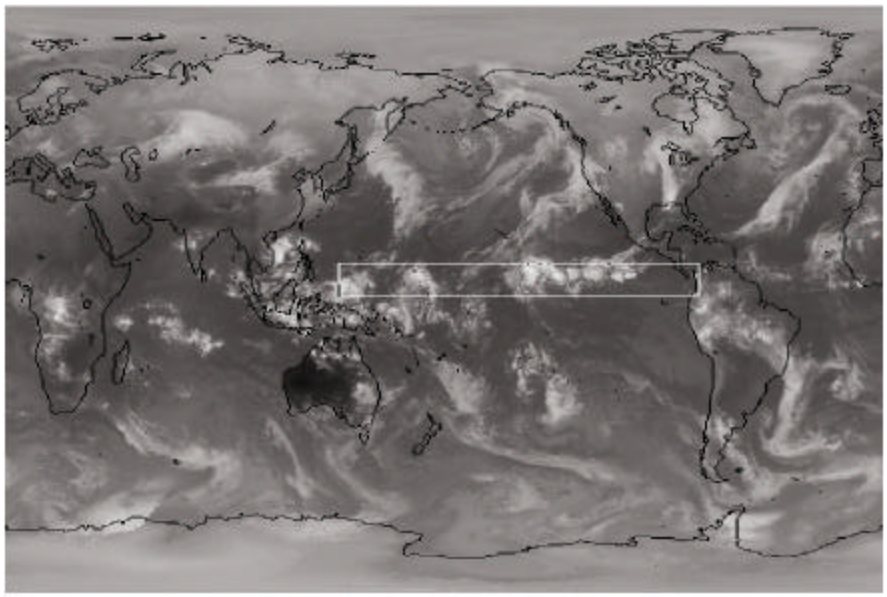

Figure 5: Global Cloud Image (brightness temperature) at 06Z on Nov 17, 1987.

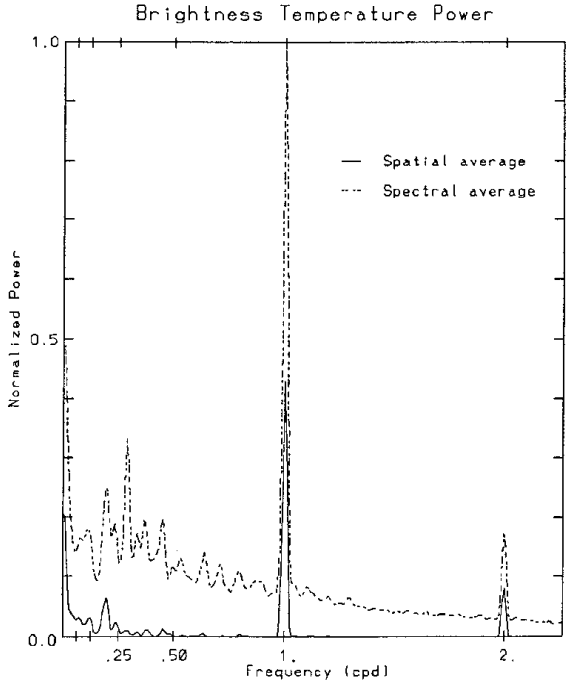

Figure 6: Frequency spectrum of cloud over tropical Africa: Ensemble average of spectra at individual 0.5° locations (dashed) vs spectrum of areal average (solid).

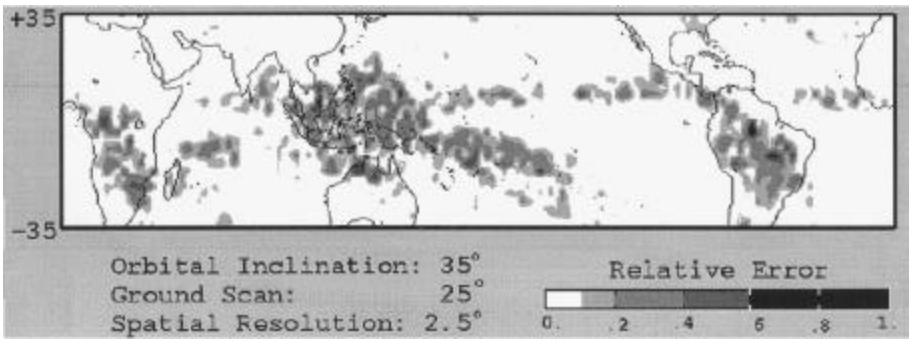

Figure 7: Relative bias from diurnal aliasing after averaging asynoptic observations over 1 month. Derived from a precessing orbit with a WFOV (25°ground scan).

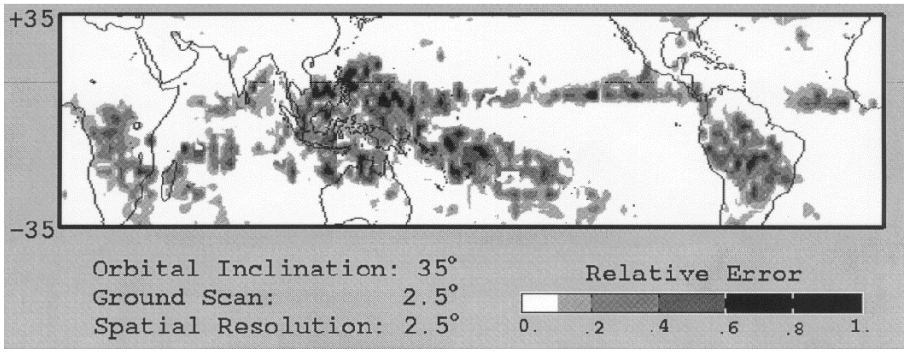

Figure 8: As in Fig. 7, but for a NFOV (2.5°ground scan).

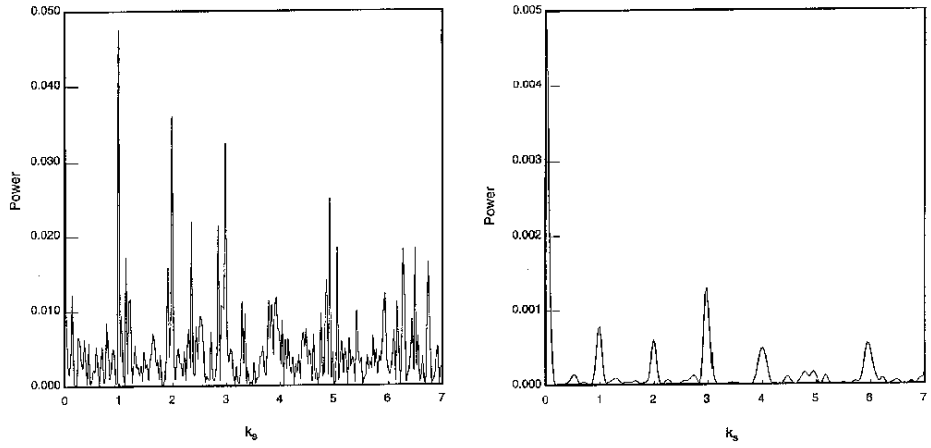

Figure 9: Power spectrum of cold cloud, as function of asynoptic wavenumber k_s, (a) from raw asynoptic data and (b) after processing to reject incoherent variance.

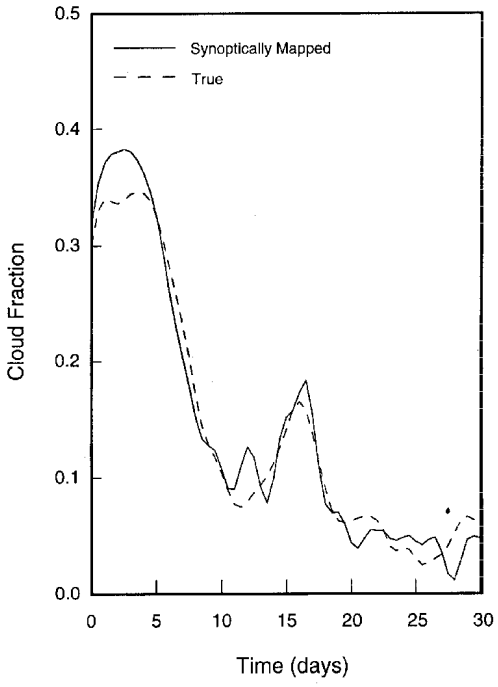

Figure 10: Large-scale evolution of cold cloud over central Pacific (a) in synoptically-mapped behavior and (b) actually present in GCI.

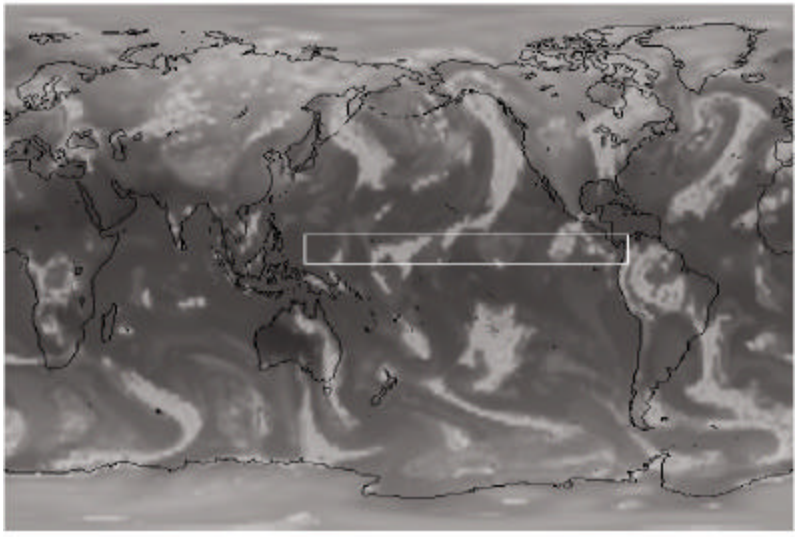

Figure 11: As in Fig. 5, but simulated in a 2-day forecast by the BMRC model.

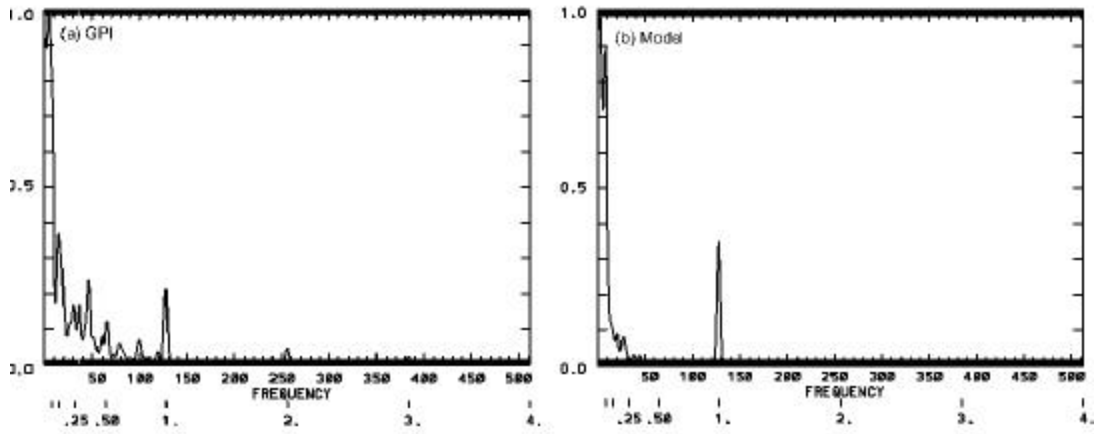

Figure 12: Power spectra of area-averaged precipitation over equatorial Pacific, indicated in Fig. 5, (a) represented in the GCI and (b) simulated by the COLA model.

BLENDING PRECIPITATION DATA SETS FROM MULTIPLE SOURCES AT SHORT TIME SCALES

F. Joseph Turk
Marine Meteorology Division, Code 7541, Naval Research Laboratory
Monterey, California 93943, USA

ABSTRACT

Despite advancements from recent passive microwave-based meteorological satellite missions, the identification and quantification of precipitation on short time scales (e.g, 3-6 hours) from satellites remains an elusive quantity. Yet the needs for a timely precipitation analysis continue to grow, in numerical weather prediction, hydrological, aerosol and land surface models, all of which are fundamental to day-to-day military operational support. Additionally, very few raingauge networks operate with the necessary spatial density and time resolution required for validation of a short-time scale, satellite-based precipitation analysis. Observationally, the main issue remains the lack of adequate time sampling throughout the day; new sensors such as the Advanced Microwave Scanning Radiometer (AMSR) on EOS-Aqua, the Advanced Microwave Sounding Unit (AMSU-B) on the NOAA satellites, and the Tropical Rainfall Measuring Mission (TRMM) have narrowed this gap. However, at short time scales other issues arise, relating to inter-sensor bias, cloud geometry (each satellite views from a different perspective), all of which combine to place a fundamental limit on how accurately a short-term-average precipitation estimate can be retrieved.

Recent investigations have emphasized other means to blend additional datasets, such as operational rapid-update geostationary-based thermal infrared (IR) data, with the various passive microwave (PMW) instruments based on low Earth-orbiting (LEO) satellites. Since these data in fact represent the diurnal variation of clouds and can often lead to erroneous assignment of precipitation to cold non-precipitating clouds or miss significant rain from warm-cloud top situations, the blended scheme tries to use the IR data to guide the PMW data during the revisit time (in-between successive overpasses). Recent validation efforts using densely spaced raingauges with a 1-minute update cycle has shown that while this type of technique produces generally unbiased estimates on daily/1-degree time and space scales, it tends to underestimate at shorter time scales and with an associated increase in RMS error. This presentation will show some current uses and underlying limitations of these blended datasets, and highlight other ongoing efforts to improve the quantification and error characteristics of short-time scale satellite-derived precipitation.

1. INTRODUCTION

The past two decades have witnessed the rapid evolution of the low Earth-orbiting (LEO) passive microwave (PMW) imaging sensor from a research setting into routine operational settings. The conically-scanning, sun-synchronous orbiting Special Sensor Microwave Imager (SSMI) imagers onboard the Defense Meteorological Satellite Program (DMSP) satellites launched between 1987 and 1999 were joined by the joint United States/Japan Tropical Rainfall Measuring Mission (TRMM) Microwave Imager (TMI) in 1997, and the Advanced Microwave Scanning Radiometer (AMSR-E) aboard the Earth Observing System (EOS) Aqua in 2002. The Advanced Microwave Sounding Unit-B (AMSU-B), an across-track scanning humidity sounder onboard the National Oceanic and Atmospheric Administration (NOAA) operational LEO satellites, has an operational rainfall product which is distributed by the National Environmental Satellite Data Information Service (NESDIS) Microwave Surface and Precipitation Products System (MSPPS) (Weng et.al, 2002). A variety of conditions make short-time scale satellite-derived precipitation problematic to validate. The changing time and three-dimensional spatial scales of global precipitation processes, the intermittent and unequally spaced satellite revisit, the instantaneous nature of a moving-platform satellite observation, the characteristics of the validation system, among others, each effect must considered in order to properly derive and interpret validation statistics. To attempt to validate a satellite-based precipitation analysis at a daily or sub-daily time scale and a sub-degree spatial scale requires a validation system with a dense, homogeneous spatial coverage and a time sampling rate fast enough (and extended over a long enough period of time) to coordinate meaningful comparisons with the instantaneous nature of moving-platform satellite-based observations, and some means to supplement (or account for) the intermittent LEO overpass schedule. Overall, when all of the above-mentioned operational LEO satellite platforms are taken into account (three DMSP, one TMI, and three NOAA as of early 2003), orbit calculations show that the resultant worst-case revisit still hovers near six hours in the tropical latitudes.

With the fundamental intermittent nature of PMW observations, the idea of capitalizing on the frequent, routinely scheduled infrared (IR) observations available from geostationary operational meteorological satellite platforms has received increasing attention in recent years (Adler et.al, 1993; Vicente, 1994; Levizzani et.al, 1996; Kidd et.al, 1998; Miller et.al, 2000; Todd et.al, 2001; Morales and Anagnostou, 2002; Dietrich et.al, 2001; Grecu et.al, 2000; Ba et. al, 2001; Grose et. al, 2002; Kuligowski, 2002). This article focuses specifically upon validation and performance of a particular blended-satellite technique at various small spatial and short time scale combinations, using raingauge data the densely spaced, 1-minute reporting Korean Meteorological Administration (KMA) Automated Weather Station (AWS). Some underlying limitations of the expected performance of this and other types of sub-daily blended satellite techniques are discussed.

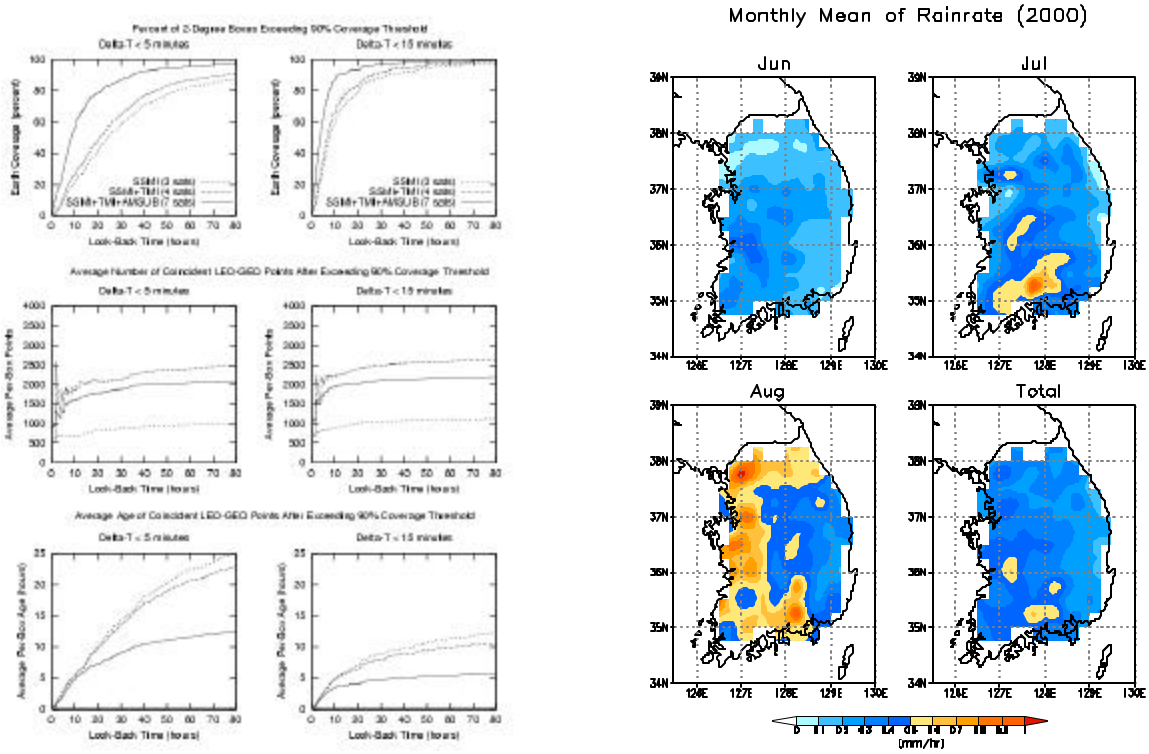

Figure 1 Left side: (top) Percentage of 2-degree boxes covered with time/space coincident IR-PMW observations over the Earth from 60S-60N latitude, as a function of the look-back time, and the number and type of Low Earth Orbiting (LEO) satellite sensors used. (middle) Average number coincident observations in each 2-degree box. (bottom) Average age in hours of the coincident observations in each 2-degree box. The maximum allowed time and space offsets between the LEO-based microwave sensor pixel and the geostationary IR pxel are 5 minutes and 10 km, respectively. Right side: Same as left side panels, but for a maximum allowed time offset of 15 minutes. **Figure 2**. Maps of the monthly mean rainrate over the South Korean peninsula for June, July and August 2000.

2. BLENDED TECHNIQUE DESCRIPTION

The blended technique developed at NRL is based upon the underlying collection of time and space-intersecting pixels from all operational geostationary orbiting IR imagers and LEO PWM imagers. In order to blend the disjoint LEO PMW and geostationary IR measurements in an automated and adaptive manner, the blended technique starts by subdividing the Earth into a 2-degree/pixel grid (60 lines by 180 samples) with a finer, 0.25-degree/pixel grid (480 lines x 1440 samples) nested inside it (the reason for these values are discussed below) between 60N and 60S. As new PMW datasets arrive, the PMW-derived rainrate pixels are paired with their time and space-coincident geostationary 11-um IR brightness temperature (T_B) data, using a 15-minute maximum allowed time offset (denoted by ?t) between the pixel observation times and a 10-km maximum allowed spatial offset (denoted by ?d) as depicted in Figure 1.

Prior to this, the geostationary data are averaged to the approximate resolution of the PMW rainfall datasets (30-km for SSMI, 10-km for TMI, and between 15-50 km for AMSU-B depending upon scan position), and parallax-induced geolocation displacements are accounted for using the procedure of Vicente et. al. (2002). Each collocated data increments histograms of the IR T_B and the PMW rain rate in the nearest 2^o box, as well as the eight surrounding boxes (this overlap assures a fairly smooth transition in the histogram slopes between neighboring boxes). As soon as a 2^o box is refreshed with new LEO data, a probabilistic histogram matching relationship (Calheiros and Zawadski, 1987) is updated using the PMW rainrate and IR T_B histograms, and a T_B-R lookup table is created. To assure that the most timely rain history is maintained, the histograms of these coincident data are accumulated backwards from the current clock time (the "look-back" time) until the spatial coverage of a given 2-degree box exceeds a 90 percent coverage threshold (the inner 0.25-km/pixel mesh is fine enough to enable an approximation of the percent coverage).

Figure 1 shows the overall percentage of 2-degree boxes that reach this coverage threshold as a function of the look-back time and the type of LEO satellites used in the coincident pixel alignment procedure. The addition of the three AMSU-B instruments to the three SSMIs and the TMI (7 satellites, dotted line) permits 90% of the Earth between 60S-60N latitude to be covered with coincident data observations within 15 hours of look-back time, with an average of

about 2000 coincident observations per box. With three SSMIs and the TMI (4 satellites, dashed line), the same total Earth coverage is reached after 30 hours, but with an average of 2500 coincident observations per 2-degree box (this is due to the fact that the ASMU-B data are coarser than the TMI, and although they may arrive prior to the TMI data, they are less in number). The bottom panel demonstrates that for 90 percent Earth coverage, the average age of the data in each 2-degree box is about 4 hours when the 7-satellite combination is used, significantly shorter than the 8-hours in the 4-satellites case and 10-hours in the SSMI-only (3 satellites) case. For comparison, Figure 2 also illustrates these same statistics, but with a smaller maximum allowed ?t=5 minutes. Under these circumstances, it takes about 35 hours to achieve the 90% Earth coverage for the 7-satellite case and the average age of these data are about 10 hours. While the smaller time offset is preferred in order to capture as nearly time-coincident data as possible, with the current 7-satellite configuration it comes with the expense of increased age of coincident data observations. With this inherent tradeoff in mind, all results discussed hereafter used ?t=15 minutes and ?d=10 km in the PMW-IR coincident data alignment procedure.

This lookup table update process is constantly ongoing with operationally arriving LEO and geostationary data. The transfer of this information to the stream of steadily arriving geostationary data is then a relatively simple lookup table procedure. For each newly arrived geostationary dataset, the IR channels are map-registered onto a global, 0.1-degree rectangular map projection for all pixels whose satellite zenith angle is less than 70 degrees. For each 0.1-degree pixel, the closest 2-degree histogram box and the eight surrounding boxes are located, and an inverse-distance weighted average rainrate is computed from these nine lookup table-derived rainrates (this minimizes discontinuities across histogram box boundaries). Lastly, NWP forecast model 850 hPa wind vectors from the Navy Operational Global Atmospheric Prediction System (NOGAPS) forecast model are combined with a 2-minute topographic database, and a correction is applied in regions of likely orographic effects on both the upslope and downslope (Vicente et. al, 2002). The previous 1-hour time history of the 11-um IR brightness temperature is analyzed for regions of active cloud top temperature growth or decay, and scaling factors are applied to intensify and lighten the overall rainrate. The use of a common 0.1-degree global map projection for all geostationary satellites greatly speeds up the computation of rainfall accumulations, and compensates for the coarser resolution of geostationary IR data at higher latitudes. At specified synoptic time intervals (usually every three hours), the rainfall accumulations are updated as far back in time as desired by backwards time-integrating.

The blended satellite technique is autonomous and self-adapting, and the adjustable parameters are the histogram box size, allowable pixel collocation time and space offsets (?t and ?d, respectively), and minimum spatial coverage of each box required to initiate its lookup table update. As additional LEO satellites are added to the blending procedure, presumably the histogram box size and allowable space/time offsets can be made smaller, which should better capture individual smaller-scale rainfall systems, although this remains to be examined when data from upcoming LEO platforms are available. In operational settings, one or more LEO datasets may be missing or arrive later than a data cutoff time. To limit this, we set a maximum look-back time of 24-hours, which may temporarily disable the blended technique over certain parts of the Earth where the overall LEO revisit time is the longest. We have resorted to using only the common 11-um channel at this point since it is common to all current geostationary satellites, but other formulations should be used to relate the PMW and IR data to take full advantage of the expanded thermal and solar spectral capabilities offered in the MSG and GOES-R series of geostationary satellites. Already, Marzano et. al. (2002) have tested multivariate probability matching and nonlinear multiple regression techniques for the PMW-IR blending. We are currently examining the use of the expanded channels aboard the Moderate Resolution Imaging Spectrometer (MODIS) in preparation for use with the Meteosat Second Generation (MSG) Spinning Enhanced Visible and Infrared Imager (SEVIRI) activation later in 2003 (Schmetz et. al, 2002).

3. VALIDATION WITH THE KMA AWS NETWORK

The Korean Meteorological Agency (KMA) maintains an operational, densely spaced Automated Weather Station (AWS) over the southern Korean Peninsula, consisting of nearly 500 tipping-bucket, uniformly-spaced, one-minute updating rain gauges (approximately 40 gauges per 1-degree box). AWS data were collected during June-August 2000 along with the individual hourly, instantaneous rainfall datasets produced by the blended satellite technique (the GMS-5 satellite is the only geostationary satellite that provides coverage and its refresh rate is hourly beginning at 30 minutes after each hour, and the Korean Peninsula is imaged about 8 minutes after the frame start time). Figure 2 depicts the shaded color maps of the mean monthly rainrate over the Southern Korean peninsula during June, July and August 2000.

During this time, the NOAA-15/16/17 satellites were not yet incorporated into the blended technique (the three SSMIs and the TMI formed the underlying LEO constellation), giving a LEO revisit over Korea of about 4 hours on average and 10 hours worst-case. Considering that an individual satellite observation represents an approximate 0.1-degree area average, whereas the gauge measurement represents a small area less than 1 m^2, South Korea is divided into smaller boxes, ranging from 0.1 degrees to 3 degrees on a side, where relatively homogeneous gauge distributions are found. Due to the inhomogeneity of the rain within the spatial averaging box and very small areas represented by individual gauges, a direct comparison of instantaneous (i.e, pixel-based) satellite-based retrievals and gauges is inherently limited. For intermittent and sporadic rain events, the rain may fall between but not into individual gauges, or the rainfall pattern

may evolve and move between the gauge locations. Using the AWS network and various IR-based rainfall techniques over a one-month period, Oh et.al (2002) investigated the impact of the spatial rain inhomogeneity by analyzing the number of rain-detected gauges in individual 1-degree boxes. They found that the satellite algorithm validation was more likely to fail for sporadic and weak rain events when the number of rain-detecting gauges per 1-degree box was less than 15. However, in some cases, isolated convective rain events may be characterized by a small number of rain-detecting gauges, so a simple minimum-gauge criterion is not necessarily sufficient in all cases. In the discussion to follow, it must be therefore be remembered that unambiguous interpretation is not always possible with gauge-satellite comparisons, especially for sporadic rain events.

The instantaneous estimate from the blended satellite technique essentially consists of transferring the past-time PMW-IR history (via the lookup tables) to newly gathered IR radiances, whose information content originates at or near the physical cloud top height, whereas the gauge data is a purely ground-based observation. Therefore, to account for the fallout time of the hydrometeors, the gauge data were first averaged over time windows varying between +/-1 to +/-30 minutes, centered about the GMS-5 observation time. Then, at each spatial resolution, these data were time-integrated over various time intervals ranging from one hour (the minimum time interval) to 30 days. That is, the original data were fixed at one spatial scale and then integrated over the various time scales, then repeated for the next spatial scale, and so on. This allows the blended technique validation to be performed in a two-dimensional, space-time fashion. Most importantly, the 1-minute time resolution of the KMA network allows individual, instantaneous satellite pixels to be paired in time with the corresponding rain gauge pixels prior to any temporal averaging.

For example, Figure 5 shows the scatter plots of the blended satellite (R_S) vs. gauge (R_G) comparison at a 1-degree spatial scale and for six time scales ranging from 1-hour to 24-hours, where the AWS-GMS time window was fixed at +/-10 minutes. As expected, the correlation improves with longer time averaging, but the bias remains near zero or slightly negative, with a large variance. The 24-hour plot demonstrates that when $R_G < 1$ mm hr^{-1}, the blended technique often assigned light rain to regions where $R_G = 0$. While it is difficult to unravel an exact cause of these characteristics, it is possible that this is related to the PMW algorithm rain/no-rain screening. Over land, a version of the NESDIS operational SSMI algorithm (Ferraro et. al, 1997) is used in the Version-5 TMI 2A12 rainfall algorithm (Kummerow at.al, 2001). Under certain conditions, light rain can be misidentified over a variety of Earth surfaces that appear to scatter radiation similar to a precipitating cloud (Bauer et.al, 2000; Conner and Petty, 1998; Ferraro et. al, 1998). In the automated histogram matching procedure, these (falsely-identified) light rain pixels get paired with their corresponding IR T_B, which is often larger (warmer) than other localized pixels that were correctly identified as rainfall. The end result can at times be a very light rainfall (under 0.5 mm hr^{-1}) that incorrectly gets assigned to regions in subsequent IR imagery, until these falsely-identified PMW points are discarded from the suspect 2-degree histogram box (usually after the next LEO overpass). The opposite effect also occurs, when the PMW algorithm rain/no-rain screen fails to identify regions of light rain. That is, these no-rain pixels get paired with a smaller (colder) IR T_B compared to other localized pixels. The result is that the zero-rain IR temperature threshold gets assigned too small of a value and the lookup table assigns zero or a very small value to subsequent IR imagery. While we cannot say for certain that misses and false alarms by the PMW screening algorithm are the cause of this, one can state that owing to its very nature, any caveats of the PMW instantaneous rain algorithms eventually manifest themselves in the blended technique results. The amount of time that these (or other) PMW data are retained in the blend is determined by the tuning parameters described in Section 2 (box size, percent coverage, ?t and ?d).

Figure 3 depicts the results from the analysis at this and other space and time scales in a two-dimensional format, where the spatial average and averaging period determines the abscissa and ordinate, respectively. The correlation, mean bias and root-mean-square error (RMSE) are each contoured for AWS time windows (gauge averaging time centered about the GMS observation time) of +/-10 minutes (other time windows are not illustrated here). Different time windows produce different results, owing to the variable fallout times of the hydrometeors from within the cloud, and the increased number of gauges in the average as the window is widened. However, there appears to be a sharp improvement when the time window is widened to +/-10 minutes, which a typical hydrometeor fallout time in tropical clouds (Soman et.al, 1995).

As expected, all three parameters improve as either the averaging period is increased or the grid size is coarsened. The contours do not flow smoothly at the longest time intervals due to the resultant small number of data points available from the finite 3-month period. Likewise, the small size of the Korean Peninsula produces a small number of data points when the data are averaged over the coarsest space scales. The blended technique is biased slightly negative (-0.1, or 10% low) once the time interval exceeds 3 days, falling to about –0.35 (35% low) at 3-hour/0.25-degree scales. One possible explanation for the bias behavior is that as the time scale is shortened, extreme heavy precipitation events are less likely to be captured by a LEO overpass. Since the nature of the blended technique is to retain some of the most recent rainfall history (a residual "memory effect"), there is a gradually increasing (rather than sudden) negative bias.

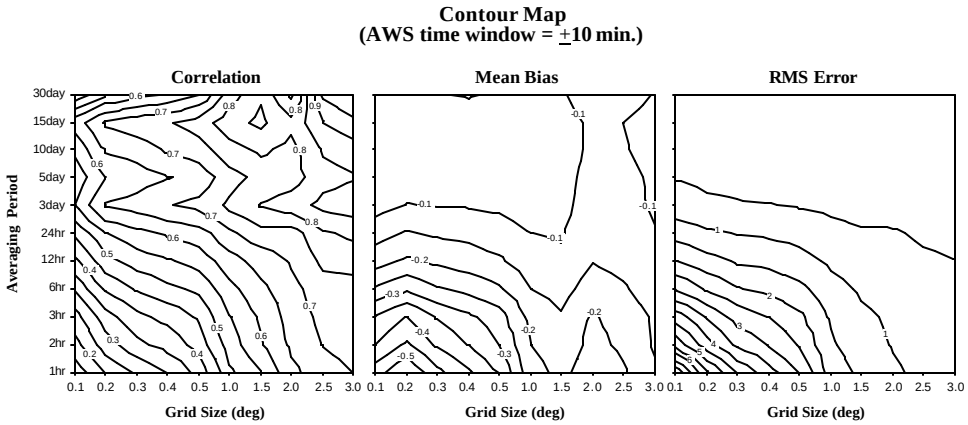

Figure 3. Space-time contour plots of the correlation coefficient, root mean square error and mean bias for an AWS time window average of +/-10 minutes. The time window is centered about the time of the GMS satellite observation of Korea. The abscissa and ordinate of each contour plot denotes the spatial and temporal scales, respectively, used to average the gauge data and the blended satellite technique estimated rain.

The RMSE is about 0.5 mm hr^{-1} for time intervals exceeding 3 days, and degrades to near 3.5 mm hr^{-1} at 3-hour/0.25-degree scales. The correlation coefficient can be as high as 0.8 for 12-hour averages, but only when the grid size exceeds 2.5 degrees. Most notably, the correlation begins to fall off quickly once the time average drops below one day, and/or the spatial scale falls under 1-degree, and this same sort of behavior is evident in the RMSE, and less so in the mean bias. This could be because the RMSE is more affected by the relatively few large precipitation events, whereas the correlation is affected by the large number of zero or near-zero rain rate points. As the time and/or space scale shrink, there are fewer heavy rain events, and the large number of zero or small rain rates, which show a large scatter, dominates the correlation coefficient.

Inherent in the inner workings of this type of blended technique is a residual "memory effect" whereby a certain amount of previous-time PMW information is retained in the statistical blend, and provided to subsequent geostationary update cycles. The effect is dependent upon the LEO revisit time, which at the latitude of Korea is about 12-hours (worst case) for the 4-satellite (3 SSMI and the TMI) constellation. As mentioned, the current 2-degree box size for the statistical matching represents a tradeoff between the overall revisit from the intermittently-spaced LEO satellite constellation (longer revisit requires a larger box size) and the need to capture "localized" rainfall characteristics and still have a sufficiently large number data points to perform a statistical histogram matching (small scale rainfall requires a smaller box size). The rapid decay of the correlation and RMSE statistics below the daily time scale may be reflecting the fact that below this scale, the blended technique estimates are often tuned with rainfall information from a somewhat earlier stage (several hours earlier) in the localized rainfall evolution, and don't always correlate well with the current rainfall evolutionary state. At time scales greater than one day, the correlation remains quite high even at the finest spatial scales, suggesting that this type of memory effect may average away past a certain time scale. While this is a plausible explanation, there are certainly other factors at work, most notably the nature of sporadic and intermittent rain evolving over a limited number of gauges. By analyzing the three month period, there are many short time-scale periods that are averaged together, some with intermittent, sporadic rainfall and others with more widespread rainfall, therefore the gauge-satellite effect should be averaged to some undetermined extent. Even so, we can state that below some minimum combination of space and time scales, there is most likely dependence between the overall LEO constellation revisit and the performance of this type of blended technique.

For NWP rainfall data assimilation requirements, the rainfall estimation error should be specified as a function of the average rain rate over the estimated space-time interval (e.g, percentage error at 1, 5, 10 mm hr^{-1}, etc). NWP variational assimilation techniques typically are based upon a minimization function, which requires knowledge of both the forecast and the observation (rainfall analysis) errors. If the forecast error is large, then the observed rainfall analysis will be increasingly allowed to contribute to the model initialization, and vice versa. The 3-hour/0.25-degree RMSE of 3.5 mm hr^{-1} was computed for all rain rates, and this would translate to a 35% error at 10 mm hr^{-1}.

The KMA gauge analysis provided validation over the three month summer interval, which are indicative of summer monsoon wet conditions, and were done during a time when the AMSU-B and AMSR sensors had not yet been added to the LEO constellation used in the blended technique. To examine the overall characteristics and performance of the technique, a longer validation time interval is needed, preferably one that covers both tropical and mid-latitude rainfall regimes and summer and winter seasons.

3. CONCLUSIONS

We have presented a series of over-land validation statistics from comparisons between satellite-derived rainfall estimates from a blended IR-PMW precipitation technique and ground-based rainfall observations gathered from operationally maintained raingauge networks in Korea. The bias, RMS error, and correlation coefficient were computed at various space and time scale combinations owing to the gauge density and the 1-minute sampling capabilities of the Korean AWS network. While precise gauge-satellite comparisons are by nature not truly possible, the gauge density and the 1-minute sampling capabilities of the Korean AWS network does reduce (but not eliminate) fundamental spatial and temporal offsets between observations and estimates, and provides a basis for gathering error statistics at sub-daily time scales and sub-one-degree spatial scales. Finer than approximately 1-day and one-degree time and space scales, respectively, a rapid decay of the error statistics was obtained by trading off either spatial or time resolution. Beyond a daily time scale, the blended estimates were unbiased and with an RMS error of no worse than 1 mm day^{-1}.

In general, the blended technique performed very well in the heavier, convective-style rain; over the mid-latitudes, the performance suffered for both summer and winter seasons. The current orographic correction scheme does not always flag probable orographic uplift regions (it is dependent upon an accurate forecast analysis of the low-level flow), and the enhancement factors do not yet appear to scale enough in regions of very steep terrain. Suggested improvements include a more qualitative usage of the time dimension available from 15-minute update times characteristic of GOES and MSG, as one means to capture information on cloud evolution in-between the intermittent PMW overpasses. Better characterization of the rainfall estimates between the individual PMW sensor types, and the adoption of one satellite as the "reference" satellite rainfall estimate is needed to reduce artifacts that result when the various SSMI, TMI, AMSU-B and AMSR rainfall estimates are blended together over short time scales.

ACKNOWLEDGEMENTS

The author gratefully acknowledge the support of his research sponsors, the Office of Naval Research, Program Element (PE-060243N) and the Oceanographer of the Navy through the program office at the Space and Naval Warfare Systems Command, PMW-155 (PE-0603207N).

REFERENCES

Adler, R.F., A.J. Negri, P.R. Keehn, I.A. Hakkarinen, 1993: Estimation of monthly rainfall over Japan and surrounding waters from a combination of low-orbit microwave and geosynchronous IR data. *J. Appl. Meteor*, **32**, 335-356.

Ba, M., and A. Gruber, 2001: The GOES Multispectral Rainfall Algorithm (GMSRA). *J. Appl. Meteor*., **40**, 1500-1514.

Bauer, P., Burose, D. and J. Schulz, 2000: Rain detection over land surfaces using passive microwave satellite data. ECMWF Tech. Memo. No. 330, ECMWF, Reading, England.

Calheiros, R.V. and I. Zawadzki, 1987: Reflectivity rain-rate relationship for radar hydrology and Brazil. *J. Clim. Appl. Meteor.*, **26**, 118-132.

Conner, M.D. and G.W. Petty, 1998: Validation and intercomparison of SSMI rain rate retrieval methods over the continental United States. *J. Appl. Meteor*., **37**, 679-700.

Dietrich, S., Solomon, R., Adamo, C., and A. Mugnai, 2001: Rainfall monitoring at the geostationary scale: Potential of lightning data in a rapid update approach. *Proc. 3rd EGS Plinius Conf. on Mediterranean Storms*, Baja Sardinia, Italy, 1-3 October.

Ferraro, R.R., 1997: Special sensor microwave imager derived global rainfall estimates for climatological applications. *J. Geophys. Res*., **102**, D14, 16715-16735.

Ferraro, R.R., E.A. Smith, W. Berg, G.J. Huffman, 1998: A screening methodology for passive microwave precipitation retrieval algorithms. *J. Atmos. Sci.*, **55**, 1583-1600.

Grecu, M., Anagnostou, E.N., and R.F. Adler, 2000: Assessment of the use of lightning information in satellite infrared rainfall estimation. *J. Hydrometeor*., **1**, 211-221.

Grose, A., E.A. Smith, H.S.-Chung, M.-L. Ou, B.J. Sohn, F.J. Turk, 2002: Possibilities and limitations for QPF using nowcasting methods with infrared geosynchronous satellite imagery. *J. Appl. Meteor.*, **41**, 763-785.

Kidd, C., D. Kniveton and E.C. Barrett, 1998: The advantages and disadvantages of statistically-derived, empirically-calibrated passive microwave algorithms for rainfall estimation. *J. Atmos. Sci.*, **55**, 1576-1582.

Kuligowski, R. J., 2002: A self-calibrating real-time GOES rainfall algorithm for short-term rainfall estimates. *J. Hydrometeor.*, **3**, 112-130.

Kummerow, C.D., Y. Hong, W.S. Olson, S. Yang, R.F. Adler, J. McCollum, R. Ferraro, G. Petty, D.B. Shin, T.T. Wilheit, 2001: The evolution of the Goddard Profiling Algorithm (GPROF) for rainfall estimation from passive microwave sensors. *J. Appl. Meteor.*, **40**, 1801-1817.

Levizzani, V., F. Porcu, F.S. Marzano, A. Mugnai, E.A. Smith and F. Prodi, 1996: Investigating a SSM/I microwave algorithm to calibrate Meteosat infrared instantaneous rain rate estimates. *Meteo. Appl.*, **3**, 5-17.

Marzano, F.S., Palmacci, M., Cimini, D., and F.J. Turk, 2002: Statistical integration of satellite passive microwave and infrared data for high-temporal sampling retrieval of rainfall. *Proc. Int. Geosci. Rem. Sens. Symp.* (IGARSS-2002), Toronto.

Morales, C. and Anagnostou, E.N., 2002: Extending the capabilities of rainfall estimation from satellite infrared via long-range lightning network observations. *J. Hydromet.*, accepted.

Miller, S.W., P.A. Arkin, R. Joyce, 2000: A combined microwave/infrared rain rate algorithm. *J. Rem. Sens.*, XX-XX.

Oh, H.J., B.J. Sohn, E.A. Smith, F.J. Turk, A.S. Seo and H.S. Chung, 2002: Validating infrared-based rainfall retrieval algorithms with 1-minute spatially dense raingauge measurements over the Korean peninsula. *Meteor. Atmos. Physics*, **81**, 273-287.

Schmetz, J., Pili, P., Tjemkes, S., Just, D., Kerkmann, J., Rota, S., Raiter, A., 2002: An introduction to Meteosat Second Generation (MSG). *Bull. Amer. Meteor. Soc.*, **83**, 977-992.

Soman, V.V., J.B. Valdes and G.R. North, 1995: Satellite sampling and the diurnal cycle statistics of Darwin rainfall data. *J. Appl. Meteor.*, **34**, 2481-2490.

Todd, M. C., C. Kidd, D. Kniveton, and T. J. Bellerby, 2001: A combined satellite infrared and passive microwave technique for estimation of small-scale rainfall. *J. Atmos. Ocean. Tech.*, **18**, 742-755.

Vicente, G.A., Davenport, J.C., Scofield, R.A., 2002: The role of orographic and parallax correction on real time, high resolution satellite rain rate observation. *Int. J. Rem. Sens.*, **23**, 221-230.

Vicente, G.A., 1994: Hourly retrieval of precipitation rate from the combination of passive microwave and infrared satellite measurements. Ph.D. dissertation, Univ. of Wisconsin, Madison, WI, USA.

Weng, F., R.R. Ferraro and N.C Grody, 2002: Advances in AMSU non-sounding products. *Proc. 12th Int. TOVS Study Conf.*, 26 February-12 March, Lorne, Victoria, Australia.

The Australian Operational Daily Rain Gauge Analysis

Beth Ebert and Gary Weymouth
Bureau of Meteorology Research Centre, Melbourne, Australia
e.ebert@bom.gov.au

Daily rainfall data and analysis procedure

The Australian Bureau of Meteorology produces objective analyses of daily rainfall that can be used for hydrological applications, validation of model forecasts and satellite rainfall estimates, and climate monitoring. The analyses give accumulated daily rainfall for 00-24 UTC on a 0.25º grid over the land area of Australia. The latitude range of 10ºS to 45ºS allows tropical, sub-tropical, and mid-latitude regimes to be investigated.

Two rainfall analyses are produced, one in near-real time, and the other a few months later. The operational near-real time analysis is based on 9 a.m. gauge observations of 24-hr accumulated rainfall at up to 2000 synoptic and telegraphic stations, and is available a few hours after the observations are made. Figure 1 shows the location of rain gauges in Australia. The populated regions of eastern and southwestern Australia contain high gauge densities, 5-20 per 1º latitude/longitude box, while some desert regions in western and central Australia have few or no gauge observations.

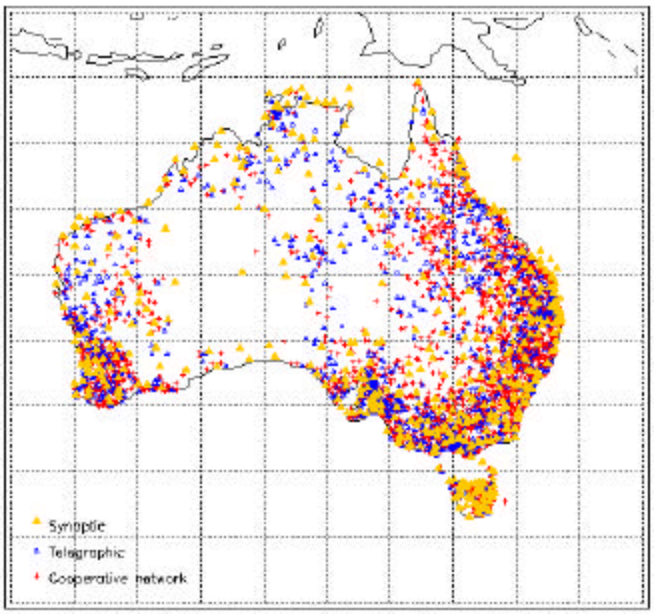

Figure 1. Australian rain gauge locations.

The 9 a.m. LST observation time corresponds to between 22 and 01 UTC, depending on season and time zone. These readings are assumed to approximate the rainfall accumulation between 00 and 24 UTC. Analysis errors associated with the timing mismatch are usually negligible, and tend to be very much smaller than those associated with the satellite estimates or NWP forecasts that they may be used to validate.

After automatic range and buddy checking to eliminate erroneous data, a three-pass Barnes successive corrections scheme is used to map the gauge data onto a 0.25º grid over the land area of Australia (Weymouth *et al*., 1999). Analysis is not attempted in regions with no gauge coverage. The Barnes scheme estimates the rainfall at a gridpoint as a weighted average of surrounding observations, where the weights are inversely related to the distance from the gridpoint using a Gaussian weighting function. The first pass uses a length scale that is large compared with the correlation scale of the data, resulting in a relatively smooth rainfall field. Inner passes, which yield incremental refinements to the initial rainfall field, use shorter length scales so that relatively greater weight is assigned to observations close to an analysis grid point. The inner passes control the level of detail provided in the analysis, effectively acting as a filter for the data.

The operational daily rainfall analyses produced using the 3-pass Barnes scheme have been compared against analyses made using more sophisticated schemes such as Statistical Interpolation (SI) and Indicator Kriging (a scheme that uses IR satellite data to detect rain-free gridpoints before performing a kriging analysis over the remaining area; Sun *et al*., 2002). Results showed that their bias and RMS errors differed by no more than a few percent. For daily rainfall over

Australia (at least), the errors associated with incomplete spatial sampling appear to be much more important than the choice of analysis scheme. These errors are investigated further in the next section.

The more complete "climate" daily rainfall analysis incorporates more than 4000 additional gauge observations from the Cooperative Network (see Fig. 1), and is produced a few months after the event. The gauge density is improved in most regions, increasing to 15-50 per 1º latitude/longitude box in populated areas. The "climate" analysis uses variable, as opposed to fixed, length scales to take best advantage of the improved sampling in data-dense regions. In addition to being more accurate, this analysis product has reduced bias compared to the near-real time product because the observations of zero rainfall from telegraphic stations (normally non-reporting in real time) are included (Weymouth *et al.*, 1999).

Analysis errors

The usefulness of the rainfall analyses is limited without some knowledge of their expected errors. This is important for using these rainfall estimates in data assimilation and merging schemes, estimating uncertainties in hydrological or other products that may use rainfall data as input, and properly accounting for uncertainty in "ground truth" when validating other precipitation estimates (e.g., Krajewski *et al*., 2000). In this section we present some results from an investigation on the accuracy of daily rainfall analyses produced using an experimental SI scheme. As previously mentioned, the analysis errors differed little from those of the 3-pass Barnes scheme, so the following results can be taken as representative of the operational products.

The magnitude of the analysis errors depends to a large extent on how well the observational network samples the natural variability of the rainfall. In Australia the correlation length scale (where $r(x)$ drops to $1/e$ $r(x=0)$) is about 350 km in winter, when most Australian rainfall is associated with mid-latitude synoptic scale systems, and decreases to around 110 km during tropical summer, when convection is the primary regime. This means that in order to adequately sample daily rainfall, stations should be closer together in the tropics than elsewhere (unfortunately not the case, see Fig. 1). As a result analysis errors are expected to be larger there than in other regions and seasons.

Cross-validation techniques are commonly used to compute statistics of analysis errors at the point scale. Unfortunately, direct calculation of *grid-scale* analysis errors requires large numbers of independent observations. However, by making some reasonable assumptions about the independence of analysis errors, it is possible to use an error separation method similar to that described in Krajewski et al. (2000) to estimate their magnitudes.

Suppose two independent analyses X_1 and X_2 are produced by randomly dividing the spatial observations in half and analysing each set separately. The variance of their difference is

$$\begin{aligned} \mathrm{var}(X_1 - X_2) &= \mathrm{var}[(X_1 - X_t) - (X_2 - X_t)] \\ &= \mathrm{var}(X_1 - X_t) + \mathrm{var}(X_2 - X_t) - \mathrm{cov}[(X_1 - X_t), (X_2 - X_t)] \end{aligned}$$

where X_t is the true value and $(X_1 - X_t)$ and $(X_2 - X_t)$ are the (unknown) analysis errors. We can expect the analysis errors to be independent of each other, since they were generated from different observations. This means we can neglect the covariance term. Given the parallel method of producing the two analyses, we can also expect that their error variances are approximately equal, i.e., $\mathrm{var}(X_1 - X_t) = \mathrm{var}(X_2 - X_t)$, and, for a sufficiently large observational dataset, a reasonable approximation to $\mathrm{var}(X - X_t)$, the error variance of the analysis based on all data. We thus arrive at a simple approximation for the analysis error variance,

$$\mathrm{var}(X - X_t) = \mathrm{var}(X_1 - X_2) / 2 \, .$$

The standard error is the square root of the variance, normalized by the mean value.

This approach was used to estimate analysis errors for the Australian rainfall data. Figure 2 shows the analysis standard error s/R decreasing with increasing station density as spatial sampling is improved. It also decreases with increasing rainfall accumulation. Similar behaviour was demonstrated by Huffman (1997) and others for satellite precipitation analysis errors.

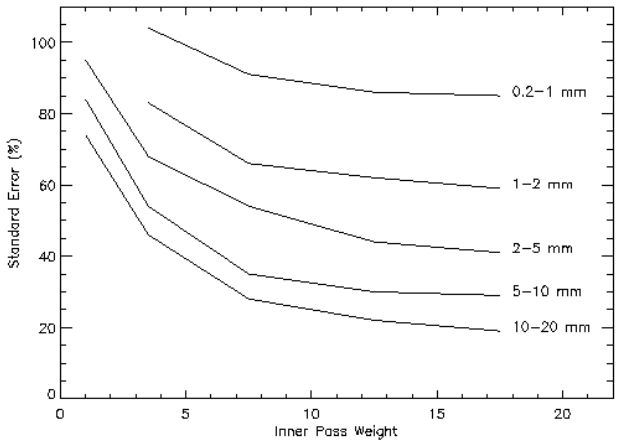

Figure 2. Standard error (%) in 0.25º grid boxes as a function of summed inner pass weight from the Barnes analysis (related to station density), for five ranges of daily rainfall accumulation.

The percent standard error in Fig. 2 can be empirically fit by a function of the form,

$$\frac{s}{R}(\%) = a + b \ln W + cR^{-1/2}$$

where W is the summed inner pass weight, R is the analysed rain accumulation, and the coefficients have the values a=65, b=-21, and c=50. This expression can be used to generate error estimates to accompany the rainfall analyses.

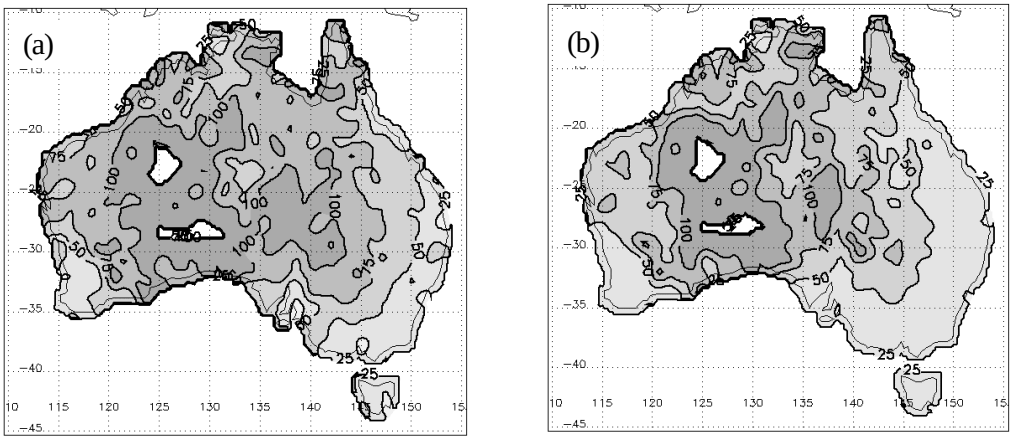

Figure 3. Annual mean analysis error standard deviation, expressed as a percentage of annual mean rain during January-December 2000, for (a) near-real time daily analyses, and (b) "climate" daily analyses.

The spatial distribution of analysis errors (Figure 3) shows that the standard errors average between 25% and 50% in eastern and far southwestern Australia, but can exceed 100% in the sparsely sampled regions of central Australia. Tropical values range between 50% and 100%, with lower errors in the "climate" daily analyses than in the near-real time analyses. Note that errors on any given day are likely to be much lower, or even zero, in areas with no observed rainfall, or much higher in the case of regions with convective rainfall.

The analysis errors can be reduced somewhat by spatial averaging. Because the rain field is spatially correlated, the error reduction is less than would be predicted for independent samples. For the Australian analyses, averaging from a 0.25º grid scale to a 1º grid scale decreases the analysis errors by only about 25%.

Future work

BMRC is working toward producing a combined rain gauge-radar analysis over Australia on hourly and daily time scales. The greatest improvements in the daily rainfall analyses are expected to be in the coastal regions of western and tropical Australia that have radar coverage.

Recommendations

1. Make use of Australian gauge data and gridded analyses for hydrological applications, validation of NWP forecasts and satellite precipitation estimates, and climate monitoring.

2. Provide error estimates with the analyses, to assist users in making the most sensible use of the data.

3. Encourage the development and use of validation methodologies that account for the uncertainties in the "ground truth" data.

4. Make use of the full gauge "climate" Australian dataset, not just the values put out on GTS, in producing merged rainfall analyses.

Obtaining Australian daily gauge data and gridded analyses

The near-real time daily rain gauge data and gridded analyses can be downloaded via FTP from the Bureau of Meteorology's National Climate Centre at the URL,

ftp://ftp.bom.gov.au/anon/home/ncc/www/rainfall/totals/daily.

The more complete "climate" rain gauge data and analyses, based on up to 6000 observations per day, can be obtained on request from the first author.

References

Huffman, G.J., 1997: Estimates of root-mean-square random error for finite samples of estimated precipitation. *J. Appl. Meteor.*, **36**, 1191-1201.

Krajewski, W.F., G.J. Ciach, J.R. McCollum, and C. Bacotiu, 2000: Initial validation of the Global Precipitation Climatology Project monthly rainfall over the United States. *J. Appl. Meteor.*, **39**, 1071-1086.

Sun, X., M.J. Manton, and E.E. Ebert, 2003: Regional rainfall estimation using double-kriging of raingage and satellite observations. *BMRC Research Report No. 93*, 41 pp.

Weymouth, G., G.A. Mills, D. Jones, E.E. Ebert, and M.J. Manton, 1999: A continental-scale daily rainfall analysis system. *Australian Meteorol. Mag.*, **48**, 169-179.

Towards an Adaptive Method for Spatial Interpolation of Global Rain Gauge Data

Reading, March 11-13, 2003

Jürgen Grieser

Global Precipitation Climatology Centre
Deutscher Wetterdienst, P.O.Box 10 04 65, 63004 Offenbach, Germany
Juergen.grieser@dwd.de

Introduction

Gridded precipitation data are important information for many applications. The analysis of droughts and floods are only two examples.

The quality of estimated precipitation fields depends on many influences. From a pure climatological view the precipitation pattern consists of a deterministic and a stochastic part. The first should be subject to deterministic methods, whereas the latter should be subject to geostatistical methods. Both kinds of methods should be flexible to deal with the regional climatic and geographic conditions as well as with the station density provided.

The Global Precipitation Climatology Center (GPCC) has a large database of monthly precipitation data (over 50.000 stations worldwide). These data are thoroughly tested for outliers as well as errors in the station meta data like location and elevation. For the main portion of these stations precipitation data are available since 1986. However, for some 1000 stations also longer time series are acquired.

Aims of the new Project

It is one aim of a current project to use this large and quality controlled database to achieve more information about the optimal way to interpolate monthly global precipitation fields over land, with special regard to the different climatological and geographic conditions as well as station density. Furthermore, this knowledge finally may result in long time series of best estimates of gridded worldwide precipitation data as well as estimates of their uncertainty.

In a first step local altitude dependencies are estimated and averaged for the Koeppen climate zones each by each and for each calendar month see (Fig. 1). Furthermore, averaged local horizontal climate gradients are estimated for different regions and seasons. As a result it can be seen that the deterministic portion of spatial variability depends on the season and region under investigation. This reveals that it should not be neglected as part of the interpolation procedure. However, the actual altitude dependency depends strongly on the local. Therefore, the altitude function has to be fitted for each grid point and month.

In a second step the empirical semivariograms are calculated again for the different climate zones and calendar months. This gives the opportunity to learn about the regional and seasonal scales of precipitation. A comparison of these scales with the regional effective station distance should reveal information about the sampling error. Eventually this may be used to learn about the station density necessary to obtain reliable estimates under certain conditions.

In a third step different geostatistical methods are intercompared for well defined artificial spatial patterns (see Fig. 2). This allows to investigate how well different patterns are reproduced by different methods. Also from this artificial examples information can be drawn about the impact of different station densities and distributions, given different methods of interpolation. As a result this step should offer enough information to decide which method provides the most reliable gridded data. Furthermore it may provide the information necessary to investigate the average error of the method under certain conditions.

Another point under investigation is the station distribution as well as the amount of stations used to interpolate a grid point value. Though more data means a better statistical basis, it also means that more distant stations have to be taken into consideration. With respect to this, more data does not necessarily mean better results. Experiments are planned to get the optimal number of stations to be used or the optimal distance up to which stations should be taken into account.

By means of a shadow correction stations hidden behind other stations should get less weight in the averaging procedures compared to stations that represent a large portion of a grid points neighbourhood. First experiments reveal that this leads to a further improvement of the gridded data.

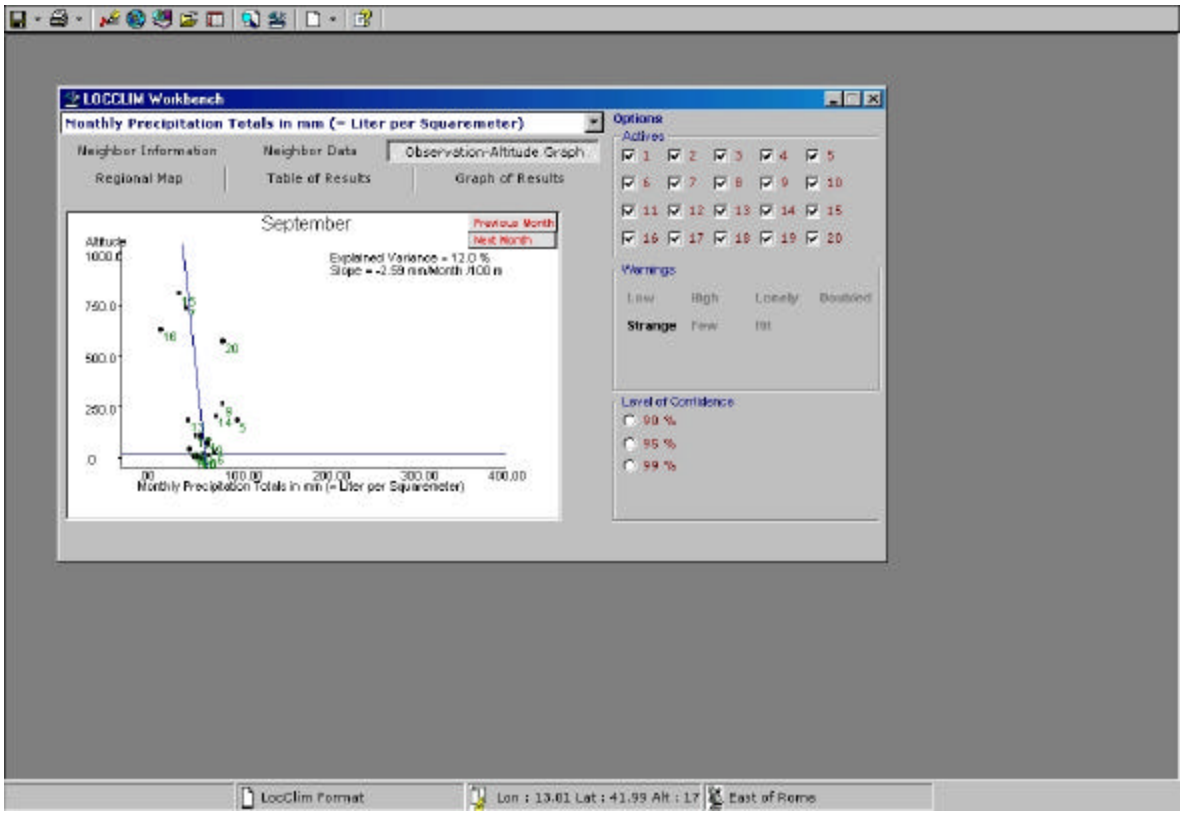

Figure 1: Investigation of local altitude dependence of precipitation. In this example the altitude dependence explains about 12% of variance. Outliers are detected and marked as strange data.

Dubious data, which may not fit to the group of neighbouring stations should be indicated and treated separately. We saw that dubious data can be found by a simple cross check.

Furthermore, the jackknife error should be given for all the estimates in order to provide a measure for the accuracy of the actually interpolated value.

Finally all the information gathered from the experiments will be used to obtain an adaptive interpolation procedure to optimally fit the local and seasonal climatic conditions, the given station densities and the geographic margins best.

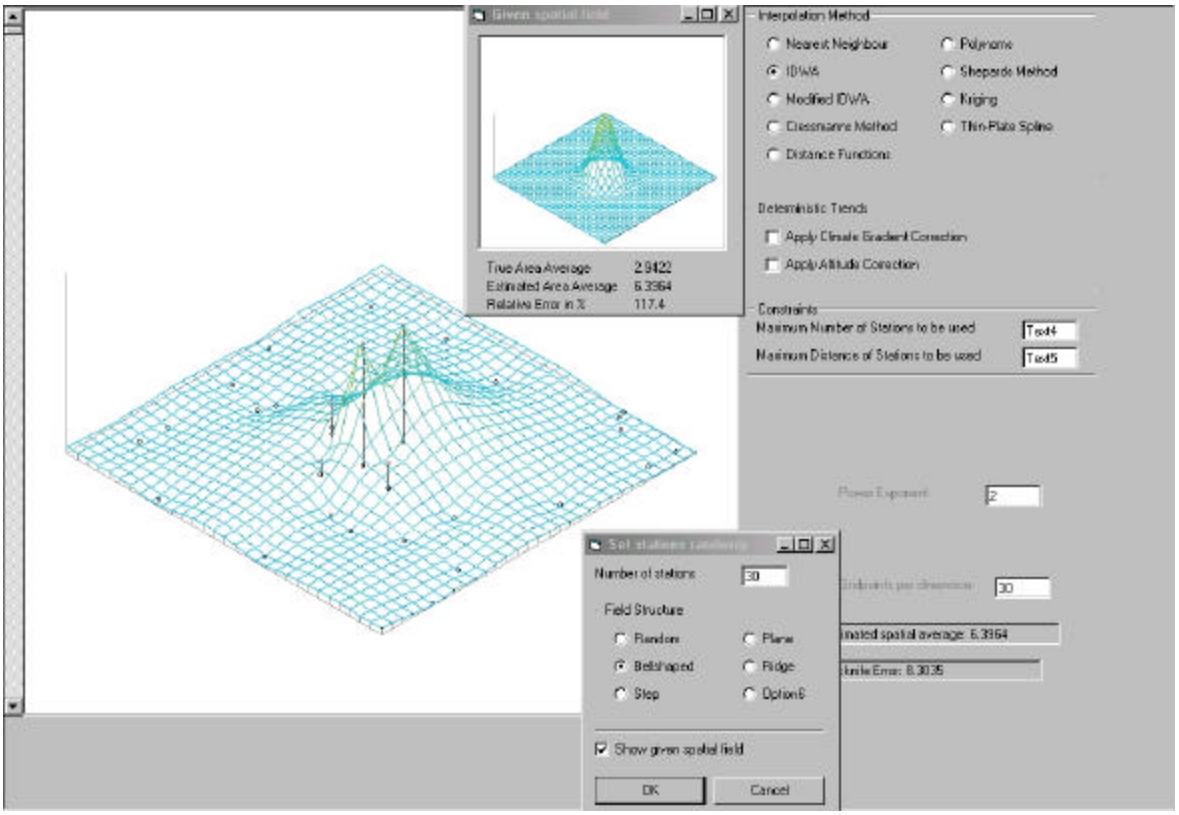

Figure 2: Investigation of the influence of station density and interpolation method. For the example of a bell shaped precipitation pattern and effective station distances equal to the scale of the bell the regional precipitation is overestimated by a factor of 2. Moreover, the shape is not correctly reproduced.

STRATEGY OF ERROR ANALYSIS AND REDUCTION IN THE PERSIANN SYSTEM

X. Gao, S. Sorooshian, and K. Hsu
Dept. of Hydrology and Water Resources
University of Arizona, Tucson, AZ, USA

ABSTRACT

Error analysis and reduction for satellite-based global precipitation data become increasingly important with the growing availability and popularity of such data. At the University of Arizona (Tucson, AZ USA), a system of Precipitation Estimation from Remotely Sensed Information using Artificial Neural Networks (PERSIANN) has been developed to provide global, real-time precipitation monitoring at relatively high temporal and spatial resolutions (6-hourly and $0.25^\circ \times 0.25^\circ$) using information from multiple sensors and multiple satellites. (http://www.hydis.arizona.edu). A strategy for PERSIANN data quality control and improvement has been made to guide our ongoing research. In this workshop, our discussion focuses on the "error estimation" of the PERSIANN data that is defined as the PERSIANN precipitation estimates associated with the observations (i.e., $P_{est} - P_{obs}$). Another equally important issue about the "observation error" (i.e., $P_{obs} - P_{true}$) will not be discussed here. However, according to following relation:

$$(P_{est} - P_{true}) = (P_{est} - P_{obs}) + (P_{obs} - P_{true}) \quad (1)$$

(Estimation Error of Rain) = ***(Error Estimate)*** + ***(Observation Error of Rain)***

"error estimate" will lost its significance to represent the "estimation error of rain", if the "observation error of rain" is large and unknown.

In order to conduct qualified error analyses, we plan to use 15 validation sites worldwide (Fig. 1); each of these observation sites have an area size greater than $0.25^\circ \times 0.25^\circ$ and include continuous radar and/or rain-gauge rainfall data for three months. For gauge-only sites, we also require at least 30 rain gauges per $0.25^\circ \times 0.25^\circ$ square area. The validation problem becomes even serious over oceans and mountains because of the lack of reliable ground-based measurements. Precipitation radar (PR) onboard the TRMM satellite provides unique data for the cross-examination of satellite precipitation estimates (in case the PR data have yet been used in the algorithms). Fig. 2 illustrates the sampling frequency of TRMM/PR in June 1999, in which most equatorial areas only receive less than 15 (instantaneous) overpasses per month, and the number of sampling increases to about 30 times per month toward the edges of the PR coverage area. Such low-sampling frequency is the key issue unsolved for the error estimate of satellite rainfall.

Two categories of investigations are planned to evaluate and enhance the PERSIANN data quality: (1) the statistical analyses of the PERSIANN data, and (2) the model (system) analyses, namely the selection and classification of input variables used to retrieve surface rainfall and the model structure. Model analysis is a significant issue, but will not be discussed here.

The statistical analyses include two successive procedures of bias analysis and variance analysis. In comparison with GPCC global (monthly, $1^\circ \times 1^\circ$ gridded) rain-gauge data, systematic positive bias (overestimation) was discovered in the PERSIANN rainfall estimates over land. Using ratios of concurrent GPCC and PERSIANN rainfall amounts at monthly, $1^\circ \times 1^\circ$ resolution as the correcting factors, the biases of PERSIANN estimates at different resolutions are adjusted proportionally. In Fig. 3, the NEXRAD rainfall data (NCEP/Stage IV, in July and August 2001) over the continental United States within the domain of 20°N-50°N, 80°W-120°W are used as independent references to evaluate the RMSE (Root Mean Square Error) and bias of the PERSIANN daily and $0.25^\circ \times 0.25^\circ$ estimates. The results indicate that the simple process is effective and necessary for the PERSIANN data, especially when the correcting ratios are large, such as in the month of July.

Preliminary variance analyses for the PERSIANN data explored certain important features common to satellite rainfall estimates. (a) Variance of rainfall estimates increase with the estimated rain rates. Based on this feature, rainfall estimation algorithms should apply different input-rainfall retrieval relations within different ranges of rain rate. Fig. 4a illustrates that, as the variation range of infrared brightness temperature (the major input variable of PERSIANN) is divided into smaller subdivisions, the estimated rain rate (mean) becomes more specified, and the estimation uncertainty (standard deviation) is also changed. In Fig. 4, each time an interval of brightness temperature is divided into two subdivisions, the mean and standard deviation in the colder subdivision (on the left side) increase, while both values in the warmer subdivision decrease. This indicates that the variance of estimates monotonically increases with the mean value of the rainfall estimate. Fig. 4b shows that the variance over the entire range is improved slightly with the increase of the subdivision number, especially when the split is made in high standard deviation intervals. Therefore, more

research attention should be paid on intensive rainfall estimation. Fig. 4b also shows that, when the input is improved by adding visible cloud images, the variance reduces substantially. (b) Variance of estimate can be reduced through averaging rainfall over time and space scales. In an experiment, the PERSIANN data over three $4^\circ \times 4^\circ$ areas (Fig. 5) are averaged from daily and $0.25^\circ \times 0.25^\circ$ resolutions down to monthly and $1^\circ \times 1^\circ$ through a series of spatial and/or temporal integrations. The variances calculated from different scales are plotted, which forms a similar monotonic 2D surface in the time and space coordinates for each individual area. In Fig. 5, the variance of rainfall estimate is quasi-linearly reduced over spatial average, while the variance shows sharp reductions from 1- to 5-day integrations, and a stable, decreasing gradient from 10-day or longer integrations. Obviously, this is good news for large-scale climate analysis; however, it should be mentioned that the major reason for the uncertainty improvement is because of the involvement of a large number of no-rain events through the average, and that information about the distribution of high rainfall intensity has been smoothened through the same processing.

In summary, variance analysis for unbiased data is the basis for many statistical techniques of error analysis, such as merging of multiple precipitation data sets, optimal interpolation, Kalman filtering, and variational approaches. Quantitative characterization of variance in satellite rainfall estimates in different conditions and at different scales provides the much-needed information for the scientific uses of these data in the methodology of comparison, validation, and assimilation.

ecipitation Climatology Centre

r Wetterdienst

Operational processing, quality-control and analysis of precipitation data at the GPCC

Udo Schneider and Bruno Rudolf, Deutscher Wetterdienst, Offenbach a.M., Germany

1 Background and objectives

The main task of the GEWEX Global Precipitation Climatology Project (GPCP) is the compilation of global gridded precipitation data sets on the basis of the available observing systems, i.e. conventional surface networks and remote sensing data. The products are required for verification of global climate model simulations, the investigation of climate variability and special phenomena such as El Niño/Southern Oscillation, as well as the determination of the Earth's water balance and budgets (WCRP, 1990).

The GPCC (Global Precipitation Climatology Centre) is the in-situ component of the GPCP. Its function within GPCP is the analysis of global land-surface precipitation by interpolation of raingauge data on an operational basis. The specific requirements are:

- High accuracy of the gridded results (desired error of monthly precipitation totals < 10%),
- Gridded analysis results are accompanied by information on analysis quality/error estimates.

The major problems in this context are:

- Errors in the reported precipitation data and station meta information,
- Sampling errors (depending on the variability in the precipitation field and the density of the station network),
- Systematic errors in raingauge-measurements.

Dealing with the difficulties mentioned above the following points are very important:

- A thorough quality-control (QC) of precipitation data and station meta information,
- A high density and a good spatial coverage of the station network,
- Analyses have to be corrected for the systematic gauge-measuring error.

2 GPCC data base

In-situ rain gauge measurements still provide the most reliable information to analyse area-mean precipitation for the land-surface. All station meta data, as well as the precipitation data are archived in an Oracle-based relational data base management system (RDBMS). In merging the data from different sources the quality-control (QC) and harmonization of the station meta information is crucial. A thorough QC is necessary to detect errors in the station meta data (especially geogr. coordinates) and a harmonization is required to ensure consistency of time series and to avoid dublettes, as far as possible, in the merged data set.

2.1 Near real-time GTS data

Via the WMO World Weather Watch Global Telecommunication System (GTS) data can be obtained near real-time from synoptic weather reports (at least with a daily resolution) and monthly climate reports. Monthly precipitation data are routinely obtained at GPCC from 3 sources: (1) monthly totals calculated at GPCC from SYNOP reports received at DWD, Offenbach, (2) monthly CLIMAT reports received also at DWD, Offenbach, and (3) monthly totals calculated at CPC/NCEP from SYNOP reports received at NCEP, Washington DC.

The data from these sources, which are checked and merged by GPCC in order to improve the spatial coverage and data quality, form the basis of its monitoring of global monthly precipitation (see section 5). The total number of stations with monthly precipitation data available via GTS has somewhat increased over time and has reached ca. 7,000 stations during recent years (Fig. 1, left).

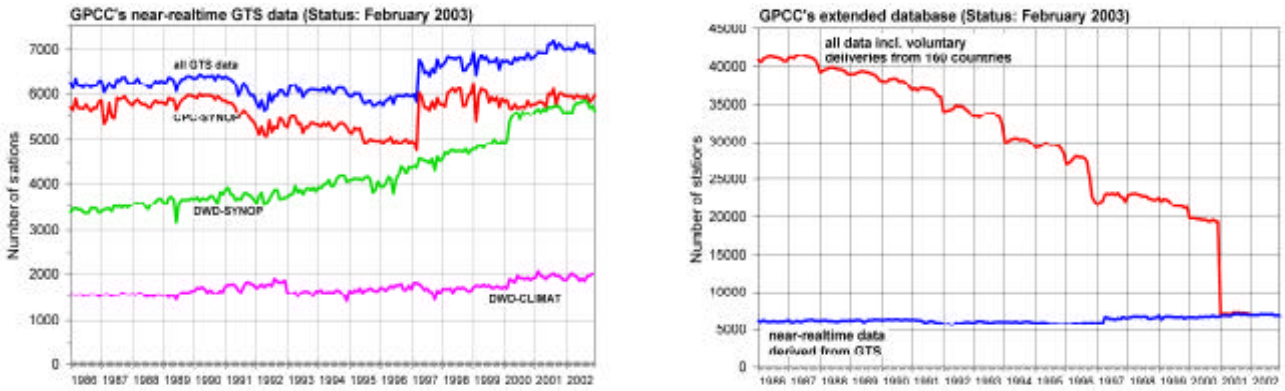

Fig. 1: Availability of precipitation data as a function of time since 1986 for (left) the data received via GTS and (right) GPCC's full data base including the delivered national/regional data collections.

2.2 GPCC's Full data base

Owing to the large variability of precipitation in space and time the GPCC is acquiring additional precipitation data from national weather services, hydrological institutes etc. to enlarge the data base. So far, institutes from about 160 countries have supplied additional data on a voluntary basis, following WMO requests and bilateral contacts of GPCC. GPCC's full data base includes monthly precipitation totals of more than 50,000 stations for which any monthly precipitation data are available in the period since 1986. According to the GPCP Implementation and Data Management Plan (WCRP, 1990) 1986 originally was defined as the starting year for the evaluation period.

The year with the best data coverage is 1987 with data of ca. 41,000 stations available. The decrease during the last years (ca. 28,000 stations in 1995, less thereafter) is caused by the delay of the data delivery and the time required by the GPCC to process and check these data sets before loading them into the RDBMS .

2.3 Historical extension of GPCC's data base

Following recommendations from GCOS, GEWEX and CLIVAR the GPCC is working on the historical extension of its data base. Therefore GPCC, in co-operation with the University of Frankfurt a.M., in Oct. 2001 started a research project*[10] „Variability Analysis of Surface Climate Observations" (VASClimO), which is aiming at the following main goals:

- the compilation of a comprehensive global climate data base for precipitation, snow cover, surface air temperature (average and extremes) and mean sea level pressure, including existing historical data collections and additional data to be acquired (performed at GPCC) and
- a detailed statistical analysis of the data set (mainly performed at Univ. Frankfurt a.M.).

The subproject at GPCC can build upon the data base available at the GPCC consisting of precipitation data and meta data of more than 50,000 stations world-wide. However, most of the time series start as late as 1986. Some large data collections already available at GPCC, such as from CRU (Univ. East Anglia, Norwich, UK), GHCN (NCDC, Asheville, NC) and FAO (Food and Agriculture Organization of UN, Rome, Italy) are including a large amount of historical climate data. These data collections will be integrated into the GPCC data base to cover also the historical period (Fig. 2). Some time series are even extending back to the early 18th century.

*[10] *The project is sponsored within the German Climate Programme (DEKLIM) by the Federal Ministry for Science and Education of Germany.*

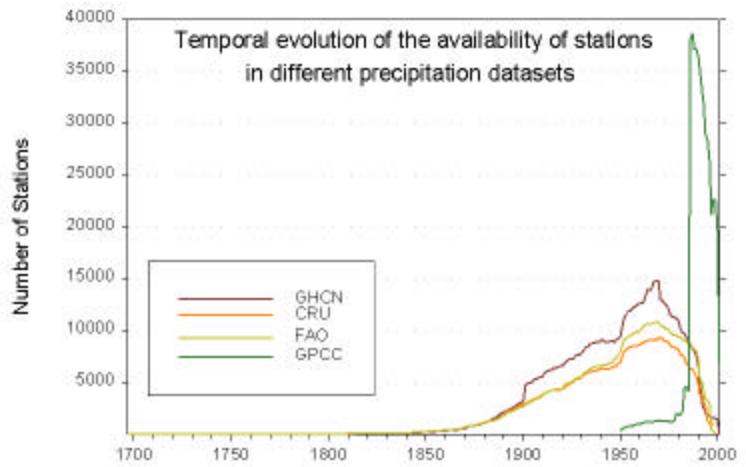

Fig. 2: Availability of precipitation data (number of stations with full year of data) as a function of time for the GHCN, FAO and CRU precipitation data set, as well as for the GPCC data base.

These data sets are currently quality-controlled and loaded into the database (11,868 precipitation time series from CRU, 22,654 precipitation and 7,280 temperature time series of the GHCN, as well as 13,530 precipitation and 5,996 temperature time series of the FAO). Checking the historical data collection from CRU and loading into the GPCC data base has almost been completed. Several significant errors in the station meta data have been detected and could be corrected (examples are given in section 3 and in the presentation). Checking the station meta information of the other historical data collections and loading them into GPCC's data base is in progress.

3 Quality-control and harmonization of station meta information

The GPCC has developed a quality-control (QC) system consisting of different levels. The focus here is lying on the QC of the station meta data. The first step is a pre-control of the station coordinates performed during the pre-processing and reformatting of the individual national/regional data sets and updates delivered to the GPCC using the software CLIDAVIS displaying the station locations and country borders. Station co-rdinates of the global data collections can be controlled using a polygon check method testing whether the stations of a country are lying within the polygons representing the border of the corresponding country or not.

The central element in checking the meta information (especially the geogr. coordinates) of the stations is the intercomparison of the meta data in the input data files with the station catalogue (more than 50.000 stations) included in the RDBMS during the loading process. The procedure for this will be presented at the meeting and is briefly outlined in the following.

First each station record in the input data file undergoes a check of the validity of the geogr. coordinates, elevation and the country code (Alpha3-code). For each station record in the input data file similar stations are selected from the data base (DB) system. If the station meta data (WMO-ID, Nat. No., geogr. coordinates, name) is identical and the elevation of the DB station is within +-10 m of the station elevation in the data file being loaded, the data are assigned automatically to the corresponding DB station.

Alternatively the selected similar stations are grouped according to the degree of similarity in an "Inner Pool" (stations with good agreement) and an "Outer Pool" (stations with less good agreement). These data pools are evaluated further. In case of a very close matching with the DB stations (i.e. in the geogr. coordinates a difference of 0.01° is tolerated) the data are assigned to the corresponding DB station.

If there is no station with similar meta information in the DB system and no station in the vicinity, a new station record is inserted into the DB.

However, in many cases only part of the station meta information in the input data set is identical to that of DB stations, whereas part of the information differs (for example due to typing errors or rounding effects in the geogr. coordinates, a different spelling of station names etc.). These unclear cases station ("UCS") have to be clarified manually. The procedure displays all stations with similar meta data selected from the DB on a screen. Then an expert has to decide whether the data can be assigned to a DB station or if a new station record has to be inserted. In some cases the meta information in the data base has to be corrected; however in most cases where discrepancies occur these can be attributed to erroneous meta data in the input data sets. All manually clarified cases with an assignment to a DB station are stored in the UCS library, so that the system is learning and exactly the same case hasn't to be treated again.

4 Method used for operational analysis of precipitation at GPCC

GPCC is using a spherical adaptation of SPHEREMAP (Shepard, 1968) for applications on a global scale (after Willmott et al., 1985) for the interpolation of the irregularly distributed raingauge measurements to a regular grid (0.5° resolution). The interpolation method is based on an inverse distance weighting scheme, taking the directional distribution (clustering) of stations also into account.

Following external studies (Legates, 1987, 1991; Bussieres and Hogg, 1989) and internal intercomparison studies (Rudolf et al., 1992, 1994) the SPHEREMAP method was selected and implemented at GPCC in 1991 for operational objective analysis of global precipitation. These studies indicated the SPHEREMAP method being particularly suitable in analysis of global precipitation climatologies. In an intercomparison study of 4 different interpolation schemes (Bussieres and Hogg, 1989) it was the best of the empirical schemes and did a job almost as well as Optimum Interpolation.

The construction of gridded fields of area-average precipitation consists of 2 major steps: (1) interpolation of the irregularly distributed raingauge observations onto points of a regular grid and (2) to convert the grid point values to area-averages for each grid box. The area-average precipitation on a 0.5° grid is calculated by averaging the grid point values at its 4 corners. Area-average precipitation on a coarser grid (1° or 2.5°) is then calculated as the area-weighted average over the corresponding 0.5° grids.

5 GPCC products

Near real-time "Monitoring Product"

The "Monitoring Product" is based on data received via the WMO GTS (ca. 7,000 stations, details see section 2.1). These global analyses of monthly precipitation are generated on a 1° and 2.5° grid and form the in-situ basis of the combined satellite-raingauge data sets of the GPCP (Huffman et al. 1997). Generally the analysis procedure (including a high-level quality-control) is continuing on a routine monthly basis and the monitoring product is available about 1 to 2 months after the observation period. The "Monitoring Product" is now covering the period January 1986 up to Dec. 2002 and can be downloaded via Internet using the redesigned GPCC-Visualizer:
http://gpcc.dwd.de/visu_gpcc.html

Non real-time "Full Data Product"

A re-analysis based upon the full data base („Full Data Product") has been carried out for the period January 1986 up to December 1995 (ca. 28,000 to 40,000 stations). The results have been calculated on a 0.5°-grid (and 1°-grid) and have been provided to NASA/GSFC for publication on the ISLSCP-II initiative CD-ROM. After future expansions of the data base the re-analysis will be repeated from time to time. A comparative analysis to the Monitoring Product has been performed (section 6).

Both products up to now are accompanied by bulk correction factors to compensate for the systematic gauge-measuring errors, that have been derived by Legates (1987) for climatological conditions. An improved method for the correction of the systematic gauge-measuring error taking into account the weather conditions during the given month is in work.

6 Intercomparison of "Monitoring Product" and "Full Data Product"

The precipitation differences between both products are large where the precipitation itself or the gradient is large, and where the "Full Data Product" is based on significantly more rain-gauges than the "Monitoring Product". In Fig. 4 area-average monthly precipitation for the earth's land-surface is shown for the "Monitoring Product" and the "Full Data Product" over the period Jan. 1986 to Dec. 1990. The area-average monthly precipitation for the "Full Data Product" is always slightly higher (up to ca. 5%) than for the "Monitoring Product". One reason may be that the heavy rainfall events, which generally are quite local in extent, are depicted better by a dense station network. Regional differences vary largely depending on the station density (number of raingauges per grid) and the location. This emphasizes the importance of a high density of the station network, too.

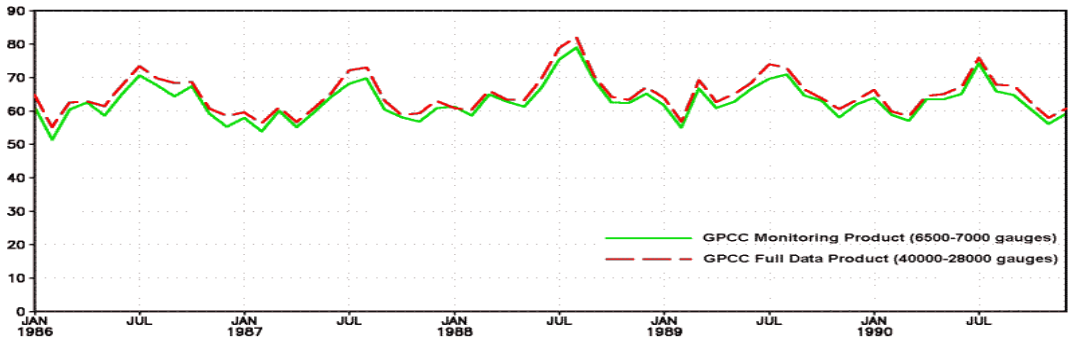

Fig. 4: Area-average monthly precipitation for the earth's land-surface for the "Monitoring Product" and the "Full Data Product" over the period Jan. 1986 to Dec. 1990.

7 Conclusions

Experience of GPCC with the processing and evaluation of the many national or regional data sets received, as well as of the global data collections (i.e. CRU, FAO, GHCN) shows that a *thorough QC not only of the precipitation (climate) data, but also of the station meta data is crucial*, because of frequently occuring errors.

Very important in this context is also the *harmonization of station meta data in merging the data sets from different sources* to ensure consistency of time series and to avoid dublettes, as far as possible, to get the best possible data base.

Compensation of the systematic gauge-measuring error is important in conventional measurements.

The *analysis method* SPHEREMAP is in operational use at GPCC since ca. 10 years. The GPCC is planning to implement a new analysis method; the selection of a new analysis technique has to be based upon statistical investigations and intercomparison studies. The meeting will be very helpful in this process. However, a new analysis technique has to be suited for operational application and the analyses for the "Monitoring Product" and the "Full Data Product" will have to be repeated then using the new methodology to create consistent data sets.

References

Bussieres, N. and W. Hogg (1989): The objective analysis of daily rainfall by distance weighting schemes on a mesoscale grid. *Atmos. Oceans*, **27**, 521-541.

Huffman, G.J., R.F. Adler, P.A. Arkin, A. Chang, R. Ferraro, A. Gruber, J. Janowiak, A. McNab, B. Rudolf and U. Schneider (1997): The Global Precipitation Climatology Project (GPCP) Combined Precipitation Dataset. *Bull. American Meteor. Soc*., **78**, 5-20.

Legates, D.R. (1987): A climatology of global precipitation. *Publ. in Climatology* **40** (1), Newark, DW, 85 pp.

Legates, D.R. (1991): Personal communication.

Rudolf, B., H. Hauschild, M. Reiss and U. Schneider (1992): Beiträge zum Weltzentrum für Niederschlagsklimatologie – Contributions to the Global Precipitation Climatology Centre. *Meteorol. Zeitschrift N.F.*, **1**, 7-84.

Rudolf, B., H. Hauschild, W. Rueth and U. Schneider (1994): Terrestrial precipitation analysis: Operational method and required density of point measurements. NATO ASI series, **I 26**, 173-186.

Shepard, D. (1968): A two-dimensional interpolation function for irregularly spaced data. *Proc. 23rd ACM Nat. Conf.*, Brandon/Systems Press, Princeton, NJ, 517-524.

WCRP (1990): The Global Precipitation Climatology Project - Implementation and Data Management Plan. WMO/TD-No. 367.

Willmott, C.J., C.M. Rowe and W.D. Philpot (1985): Small-scale climate maps: A sensitivity analysis of some common assumptions associated with grid-point interpolation and contouring. *Amer. Cartogr.*, **12**, 5-16.

More information about GPCC: http://gpcc.dwd.de

Characteristics of Precipitation as Observed by TRMM PR

Yukari N. Takayabu
Center for Climate System Research, University of Tokyo
4-6-1 Komaba, Meguro-ku, Tokyo, JAPAN Email: yukari@ccsr.u-tokyo.ac.jp

1. Introduction

Tropical Rainfall Measuring Mission (TRMM) satellite launched in December 1997 is equipped with the first space-borne precipitation radar (PR). There are several advantages of TRMM PR. First of all, it provides three dimensional rainfall structures, which enables more accurate classification of convective and stratiform rains than before. Secondly, since TRMM is unsyncronous with the sun, it can observe diurnal cycle of the precipitation.

Figure 1 shows three-year average diurnal cycles of rain in the equatorial belt of 10N-10S, analyzed separately for those over ocean and those over land (Takayabu, 2002). It was indicated that with a 0.3mm/hr rain-top detection thresholds, convective: stratiform ratio in total rain are 50:50 over ocean, and 63:37 over land at the 2-4km level. Stratiform clouds at these latitudes consists primarily of anvil clouds of mesoscale systems. It was also noticed that convective and stratiform rains over ocean experience almost synchronous diurnal cycle with a maximum in the early morning and a minimum in the afternoon. Over land, on the other hand, a significant afternoon peak in convective rain corresponds to the afternoon shower, but the stratiform rain does not have the corresponding increase in the afternoon but has a maximum in the midnight. These results indicate that rain over ocean is dominated by well organized mesoscale convective systems as shown by previous studies (e.g. Houze, 1977, Nesbitt et al. 2000), while that over land consists of two types of rain; one is the afternoon shower which is not as well organized as mesoscale systems, and the other is organized systems which is enhanced from midnight to early morning. The emphasis of this analysis is on the quantification of precipitation characteristics.

In this report, we aim to examine regional and seasonal variations of rain characteristics, focusing on several indices which became available with TRMM PR; stratiform rain fraction, convective/stratiform rain intensity, convective/ stratiform rain area, etc.

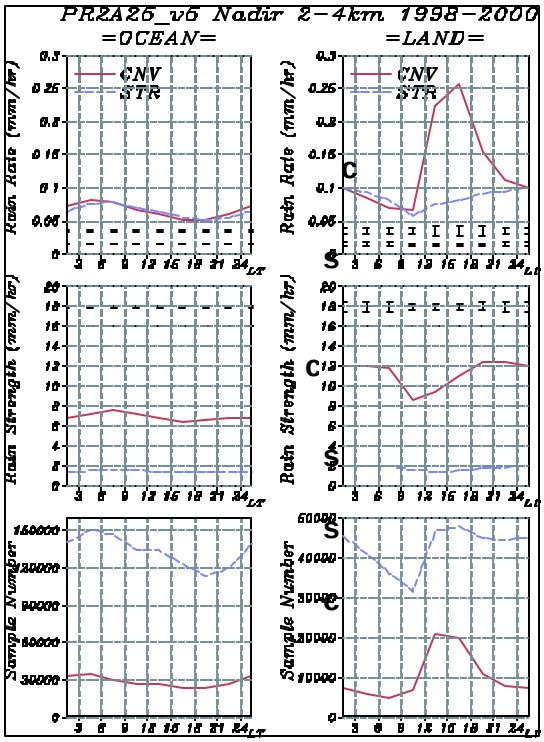

Fig. 1 Mean diurnal variation of the convective rain (solid lines) and of the stratiform rain (broken lines) for the oceanic pixels (left) and for the land pixels (right). The middle panels show the conditional mean diurnal variations under the condition of the pixels are rainy. The bottom panels show the sampled numbersfor each classes. Error bars indicate the 99% confidence intervals but plotted away from the mean values, not to obscure the mean values.

2. Data

In this study, rain rate profiles, rain flags, and method flags obtained from TRMM PR2a25 version 5 archives are utilized. Rain rate data consist of 80 vertical levels from 250m to 20,000m with a vertical resolution of 250m. Classification of rain basically follows rain flags which is determined in the PR2a23 algorithm based both on vertical method with bright-band detections and on horizontal method. Note that an alteration of the flag from the shallow sporadic stratiform rain to shallow convective rain is made, following the indication by Schumacher and Houze (2002, personal communication). Method flags are used to obtain the surface information. Rainy columns are distinguished with a rain-top threshold of 0.3 mm/hr. Most of the statistics in this report are done with only nadir data among 49 rays, except for Fig.2 which consists of all 49 ray data.

Analysis period is three years from 1 January 1998 to 31 December 2000. From January to May 1998 is in the midst of 1997/98 El Nino period. EC MWF operational analysis data for the same period are also utilized to examine the background meteorological conditions.

3. Seasonal Variations in Stratiform Rain Fraction

It has been shown that the stratiform rain fraction is larger over ocean than over land in general (see Fig. 1). However, there are finer variations over ocean as well as over land. In order to examine in details, we divided the analysis period into northern hemisphere monsoon (June-November, referred to as NHM) and southern hemisphere monsoon (December-May; SHM) seasons.

Figure 2 shows stratiform rain fraction maps for four seasons. We can observe clear seasonal variations. Especially when we focus on continental monsoon regions, such as South America, Australia, South Asia, and Africa, it is found that stratiform ratio is larger in rainy seasons and smaller in dry seasons. Over the ocean also, there is a tendency that stratiform ratio is larger over the summer hemisphere than the winter hemisphere. Note that the top panel is for January-May 1998, which is during the ENSO warm event. It is noticeable that the stratiform ratio over the central Pacific is significantly larger than other seasons, which implies that lager portion of rain is associated with well organized systems over the warmer water.

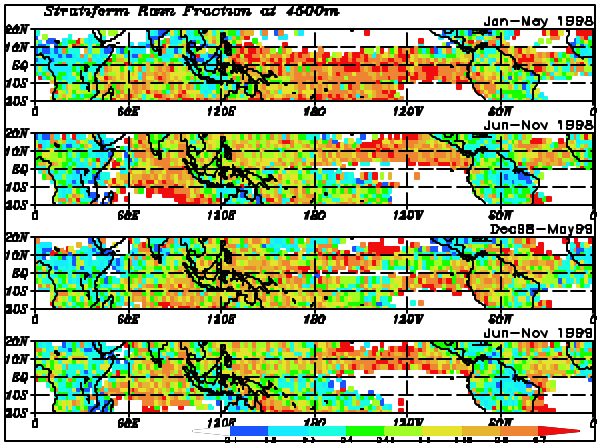

Fig. 2 Maps for the stratiform rain fraction depicted in color shades for four monsoon seasons. SHM, NHM, SHM, NHM from top to bottom. Reddish colors indicate larger fraction of stratiform rain, while bluish colors indicate more convective area. Note that the top panel shows the condition during the warm El Nino event.

Next, in order to understand such seasonal variations in precipitation characteristics in relation to atmospheric conditions, we examined the ECMWF analysis data. Six continental monsoon regions and three oceanic monsoon regions are selected as shown in Fig.3, and regional and 13-day running mean time series are constructed with PR2a25 rain data as well as with ECMWF analysis data. These averaging are necessary to overcome the sampling insufficiency due to the small swath width of PR. Figure 3 shows a scatter plot of stratiform rain fraction against the 500hPa humidity. Significant correlations are found between stratiform rain fraction and mid tropospheric humidity, both for continental monsoon regions (coefficient=0.66) and for oceanic monsoon regions (0.60). Not shown here but mid-to-upper-level humidity fields are well correlated to this stratiform rain fraction.

Considering that mid-to-upper troposphere is moistened mainly by anvil clouds, it is indeed a natural result. Still, we would like to consider two points related to this fact. First, since correlation is quantified, we may induce atmospheric humidity from observations of the stratiform rain fraction. Second point is that in the rainy season when the troposphere is more humid, the optical depth for the long wave radiation is thicker due to larger amount of water vapor. Then the atmospheric radiative cooling becomes top-heavier in the wet season than in the dry season (*e.g.* Fig.4). Since 'convective heating' associated with organized mesoscale systems consists of real convective heating and anvil heating, larger stratiform rain fraction results in top-heavier 'convective heating'. We would like to point out that top-heavier 'convective heating' is in the sense of balancing the top-heavier radiative cooling in the rainy season, and the other way round in the dry season.

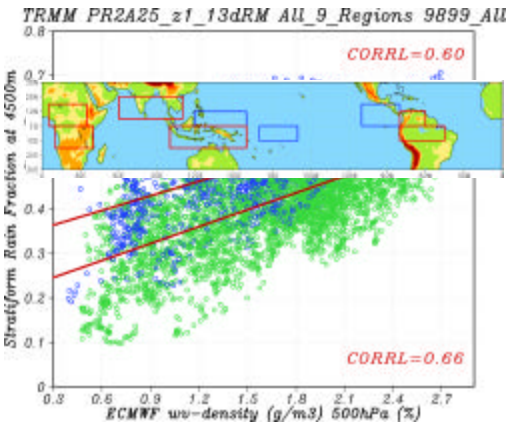

Fig. 3 Scatter diagram between ECMWF humidity (g/m3) and stratiform rain ratio. Both values are applied averaging in the 6 continental and 3 oceanic monsoon regions indicated in the above map and 13-day running means. Green dots indicate those for continental regions and blue dots indicate those for oceanic regions. Correlation coefficients are 0.66 and 0.60 for continental and oceanic data, respectively.

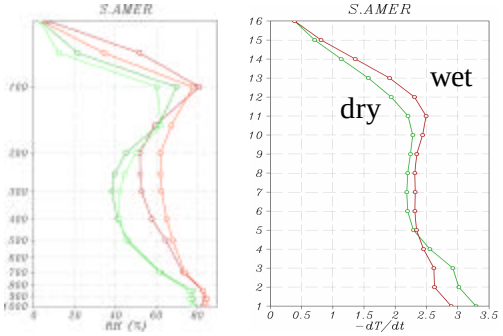

Fig.4 Humidity profiles obtained from ECMWF operational analysis (a) and cloud-free-sky radiative cooling (K/day) profiles calculated with ECMWF atmospheric data (b) over South American monsoon region. Red curves indicate those for wet season and green curves for the dry season.

4. Statistics in Seasonal variation of Precipitation Characteristics

Precipitation characteristics can be also examined with diurnal variations. Figure 5 compares those in the wet season (hereafter summer) and dry season (hereafter winter) for tropical northern hemisphere (20N-Eq, at all longitudes). Over the ocean, convective rain intensity is larger in summer than in winter by factor 1.25 in average (see Table 1), while stratiform rain intensity is not much different. At the same time, the stratiform/convective ratio of the rain area increases by factor 1.27. As a result, total rain amount is larger in summer with a slight increase of stratiform rain fraction. It is notable for the precipitation over ocean, that there is little dependence of the seasonal change on hours of the day (Fig. 6).

On the other hand, over land, summer/winter contrast in convective rain intensity and stratiform/convective area ratio are both found to be smaller (Table 1). Examining the monthly time series (Fig.6), there is considerable seasonal change in the convective intensity but not in the latter. The small contrast for convective intensity in Table 1 is attributable to the definition of two seasons; the value already increases in early summer from April to May which is included in our 'winter'. Significant dependence on

seasonal change among the hours of day is found for precipitation characteristics over land (Fig.6). Smaller variations in convective intensity and in stratiform/convective ratio in area are found in the afternoon (15-18LT), while much lager variation is found for early morning (00-03LT) rain. This result may be an indication that nighttime rain has separate origins from afternoon showers.

Note that as seen in Table 1, the stratiform rain fraction is slightly less than 50% over ocean, while slightly less than 40% over land, in general. However, only southern hemispheric summer over land, the value (43%) is larger than usual. It is attributable to Southern American rain which is quite unique in characteristics.

It may be emphasized that there is a tendency that stratiform/convective ratio in area increases in accord with the intensification of convective rain in warmer seasons, especially over the tropical ocean. And it seems to be in the opposite sense from Lindzen et al. (2000)'s iris hypothesis, although not directly addressing the issue. Over the tropical land, characteristics of the afternoon shower vary little with season, while those of night-to-early-morning rain shows similar tendency as those over ocean.

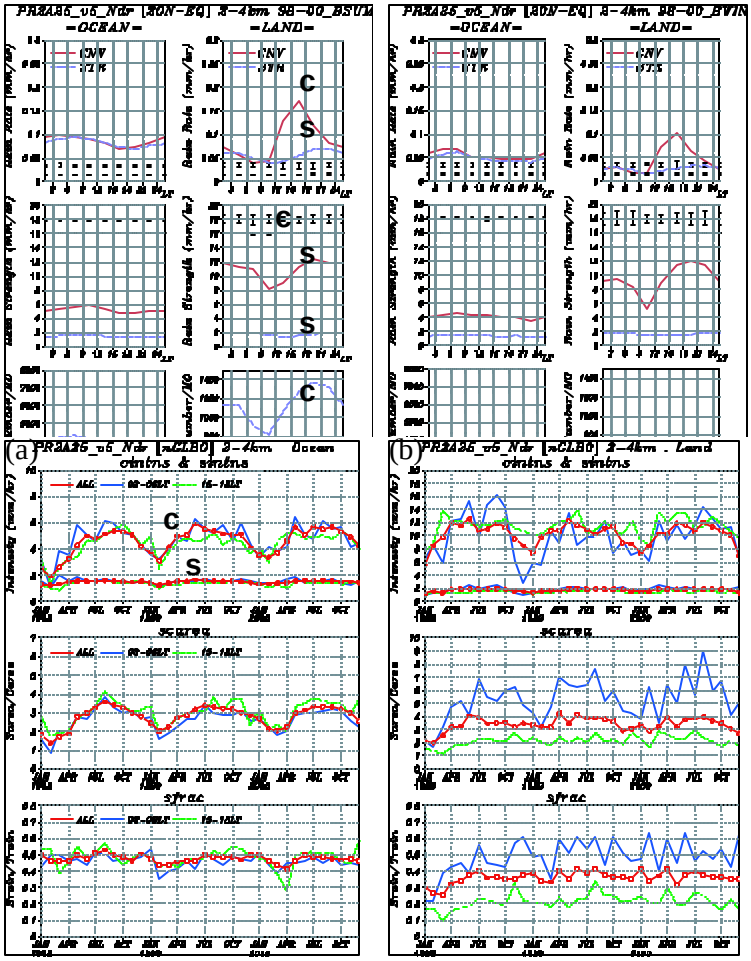

Fig. 5 Same as Fig. 1 but for those over tropical northern hemisphere region (20N-Eq, all longitudes), for NHM (left) and for SHM (right) seasons. NHM composite consists of 18 months: June-November in 1998, 1999, and 2000, while SHM composite consists of 12 months: Dec 1998-May 1999, and Dec 1999-May 2000.

Fig. 6 Monthly mean time series for indices representing precipitation characteristics. Values are, convective and stratiform rain intensity (upper), stratiform / convective rain area ratio (middle), and stratiform rain fraction in the total rain amount (bottom), over the tropical northern hemispheric ocean (a), and land (b). Thick lines with dots indicate those for daily mean values, while solid lines are for 03-06LT, dotted lines are for 15-18LT.

Lindzen, R. S., M. D. Chou, and A. Y. Hou, 2001: Does the earth have an adaptive infrared iris? Bull. Amer. Meteor. Soc., 82, 417-432.

Nesbitt, S. W., E. J. Zipser, and D. J. Cecil, 2000: A census of precipitation features in the Tropics using TRMM: Radar, ice scattering, and lightning observations. J. Climate, 13, 4087-4016.

Takayabu, Y. N., 2002: Spectral representation of rain profiles and diurnal variations observed with TRMM PR over the equatorial area.

Table 1 Statistics of precipitation obtained from TRMM PR2a25 data. Values are average contribution of convective rain to total rain rate, same for stratiform rain, convective rain intensity, stratiform rain intensity, convective/stratiform intensity ratio, and stratiform/convective area ratio, from top to bottom. Note that the values for stratiform area and stratiform intensity are sensitive to the threshold of rain detection, while others are not.

	Ocean	Ocean	Land	Land
20N-Eq, all longitudes	**Summer (NHM)**	**Winter (SHM)**	**Summer**	**Winter**
meanConv (mm/hr)	0.087 (51%)	0.056 (53%)	0.093 (62%)	0.048 (64%)
meanStrat (mm/hr)	0.082 (49%)	0.049 (47%)	0.057 (38%)	0.027 (36%)
C-intensity (mm/hr)	5.27 [1.25*w]	4.20	11.1 [1.09*w]	10.2
S-intensity (mm/hr)	1.54 [1.08*w]	1.43	1.82 [1.08*w]	1.68
Cintns/Sintns	3.42 [1.16*w]	2.94	6.09 [1.00*w]	6.08
Sarea/Carea	3.23 [1.27*w]	2.54	3.70 [1.08*w]	3.42
Eq-20S, all longitudes	**Summer (SHM)**	**Winter (NHM)**	**Summer**	**Winter**
meanConv (mm/hr)	0.065 (53%)	0.035 (54%)	0.100 (57%)	0.061 (64%)
meanStrat (mm/hr)	0.058 (47%)	0.030 (46%)	0.076 (43%)	0.034 (36%)
C-intensity (mm/hr)	4.38 [1.48*w]	2.96	10.4 [0.95*w]	11.0
S-intensity (mm/hr)	1.50 [1.13*w]	1.33	1.77 [1.00*w]	1.76
Cintns/Sintns	2.92 [1.31*w]	2.23	5.85 [0.94*w]	6.24
Sarea/Carea	2.59 [1.33*w]	1.95	4.44 [1.29*w]	3.44

MULTISENSOR-MULTISCALE PRECIPITATION DATASETS AND MODEL VERIFICATION

Efi Foufoula-Georgiou
St. Anthony Falls Laboratory, University of Minnesota
Mississippi River at 3rd Avenue SE
Minneapolis, MN 55414, USA.
e-mail: efi@tc.umn.edu
Tel: +1-612-626-0369.

1. Introduction

Multisensor validation of precipitation involves comparison of precipitation estimates at different scales, e.g., comparison of 20-30 km averages from a satellite to 2-km averages from radars to point observations from raingauges, and often to a numerical model output at another scale. A major problem arising when spatial averages of precipitation at one scale are compared to averages at another scale is the fact that precipitation variability is scale-dependent (e.g., see Fig. 1). How this variability changes with scale is a function of the inherent characteristics of the storm and varies with storm type. Moreover, even the uncertainty of the estimates depends on scale, and it differs from sensor to sensor.

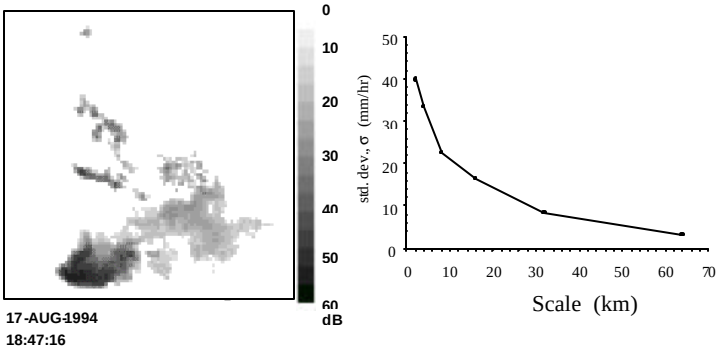

Figure 1. Radar-observed precipitation (left) from the WSR-88D (NEXRAD) radar KICT in Wichita, Kansas on 17 August 1994, along with the standard deviation of non-zero precipitation as a function of grid scale.

In a recent study, Tustison et al. (2001) demonstrated the importance of accounting for the multiscale variability of precipitation in QPF verification studies and showed that typical methods used to change the scale of observations to the scale of the model estimates impose a "representativeness error" which is nonzero even in the case of "perfect" model estimates. We propose the development of a rigorous methodology, which can explicitly account for the scale-dependent variability and uncertainty of precipitation estimates in any study involving comparison or merging of multisensor observations.

2. Background on the proposed methodology: Scale-Recursive Estimation

The proposed methodology largely utilizes a stochastic scale-recursive estimation (SRE) technique introduced by Chou et al. (1994). This technique can optimally merge observations of a process at different scales while explicitly accounting for their uncertainty and variability at all scales. It requires the specification of a model (called multiscale model) describing how the process variability changes with scale. This multiscale model is defined on an inverted tree structure (see Figure 2) and the estimation algorithm is developed along this tree in two steps. One step involves the multiscale model in its coarse-to-fine scale form:

$$X(l) = A(l)X(\gamma l) + B(l)W(l) \qquad (1)$$

where $?$ is an index to specify the nodes on the tree, $??$ represents the node on the tree directly above the node specified by $?$, $X(?)$ is the state of the system at scale $?$, $A(?)$ and $B(?)$ control the scale-to-scale variability of the process, and $W(?)$ is a normally distributed driving noise. This model may be used to describe any process whose coarse-to-fine scale dependence can be expressed in a linear form. The second step of SRE involves the fine-to-coarse scale form of the model:

$$X(\gamma l) = F(l)X(l) + W^*(l). \qquad (2)$$

The parameters $F(?)$ and $W^*(?)$ are defined by $A(?)$ and $B(?)$ by manipulation of (1) and (2). The incorporation of the measurements into the multiscale model is done via the measurement equation

$$Y(l) = C(l)X(l) + V(l) \qquad (3)$$

where $V(?)$ is a normally distributed measurement noise which characterizes the error variance of the measuring instrument and $C(?)$ provides the relation between the observed quantity and the state.

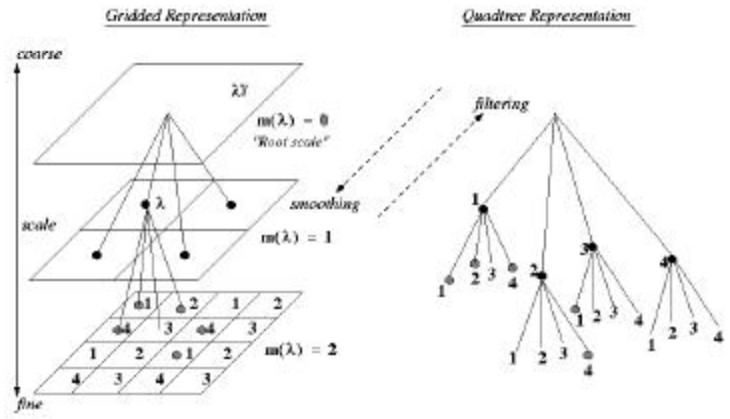

Figure 2. Illustration of the scale-recursive estimation (SRE) technique applied to precipitation measurements. Sparsely-distributed measurements at one scale (gray dots), and measurements at a coarser scale (solid dots), are placed on an inverted quad-tree and merged via filtering and smoothing to obtain estimates at any desired scale together with the uncertainty of these estimates.

Equations (1-3) form the basic equations for the scale-to-scale evolution of the process and the inclusion of its measurements. Figure 2 illustrates the inverted tree, the scale-to-scale composition of the process, and how measurements are placed on the tree for inclusion in the multiscale estimation.

The multiscale recursive estimation algorithm consists of two steps: filtering and smoothing. The filtering step uses Kalman filtering, incorporating the measurements of the process with (3) and propagating the estimates from fine-to-coarse scales with (2). The second step consists of smoothing in which the estimates from step one are merged with those predicted from (1) along the coarse-to-fine path on the tree. This algorithm has the advantage that it is extremely computationally efficient due to its recursive nature. This is especially important with large data sets available at many scales, such as those available for rainfall (e.g. raingauges, radars, satellites) and for real-time data assimilation applications.

3. Illustrative Example

Suppose one has available radar observations at 2-km resolution and satellite observations at 16-km resolution, or only a sparse network of raingauge observations but complete coverage of the area by a satellite overpass. How is one to combine these observations for obtaining an optimal (in some sense) merged product at one or more desired scales? This optimally merged product can be used to verify a numerical weather model or a precipitation retrieval at the desired scale. To demonstrate the use of the multiscale framework, a simple numerical experiment was conducted.

In all cases, a combination of observations and their uncertainties at 2 km and 16 km were provided and optimal estimates at 8km were computed using SRE (see Fig. 3). These estimates were then compared to the true 8-km averages (known to us in this constructed example) in terms of bias, RMSE, standard deviation of the whole field, and mean uncertainty of the estimates. Different scenarios of available observations were tested. A bounded lognormal cascade fitted to the 2-km field was used as the prescribed multiscale model. Table 1 summarizes the results and quantifies the potential of the method for multisensor validation studies. As was expected, increasing the density and resolution of available observations decreases the RMSE and bias in validation (i.e., produces more accurate merged fields at 8km) and increases the accuracy of the merged estimates (smaller uncertainty). More details can be found in Tustison et al. (2003).

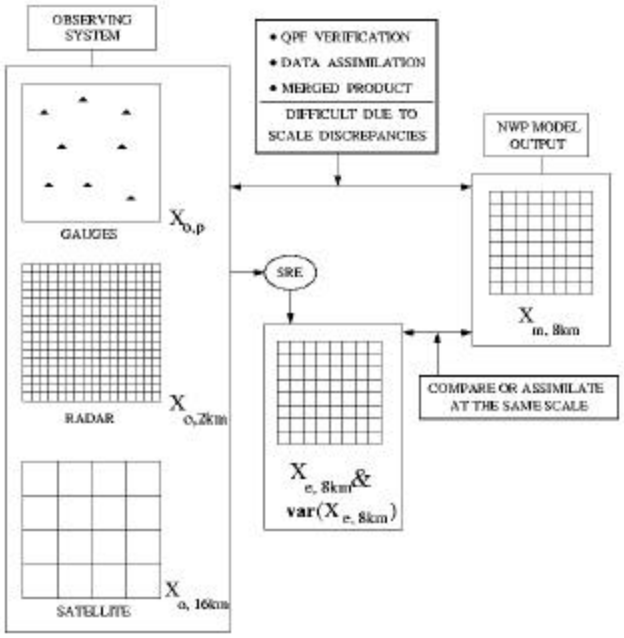

Several issues must be carefully studied before SRE can be used with confidence for multisensor validation or data merging. One of those is the sensitivity of SRE to multiscale model selection, observational error, and presence of zeros.

Figure 3. Illustration of the proposed framework for QPF Verification.

Table 1. Case studies illustrating the application of the SRE methodology for merging observations at different scales. The mean of the KEAX WSR-88D hourly accumulation field at 8 km (which was considered the "true" field in this example) was 1.99 mm, and the standard deviation, 3.01mm. All the values are given in mm.

Case	Observations	SRE estimation at 8 km			
		Bias	RMSE	σ_{est} field	Mean uncertainty of estimates
1	10% sampling at 2 km	0.40	1.13	2.47	0.32
2	50% sampling at 2 km	0.15	0.48	2.84	0.21
3	10% sampling at 2 km; 100 % at 16 km	0.17	0.84	2.80	0.30
4	50% sampling at 2 km; 100 % at 16 km	0.10	0.45	2.88	0.21

REFERENCES:

Chou, K. C., A. S. Willsky, and A. Benveniste, Multiscale recursive estimation, data fusion, and regularization, *IEEE Trans. Automat. Contr.*, 39, 464-478, 1994.

Tustison, B., D. Harris and E. Foufoula-Georgiou, Scale issues in verification of precipitation forecasts, *J. Geophys. Res.*, 106(D11), 11,775-11,784, 2001.

Tustison, B., D. Harris, and E. Foufoula-Georgiou, Scale-Recursive estimation for multi-sensor QPF verification: A preliminary assessment, *J. Geophys. Res.*, 108(D8), 8377-8390, 2003.

On the relevance of gridded rainfall observations to verify ECMWF precipitation forecasts

A. Ghelli
European Centre for Medium-Range Weather Forecasts
anna.ghelli@ecmwf.int

Introduction

General circulation models (GCM) predict precipitation on spatial scales that are different from the scales described by observations. The observed precipitation from a rain gauge will tell us something about the local precipitation pattern, but the forecasting system will in general be unable to describe such a small scale variability. Moreover, verification against irregularly distributed observed data, as SYNOPs available in real time from the Global Telecommunication System (GTS) might be, is liable to misinterpretation due to SYNOPs under-sampling the precipitation variability.

The precipitation forecast should be interpreted as an areal quantity, rather than a grid point value. Therefore verification that interpolates the forecast precipitation to the rain gauge location can only capture partially the model skill.

Ideally a precipitation analysis will appeal to a user who wants to verify his/her forecasting system if the analysis describes spatial scales comparable to the model scales, it represents the observed areal rainfall, and it is independent from any model thus guaranteeing an independent dataset for verifications. The up-scaling technique (Ghelli and Lalaurette, 2000) represents a step in this direction. The up-scaled precipitation dataset is independent of models and describes spatial scales that are the spatial scales of the precipitation forecasts. Some of the spatial variability of rainfall is maintained in the up-scaling technique.

The up-scaling technique is a simple averaging method which has shown to guarantee a fairer comparison between precipitation forecast and observed amounts. Cherubini et al (2002) show that the overestimation of most rainfall amounts is reduced when using up-scaled observations rather than point estimation of rainfall.

The up-scaling technique

The up-scaling technique is a very simple algorithm that assigns each station of the high-density dataset to a model grid-box. Each model grid-box is built around a grid-point. A simple average of all the stations comprised in the same grid-box is then calculated, and the mean value is assigned to the corresponding grid-point. Mean values will be referred to as up-scaled observations.

The up-scaling method can smooth out local maxima of precipitation, thus reducing the small-scale variability that current GCM are not likely to be able to simulate correctly. High-density network data cover only land areas and cannot currently be used in real time. The end product of the up-scaling technique is a precipitation analysis whereby the observed grid-point value is indeed an areal quantity. Moreover, data from the high- density network of rain gauges represent an independent dataset for use in verification. Because of the high density of such data, they can be used to verify models at different spatial resolution, provided the up-scaling technique is tuned for the different resolutions.

Verification measures

Any forecast system should include verification to evaluate the accuracy and skill of forecasts. Quantitative and qualitative verification help us to understand the characteristics of the forecasting system. The measures used in the present paper to test the performance of the forecast are the Frequency Bias Index (FBI) and the Equitable Threat Score (ETS).

Contingency tables (table 1) for different thresholds of 24 hour accumulated precipitation have been built. The ETS (Schaefer, 1990) is a modified version of the Threat Score rendered equitable by taking away the random forecast (R(a)). A detailed explanation of such score can be found in Wilks, 1995. The FBI is written as:

$$FBI = \frac{a + b}{a + c}$$

The ETS is written as follows:

$$ETS = \frac{a - R(a)}{a + b + c - R(a)}$$

where:

$$R(a) = \frac{(a + b)(a + c)}{a + b + c + d}$$

The FBI measures the event frequency and its value is 1 for a perfect forecast and it is larger (smaller) than 1 for an over-forecasting (under-forecasting) system.
The ETS is 0 (no skill) for a chance or constant forecast and it is 1 for a perfect forecast.

	observed yes	**observed no**
forecast yes	a (hits)	b (false alarms)
forecast no	c (misses)	d (correct no event)

Table 1: Contingency table for a generic threshold

Results

1. Precipitation forecast verification in France

The high-resolution data for the French territory has been made available by Meteo-France and it covers the period January 1997 to November 2002. There are about 4000 rain gauges reporting rainfall amounts that are accumulated over a period of 24 hours.

The FBI has been stratified by seasons thus avoiding the thinning of the sample size, which renders the statistics very noisy. The FBI is therefore calculated for December, January and February (D), March, April and May (M), June, July and August (J) and finally September, October and November (S). The FBI is then averaged over the French territory where the up-scaled observations are available. Fig. 1 shows timeseries of FBI for two different thresholds 1 mm/24h (panel a) and 5 mm/24h (panel b) and different forecast ranges.

The FBI shows that the forecasting system performs better in autumn/winter months when the FBI values are closer to 1. This period is characterised in Europe by well-organised frontal systems as opposed to summer months when convection becomes the predominant mechanism. In October 1999, the model vertical resolution was increased to 60 levels and a change in the cloud scheme was introduced. This is reflected in the FBI trend: the model over-forecasts precipitation events before autumn 1999 while after the change was introduced it performs as an almost perfect system in autumn/winter months and it slightly under-forecasts during summers. This is evident for both thresholds.

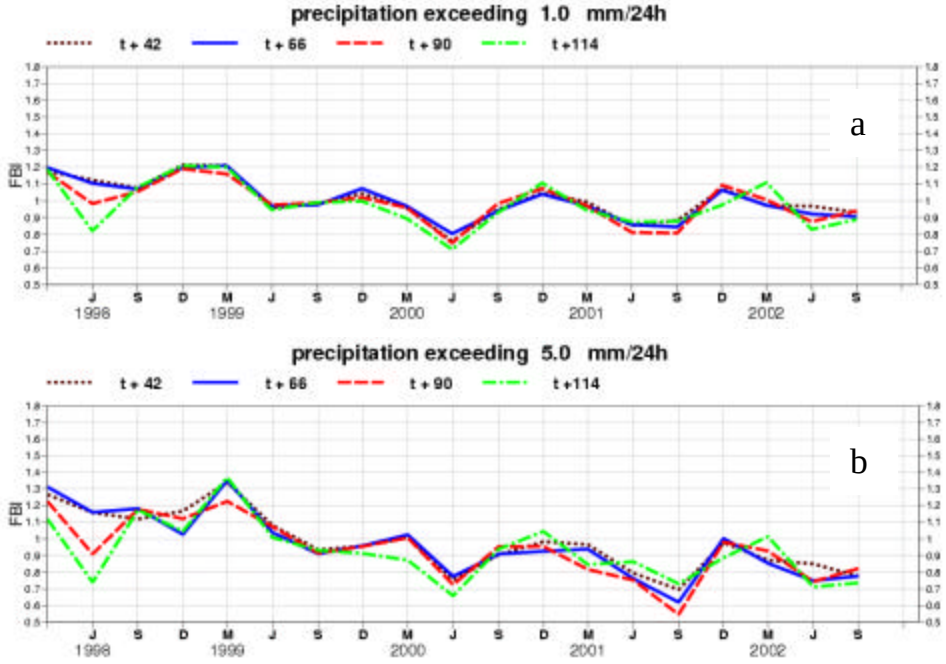

Figure 1: FBI timeseries for different forecast ranges and different thresholds: 1 mm/24h (panel a) and 5 mm/24h (panel b)

2. Precipitation forecast verification for the Douro/Duero river basin

The verification of precipitation forecasts has been extended to the catchment area of the Duoro/Duero river that runs from Spain into Portugal towards the Atlantic Ocean. The catchment area contains around 400 high-density network rain gauges and only 11 SYNOP stations available from the GTS. The area comprises 72 grid points. An assessment of the model performance has been possible because of the high resolution data made available to ECMWF by Spain and Portugal.

Standard verifications looking at the degree of match between forecast and observed value, have been described in Ghelli (2002) for a flooding episode of the river Duoro in February-March 2001. Hereafter, objective measures are presented.

FBI and ETS have been calculated for a 15-month period (January 2001 to March 2002) and they are shown in Fig. 2 as a function of the precipitation thresholds. Three different accumulation ranges have been evaluated, as the length of the rainy events is a significant factor in determining the response of the river basin. FBI (fig. 2 a) values are confined to values very close to 1 for all the accumulation ranges and thresholds. This indicates that the model only slightly over-estimates the frequency of the rainy events.

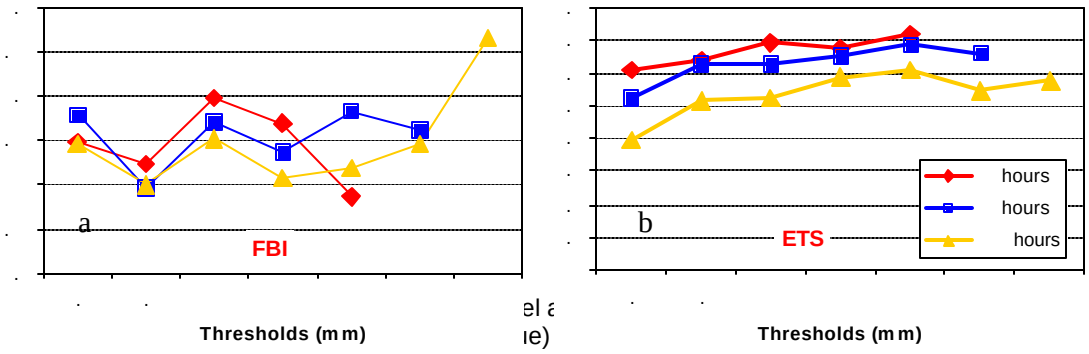

precipitation forecasts averaged over the whole period investigated.

The ETS (Fig. 2 b) shows a more skilful system for shorter accumulation times. The ETS value decreases as the accumulation range increases. Nevertheless, 5-day accumulation forecasts have still considerable value with the ETS reaching 0.6 for the 4 mm/120h threshold.

Conclusion and recommendations

In the present paper, it has been discussed the importance of precipitation observations obtained from high density observing networks. These observations, up-scaled to the model resolution, allow the spatial scales of the model to be compared to analogous observed scales. Moreover, the end product of the up-scaling procedure is a gridded analysis whereby each grid-point value represents an areal quantity.

It has been pointed out that SYNOPs available in real time on the GTS may suffer from under-sampling, hence they describe the small scale variability of rainy events partially. Verification against these irregularly distributed data is liable of misinterpretation.

The forecast verification in France has indicated that the over-forecasting of the event frequency has been reduced since autumn 1999. This reduction is linked to the cloud scheme change and the increased vertical resolution implemented in October 1999.

The paper has also shown some results from the verification of forecast precipitation for a river catchement area. These verifications could not have been done without the high-resolution data, as there were only 11 SYNOPs available on the GTS for an area of about 350x350 Km. The results show that the forecasts slightly over-forecast the number of rainy events. Moreover, the forecast has considerable skill for different accumulation ranges when the observation/forecast pairs are pooled over a 15-month period.

Obtaining precipitation data from high-density observing networks may be difficult, but where possible they should be used to verify models. This is our challenge for the future.

Acknowledgements: I am grateful to ECMWF Member and Co-operating States for providing high-density network precipitation data. I am also grateful to Dr.Tiziana Cherubini and Mr. Tamas Hirsch for discussions and help in producing the statistics.

References

Cherubini, T., A. Ghelli and F. Lalaurette (2002) Verification of precipitation forecasts over the Alpine region using a high density observing network. Wea. Forecasting, 17, 238-249

Ghelli A. and F. Lalaurette (2000) Verifying precipitation forecasts using up-scaled observations. ECMWF Newsletter, Vol. 87, 9-17.

Ghelli A. (2002) Verifcation of precipitation forecasts using data from high-resolution observation networks. ECMWF Newletter, Vol.93, 2-7

Schaefer, J.T. (1990) The critical success index as an indicator of warning skill. Wea. Forecasting, 5, 570-575

Wilks D.S. (1995) *Statistical Methods in the Atmospheric Sciences.* Academic Press, 467 pp.

Rain Gauge and Radar-Rainfall Errors

Witold F. Krajewski and Mekonnen Woldemarian Gabremichael

IIHR-Hydroscience & Engineering
The University of Iowa
Iowa City, Iowa 52242, USA

Extended Abstract

We present results of studies aimed at determination of uncertainties in rain gauge and radar rainfall estimation uncertainty. We also explore the information contained in radar-rainfall data on the spatial structure of rainfall. This is relevant to TRMM and other remote sensing products of rainfall as they may be used in regions of the world where no other information is available.

We begin with rain gauge data. First, we address the issue of random error of tipping bucket rain gauge. To date we know of two such rigorous studies on this subject. Habib et al. (2001) performed a data based simulation and estimated the error distributions as function of rainfall magnitude, time integration scale, and bucket size. Recently, Ciach (2003) conducted an experimental study and synthesized the results for two different methods of tip data processing. His results are in good agreement with the earlier study by Habib et al. (2001). A very interesting result is the scaling behavior of the errors. These results are also confirmed by analysis from the double gauge data at the Iowa City Municipal Airport. The main conclusion from these studies is that tipping bucket rain gauges, when well maintained and deployed as a pair, provide accurate observation of rainfall at scales from 10 minutes up. The errors decrease with increasing rain rate.

The second issue is that of estimating rainfall over small areas from dense cluster of rain gauges. Let us pose a question relevant to direct validation (Krajewski and Smith 2002): "How many gauges are required in a 2×2 km^2 area (equivalent to a typical radar-rainfall product) to obtain areal estimate with high accuracy (~5%)?" Answering this question requires knowledge of the spatial correlation function of the rainfall regime. Habib and Krajewski (2002) estimated such a function for Florida summer rainfall. Krajewski et al (2003) estimated it for five different locations around the world. Based on these studies we consider two cases: exponential correlation with the correlation distance of 5 km and 15 km. In the first case we need about 20 gauges uniformly covering the pixel to reach the 5% error level. In the second case only 5-8 gauges will achieve the same objective.

The third issue addresses the question of the information contained in the radar rainfall data of the statistical structure of rainfall. We considered two functions: spatial covariance function and scale-dependent variance reduction function. Our results show that in both there is significant discrepancy between accurate estimation based on very dense network of gauges and that based on radar estimates. We attribute this difference to the random error present in the radar data. We confirm this by performing several data based simulation experiments.

Our final result is on the sampling effect of TRMM-like sampling of rainfall on inferring multiscale description of rainfall. Using full two months of radar rainfall data (every 6 minutes) and TRMM-like subsamples of the same data set, we estimated the normalized moment scaling function. The reduced sample leads to a significant bias in the estimated function.

References

Ciach, G.J., Local random errors in tipping-bucket rain gauge measurements. *J. Atmos. Oceanic Technol.*, 2003 (in press).

Habib, E., W.F. Krajewski, and A. Kruger, Sampling errors of fine resolution tipping-bucket rain gauge measurements, *Journal of Hydrologic Engineering*, 6(2), 159-166, 2001.

Habib, E. and W. F. Krajewski, Uncertainty analysis of the TRMM Ground Validation radar-rainfall products: Application to the TEFLUN-B field campaign, *Journal of Applied Meteorology*, 41(5), 558–572, 2002.

Krajewski, W.F., G.J. Ciach and E. Habib, An analysis of small-scale rainfall variability in different climatological regimes, *Hydrologic Science Journal*, 2003 (in press).

Krajewski, W.F. and J.A. Smith, Radar hydrology: Rainfall estimation, *Advances in Water Resources*, 25, 1387–1394, 2002.

Monitoring Precipitation over the Arctic Terrestrial Drainage System: Data Requirements, Shortcomings and Applications of Atmospheric Reanalysis

Mark C. Serreze, Martyn P. Clark
Cooperative Institute for Research in Environmental Sciences, Campus Box 449, University of Colorado
Boulder, CO 80309-0449, USA

David H. Bromwich
Byrd Polar Research Center, 1090 Carmack Road, The Ohio State University, Columbus, OH 43210, USA

ABSTRACT

The hydro-climatology of the Arctic terrestrial drainage plays an important role in the climate system. The primary freshwater source to the Arctic Ocean is river discharge. River discharge influences ocean salinity and sea ice conditions which can impact on freshwater fluxes through the Fram Strait and Greenland Sea into the North Atlantic. The degree of surface freshening in the North Atlantic is thought to influence the global thermohaline circulation. Changes in the terrestrial hydrologic cycle may alter soil moisture, impacting on plant communities and their grazers. Arctic soils serve as potentially significant sources of carbon dioxide and methane. Fluxes appear to respond sensitively to altered soil moisture and temperature. There is hence a clear need to monitor the Arctic system and better understand interactions between system components. The terrestrial hydrologic budget is a high priority.

A project known as Arctic-RIMS (Rapid Integrated Monitoring System) is bringing data sets and techniques together to provide readily accessible hydrologic products. Arctic-RIMS is a collaborative effort between University of Colorado, University of New Hampshire, the Ohio State University and the Jet Propulsion Laboratory. The project uses satellite data, the NCEP reanalysis, in-situ records and a permafrost/water balance model to compile fields of precipitation (P), precipitation less evapotranspiration (P-ET), ET, temperature, soil moisture, soil freeze/thaw state, active layer thickness, snow extent and its water equivalent, soil water storage and other variables. Historical time series are provided along with updates at a 1-2 month time lag. Gridded products are assembled over the complete Arctic terrestrial drainage, defined as areas emptying into the Arctic Ocean as well as into Hudson Bay, James Bay, Hudson Strait, the Bering Strait and northern Bering Sea. Here we describe a core element of Arctic-RIMS - the provision of historic time series and updates of gridded precipitation. Details are provided in the upcoming paper of Serreze et al. [2003].

Provision of gridded historic time series has in itself proven to be a daunting and at times frustrating task. The required station density to assemble quality gridded time series at a spatial scale useful for input to hydrologic models exceeds what is available over most of the Arctic drainage. The problem is compounded by large errors in the measurement of solid precipitation and degradation of the station network since about 1990, the latter due to budget cuts in both the Former Soviet Union (FSU) and Canada. For example, the station coverage for the FSU in 1996 is about half of that available in the mid 1980s. Canada is also seeing a trend toward the replacement of manual observations by automated systems, providing data of suspect quality.

To assess the impacts of station density for generating historical time series, Monte-Carlo experiments were performed for the few well-instrumented areas of the Arctic drainage in Canada. Briefly, monthly grid box time series were compiled using all the stations in 175 km grid boxes. These were taken to be the "true" time series. Time series were then compiled by randomly removing stations from the boxes, and were compared to the true time series. It is concluded that for 175 km grid cells, the Arctic station network over the period 1960-1989 is generally sufficient to estimate the mean and standard deviation of precipitation at this scale (hence the statistical distributions). However, as for most regions of the Arctic, one must obtain grid box values by interpolating from stations well outside of the grid box bounds, the true grid box time series are often poorly represented. The Monte Carlo experiments indicate that to accurately capture the true monthly time series (e.g., to get a squared correlation exceeding 0.70), one must have at least four stations per 175 km cell and more in topographically complex regions. However, only 38% of cells across the Arctic terrestrial drainage contain even a single station.

We next consider four options for monitoring precipitation: (1) make do with gridding available updates of station data; (2) make direct use of gridded precipitation forecasts from the NCEP reanalysis; (3) use the gridded observed precipitation time series and NCEP output for 1960-1989 (forecasted precipitation and other variables such as vertical motion) to develop linear regression models which can be applied to NCEP updates (a form of statistical downscaling); 4) use non-parametric methods to constrain NCEP output by the statistical distributions of the gridded

observations over the 1960-1989 period. A common thread between options 2-4 is that output could be subsequently adjusted via assimilation of any available station data updates.

The problem with Option 1 is that station coverage since 1990 is much more sparse than for earlier decades and is insufficient by itself. Regarding Option 2, NCEP forecasts of precipitation in the Arctic contain large biases (especially in summer) and cannot be used "as is" [Serreze and Hurst 2000]. Option 3 (e.g., multiple linear regression) is clearly problematic in that it requires faith in the observed gridded precipitation time series. As concluded from the Monte-Carlo simulations, the grid box time series are often of poor quality, meaning that one will be regressing against noise. The time series of individual stations represent truth (with due consideration of gauge undercatch and other biases). However, regression against station time series runs into problems of scale (relating point observations to relatively coarse scale NCEP output). Gridding the resulting station reconstructions also runs into the same problems of station density that were just discussed.

Option 4 emerges as the most viable. It recognizes that: 1) biases in NCEP precipitation forecasts are at least in part systematic; 2) systematic biases can be accounted for through re-scaling procedures (a non-parametric probability transform, see Panofsky and Brier [1963]) that require only the statistical distributions of observed precipitation rather than accurate representation of the gridded time series themselves; 3) re-scaling procedures can be applied to reconstruct precipitation from other variables, such as aerological estimates of P-ET (from the vapor flux convergence and the tendency in precipitable water), which can replace the re-scaled NCEP precipitation forecasts if they are shown to provide better skill. The utility of these P-ET fields for assessing the Arctic moisture budget has been demonstrated in several recent studies [e.g., Rogers et al., 2001].

Cross-validated correlation analyses indicate that re-scaled monthly NCEP forecasts (re-projected to a 175 km grid) have considerable skill in some parts of the Arctic drainage (squared correlations exceeding 0.50), but perform poorly over large regions. A fundamental problem, however, is that in data sparse regions, the observed gridded time series are themselves of poor quality. Hence, the term "validation" is perhaps inappropriate. In data-sparse areas, it may well be that the NCEP forecasts are performing better than is indicated from the correlations.

Treating climatology as a first guess with replacement by re-scaled NCEP values in areas where skill can be demonstrated yields a marginally useful monitoring product on the scale of large watersheds such as the Ob, Yenisey and Lena. Further improvements are realized by assimilating data from a limited array of station updates (taken as representative of the network which will be available in the next decade) via a simple replacement strategy. In turn, the product can be further improved by including aerological estimates of P-ET within the initial re-scaling procedure. In some areas, such at the Lena basin in summer, the re-scaling technique (even without data assimilation) works extremely well.

We also examined the alternative approach of reconstructing precipitation via multiple linear regression (Option 3), using as predictors the NCEP precipitation forecasts along with other reanalysis variables such as P-ET computed from wind and humidity profiles, monthly sums of upward vertical velocity (omega) at 500 hPa, zonal and meridional moisture fluxes, sea level pressure and a measure of lower-tropospheric stability. The apparent skill is comparable to that based on the re-scaling approach using NCEP precipitation and P-ET. There are issues of co-linearity between predictors. There are methods to resolve these issues, but as just discussed, the re-scaling approach is on a better statistical footing in that unlike regression, it does not assume that the observed time series are themselves accurate. Only the statistical distributions need be known. We have also used the re-scaling approaches to reconstruct precipitation at the station locations, with subsequent interpolation of the reconstructed station values to the 175 km grid cell array. In general, the results are worse than those based on first interpolating the station data to the grid cell array.

An obvious need for doing a better job is to have better observations. However, the station data base in the Arctic has always been sparse, and as mentioned, has seriously degraded over the past decade. We need to look into satellite-based precipitation retrievals. The brightest avenue, however, is having access to output from an improved atmospheric model. We have had the opportunity to examine several years of precipitation forecasts from ERA-40. While ERA-40 appears to perform little better than ERA-15, performance is much better relative to NCEP. The monitoring approach will hence transition to the use of ERA-40 as soon as significant portions of the data stream become available to us. Note that precipitation output from the NCEP-DOE AMIP-2 reanalysis is no better than that from the primary NCEP data stream. A dedicated Arctic System Reanalysis (ASR) has been proposed under the National Science Foundation (NSF) Study for Environmental Arctic Change program [SEARCH SSC, 2001]. The proposed ASR will draw on lessons learned from ERA-40 and the NCEP North American Regional Reanalysis (NARR).

References

Panofsky, H.A. and G.W. Brier, 1963: *Some Applications of Statistics to Meteorology.* Mineral Industries Continuing Education, College of Mineral Industries, the Pennsylvania State University, University Park, Pennsylvania, 224 pp.

Rogers, A.N., D.H. Bromwich, E.N. Sinclair, and R.I. Cullather, 2001: The atmospheric hydrologic cycle over the Arctic Basin from reanalyses Part 2. Interannual variability. *J. Climate*, 14, 2414-2429.

SEARCH SSC, 2001: *Study of Environmental Arctic Change, Science Plan*, Polar Science Center, Applied Physics Laboratory, University of Washington, Seattle, 91 pp.

Serreze, M.C., M.P. Clark and D.H. Bromwich, 2003: Monitoring precipitation over the Arctic terrestrial drainage system: Data requirements, shortcomings and applications of atmospheric reanalysis. *J. Hydrometeorology* (in press).

Serreze, M.C. and C.M. Hurst, 2000: Representation of mean Arctic precipitation from NCEP-NCAR and ERA reanalyses. *J. Climate*, 13, 182-201.

THE INTERNATIONAL PRECIPITATION WORKING GROUP: OPPORTUNITIES AND PERSPECTIVES

Vincenzo Levizzani
CNR-Institute of Atmospheric Sciences and Climate, Via Gobetti 101, I-40129, Bologna, Italy
v.levizzani@isac.cnr.it

Arnold Gruber
NOAA-NESDIS, Cooperative Institute for Climate Studies,
Earth System Science Interdisciplinary Center,
2207 Computer and Space Sciences Building, College Park, Maryland 20742-2465
arnold.gruber@noaa.gov

Introduction

The Coordination Group for Meteorological Satellites (CGMS) during its XXVIII meeting noted that WMO had analyzed the benefits from and agreed upon the need to foster further development of focused science groups. The success of both the International TOVS Working Group (ITWG) and the International Wind Workshop (IWW) in focusing the scientific community on a specific application area's issues and problems, strongly suggested similar benefits could be gained by development of science teams and workshops that could deal with application areas of satellite meteorology such as quantitative precipitation estimates, NWP and ocean and land surface properties. The current existence of many scientific groups operating in these areas could facilitate the task. For example, in the area of quantitative precipitation estimation, groups of scientists are currently involved in the Global Precipitation Climatology Project (GPCP) of the World Climate Research Programme (WCRP) and have already exchanged information on data requirements, algorithm development, data set production, validation and data distribution.

CGMS-XXVIII also noted that the fifty-second session of the WMO Executive Council had recommended involving relevant science groups in a systematic manner and the positive indication from the GPCP for WCRP's Global Energy and Water Cycle Experiment (GEWEX) to serve as a nucleus for such a working group. Thus, WMO strongly encouraged the formation of an International Precipitation Working Group (IPWG) with active participation by WMO and GPCP within the framework of CGMS. As a result, CGMS-XXVIII initiated the establishment of a Working Group on Precipitation, with co-sponsorship by WMO and CGMS.

The first session of the IPWG was held at the Colorado State University, Fort Collins, Colorado, USA, 20-22 June 2001. The current status of precipitation estimation from satellite-based observing systems and the plans and capabilities of proposed future satellite systems were reviewed. Draft terms of reference for the IPWG were established, which were approved at CGMS-XXIX in Capri, 23-26 October 2001.

Scope of IPWG

The IPWG is established to foster the:

- Development of better measurements, and improvement of their utilization;
- Improvement of scientific understanding;
- Development of international partnerships.Specific objectives are as follows:

1) to promote standard operational procedures and common software for deriving precipitation measurements from satellites;
2) to establish standards for validation and independent verification of precipitation measurements derived from satellite data; including:
   - *reference standards for the validation of precipitation for weather, hydrometeorological and climate applications;*
   - *standard analysis techniques that quantify the uncertainty of ground-based measurements over relevant time and space scales needed by satellite products;*
3) to devise and implement regular procedures for the exchange of data on inter-comparisons of operational precipitation measurements from satellites;
4) to stimulate increased international scientific research and development in this field and to establish routine means of exchanging scientific results and verification results; to make recommendations to national and international agencies regarding the utilization of current and future satellite instruments on both polar and geostationary platforms; and

5) to encourage regular education and training activities with the goal of improving global utilization of remote sensing data for precipitation measurements.

1st IPWG Science Workshop

The first science workshop of the CGMS and WMO International Precipitation Working Group was held at the EUMETSAT Nowcasting Satellite Applications Facility (SAF) in Madrid, Spain from 23-27 September 2002. The workshop promoted the exchange of scientific and operational information between the producers of precipitation measurements, the research community, and the user community, and developed pathways forward for a variety of activities within the IPWG. The workshop was hosted by the Instituto Nacional de Meteorologia (INM) and the SAF.

The first three days of the workshop consisted of keynote and scientific presentations in the following topical areas:

- The IPWG and Related International Projects
- Operational Estimation of Rainfall
- Missions and Instruments
- Research Activities
- Validation

An important goal of the workshop was to compile an inventory of routinely produced precipitation estimates; either operational or experimental/research. The two most important criteria for the inventory are: 1) the retrieval algorithm be published so that others can study what was done, and 2) the algorithm be in current use and producing precipitation estimates on a routine or regular schedule.

The following two days activities were focused in three working groups: Operational Applications, Research Activities, and Validation Activities. Each working group discussed activity within their topical area and developed plans for future activities with short term, intermediate and long term goals.

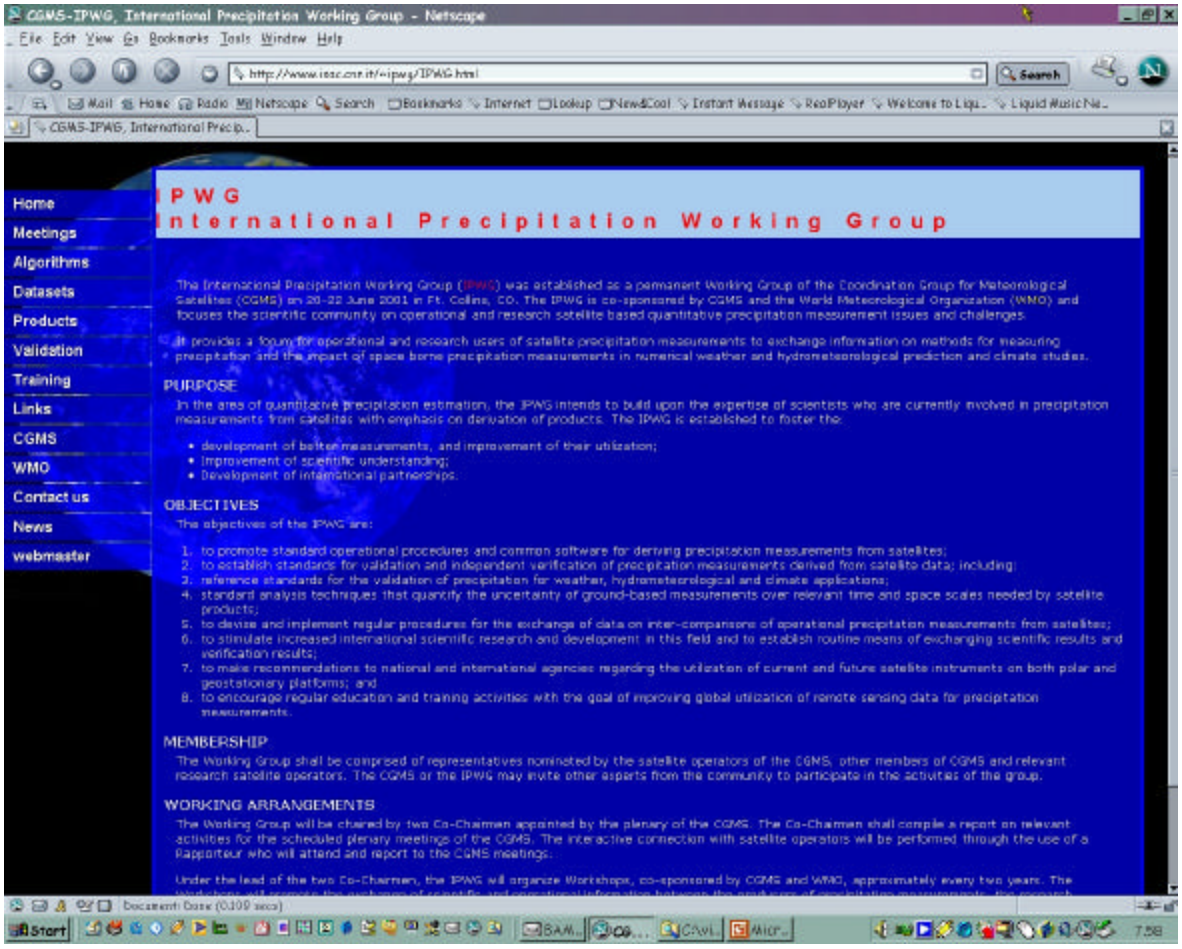

Fig. 1. The IPWG web site at the Institute of Atmospheric Sciences and Climate of the Italian National Research

Operational Applications: Recommendations

Form a subgroup for the development of instantaneous precipitation estimation export algorithms for users of geostationary and low Earth-orbiting satellite data. Collect current, operationally-oriented, instantaneous satellite-based precipitation algorithms to be made available through the IPWG website. Provide information on current and research-oriented climatological precipitation techniques. IPWG group to survey the space/time needs, accuracies needed, data latency time, and temporal coverage. Establish the IPWG web site. The web site has been established at http://www.isac.cnr.it/~ipwg/ (see Fig. 1).

Coordinate efforts and activities contemplating the use of satellite precipitation data for "non-traditional" applications. Broaden the application of satellite precipitation products by co-operation with communities other than meteorology and hydrology, e.g. snow models, irrigation models, pest and disease models, mud slide and avalanche models, dispersion models, surface pollution models and others.

Make case study satellite datasets available through the IPWG website, for further algorithm research.
Encourage continued development, refinement, and validation of the various research-status satellite sensor precipitation estimation techniques.

- MW satellite precipitation techniques; Combined or "blended" satellite precipitation techniques (IR+MW); Satellite + NWP precipitation techniques;
- Improved validation techniques to properly analyze the error characteristics of satellite-derived precipitation estimates at different space and time scales; Assimilation into NWP models at short time scales (instantaneous to 6-hourly) and relatively fine spatial scales (0.25-degree or less).

Coordinate satellite-based precipitation estimation research with the needs and requirements for climatological applications. While climate models typically analyze precipitation on time scales of one month and space scales of 2.5 degrees, there is an increasing need for daily-scale precipitation estimates and space scales approaching one-degree. These data can be produced with a latency time, but need to have data records extending back over a sufficient number of years in order to be useful for identifying long time scale variabilities.

Research Activities: Recommendations

Provide a generally accessible platform on data and algorithms for the research community. Define elements of algorithm transition required for general applications (QPE, bias/error estimate, limits of applicability, documentation, comprehensive bibliography, compliance with user requirements as defined by WMO, EUMETSAT, NASA-DAO, ESA, others - compile user requirements w.r.t. to precipitation on the IPWG web site). Set up an inventory of field campaign data with co-located satellite and ground data relevant for validation purposes, i.e. providing the necessary data sets for validation exercises. Enable co-operation and training through software libraries.
Develop new strategies on flexible and global structures for physical algorithm development, validation, and data fusion. Establishing a framework for

- Physical algorithm development (global and regional).
- Developing a testbed for algorithm validation (comparison data sets etc.).
- Product merging and blending.

The principal problem of under-constrained precipitation retrievals requires different types of analysis/retrieval approaches.
Methodology and information: more complex analysis methodologies, multiple sensors, multiple satellites, new instrument developments (e.g. geo-MW, lightning sensors, dual-frequency radars); climatological information, simplified dynamical physical models. The usefulness and complexity of the needed methodology and information depends on the application. Only by stronger constraints on algorithms special retrieval problems ca be solved such as: orographic precipitation, light precipitation, frozen precipitation, resolution enhancement [spatial (vertical/horizontal) and temporal]. Indications for future sensors should emerge based on the identified scientific outstanding areas.
In view of future sensor development a long-term strategy for frequency protection has to be developed and integrated in the current ITWG activities.

Validation Activities: Recommendations

Provide baseline validation standards for satellite precipitation algorithm(s) in terms of the needs of users in NWP data assimilation, nowcasting, hydrology, climate, and algorithm development communities.
Define validation metrics for NWP.
Define validation metrics for nowcasting.
Define validation metrics for hydrology.

Define validation metrics for climate. Ensure that members of the NWP data assimilation, nowcasting, hydrology, climate communities are represented at future IPWG meetings. Monitor performance of operational precipitation algorithms on a large scale on a daily basis, preferably in connection with NWP forecast validation. Support alternative approaches to error estimation such as physical error modeling and cloud/system classification to obtain global error estimates. Create an inventory of existing high quality reference data.

Encourage sharing of data from Intensive Observation Periods in large-scale experiments with the IPWG community, to enable improved validation of satellite rainfall estimates.

Perform and develop new methods for the error characterization of reference datasets. Encourage the use of dual-gauge systems and optimal network design in operational rain gauge networks, to improve the reliability and quality of rainfall observations. Investigate the quality and availability of surface reference networks for the validation of hard-to-measure (orographic, light, solid) precipitation. Develop an assessment software package, incorporating both basic and advanced techniques, to facilitate validation of satellite rainfall estimates by algorithm developers and users.

ACKNOWLEDGEMENTS

The authors wish to acknowledge continuing support from their home organizations (CNR and NOAA) that enables them to carry on the chair work for the IPWG. Funding was also provided to the senior author by EURAINSAT (http://www.isac.cnr.it/~eurainsat/), a shared-cost project (contract EVG1-2000-00030) co-funded by the Research Directorate General of the European Commission within the research and technological development activities of a generic nature of the Environment and Sustainable Development subprogram (5th Framework Programme).

Appendix I. WORKSHOP AGENDA

March 11, 2003 Tuesday

Welcome

9:15-9:35 Tony Hollingsworth, Arnie Gruber

Introduction

9:35-10:00 Masao Kanamitsu (SIO/UCSD)

Session I-a. Precipitation analysis procedures (GPCP, CMAP)

Chair person: Arnie Gruber

1 10:00-10:40 George Huffman and Bob Adler (GSFC/NASA)
(1) The Current Approach to GPCP Monthly and Daily Precipitation Estimates.
(2) The Multi-satellite Precipitation Analysis (MPA) in Real and Post-Real Time.

Break (10:40-11:00)

2 11:00-11:25 Pingping Xie, Yelena Yarosh, John Janowiak (NCEP/NOAA), and Phillip A. Arkin (ESSIC/UMD)
Techniques used to create CMAP and their potential improvements

Session I-b. Precipitation analysis procedures (NWP data assimilation)

Chair person: Peter Bauer

3 11:25-11:50 Philippe Lopez (ECMWF)
Precipitation assimilation at ECMWF

4 11:50-12:15 Arthur Hou (DAO/NASA/GSFC)
Precipitation assimilation at NASA Goddard

5 12:15-12:40 Bruce MacPherson (Met Office)
Precipitation assimilation at the Met Office (UK) and COST-717 collaboration in Europe

Lunch (12:40-1:50)

6 1:50-2:15 Peter Bauer (ECMWF)
Estimation of rainfall and its error characteristics from satellite observations

7 2:15-2:40 Ko Koizumi (JMA)
Precipitation assimilation to JMA mesoscale model using a 4D-Var method

8 2:40-3:05 Per Kallberg (ECMWF)
The precipitation in ERA-40

Session I-c. Precipitation analysis procedures (Other methods)

Chair person: Yukari Takayabu

9 3:05-3:30 Murray Salby (U. Colorado)
Gridding of Global precipitation from satellite measurements

Break (3:30-4:05)

10 4:05-4:30 Evgeny Yarosh, Wayne Higgins and Wei Shi (NCEP/NOAA)
High-resolution daily precipitation analysis over U.S. at CPC/NCEP

11 4:30-4:55 Joe Turk (NRL)
Blending precipitation data sets from multiple sources at short time scales

12 4:55-5:20 E. Ebert (BMO)
The Australian Operational Daily Rain Gauge Analysis

13 5:20-5:45 Jurgen Grieser (DWD)
Towards an adaptive method for spatial interpolation of global rain gauge data

5:45- **Cocktails**

March 12, 2003 Wednesday

14 9:15-9:40 Xiaogang Gao, Soroosh Sorooshian, and Kuolin Hsu
Strategy of Error Analysis and Reduction in the PERSIANN System

Session II - Observation characteristics (rain gauge and satellite)

Chair person: Beth Ebert

15 9:40-10:05 Udo Schneider (GPCC/DWD)
Operational processing, quality control and analysis of precipitation data at GPCC

16 10:05-10:30 Yukari Takayabu (CCSR/Univ. Tokyo)- Characteristics of precipitation as observed by TRMM PR

Session III. Validation and Collaboration

Chair person: Pingping Xie

Break (10:30-10:50)

17 10:50-11:15 Efi Foufoula (Univ. Minn.) - Multisensor-multiscale precipitation datasets and model Verification

18 11:15-11:40 A. Ghelli (ECMWF) - The relevance of gridded rainfall observations to verify ECMWF precipitation forecasts

19 11:40-12:05 Krajewski (U. Iowa) - Error characteristics of rain gauge and radar estimates and validation issues

20 12:05-12:30 Mark Serreze (NSIDC) - Monitoring Precipitation over the Arctic drainage: Data requirements, shortcomings and applications of atmospheric reanalysis

Lunch (12:30-1:45)

21 1:45-2:10 V. Levizzani (CNR, Italy) and Arnie Gruber (NESDIS/NOAA) - The international Precipitation working Group: Opportunities and perspectives

Discussions

2:15-5:30 Guidance to Working Group and breakout

- Analysis procedure
- Data assimilation
- Observation error characteristics

5:30- **Informal buffet in the ECMWF Restaurant**

March 13, 2003 Thursday

9:15 – 10:45 Working Group discussions continue
10:45 – 11:00 *Break*
11:00 – 1:00 Plenary Session – Report of Working Group and Recommendations

Appendix II. List of participants

Name	Affiliation	email
Bauer, Peter	ECMWF	p.bauer@ecmwf.int
Bruno, Rudolf	DWD/GPCC	bruno.rudolf@dwd.de
Buizza, R.	ECMWF	roberto.buizza@ecmwf.int
Ebert, Beth	BMRC	eee.bom.gov.au
Foufoula-Georgiou, Efi	Univ Minn	efi@umn.edu
Gao, Xiaogang	Univ. AZ	gao@hwr.arizona.edu
Grieser, Jürgen	DWD	juergen.grieser@dwd.de
Gruber, Arnold	NOAA/NESDIS	arnold.gruber@noaa.gov
Hollingsworth, Anthony	ECMWF	Anthony.Hollingsworth@ecmwf.int
Hou, Arthur	NASA/GSFC	hou@aglaya.gsfc.nasa.gov
Huffman, George	NASA/GSFC	Huffman@agnes.gsfc.nasa.gov
Kanamitsu, Masao	SIO/UCSD	mkanamitsu@ucsd.edu
Kallberg, Per	ECMWF	Per.Kallberg@ecmwf.int
Koizumi, Ko	JMA	kkoizumi@npd.kishou.go.jp
Krajewski, Witold	University Iowa	wfkrajewski@icaen.uiowa.edu
Ghelli, Anna	ECMWF	A.Ghelli@ecmwf.int
Levizanni, Vincenzo	CNR, BOLOGNA Italy	V.Levizzani@isac.cnr.it
Lopez, Phillip	ECMWF	Philippe.Lopez@ecmwf.int
McPherson, Bruce	UK Met Office	bruce.macpherson@metoffice.com
Salby, Murry	Univ Colorado	mls@icarus.colorado.edu
Schneider, Udo	DWD, GPCC	Udo.Schneider@dwd.de
Serreze, Mark	NSIDC	serreze@kryos.colorado.edu
Takayabu, Yukari	CCSR/University of Tokyo	yukari@ccsr.u-tokyo.ac.jp
Turk, Joe	NRL	turk@nrlmry.navy.mil
Xie, Pingping	NOAA/NCEP	pingping.xie@noaa.gov
Yarosh, Evgeney	NOAA/NCEP	Evgeney.yarosh@noaa.gov

Affiliations

BMRC - Bureau Meteorological Research Center
CCSR - Center for Climate System Research
DWD - Deutcher Wetterdienst
GPCC - Global precipitation Climatology Center
ECMWF - European Center for Medium Range Weather Forecasting
JMA - Japan Meteorological Agency
NASA/GSFC - National Aeronautics and Space Administration/Goddard Institute for Space Sciences
NOAA/NESDIS - National Oceanic and Atmospheric Administration/National Environmental satellite Data and Information Service
NOAA/NCEP - National Oceanic and Atmospheric Administration/National Center for Environmental Prediction
NRL - Naval Research Laboratory
NSIDC - National Snow and Ice Data Center
SIO/UCSD - Scripps Institute of Oceanography/University California San Diego

Appendix III–1. Recommendations by each Working Group

Analysis Working Group

Efi Foufoula (13th), Xiaogang Gao, Jurgen Grieser, George Huffman (Chair), Witold Krajewski (13th), Murray Salby, Pingping Xie, Evgeny Yarosh

Summary of Recommendations
(In some cases there is additional information in the corresponding item under "Detailed Summary of Discussion", below)

Data Issues

2. Difference due to instruments
   - *A study is needed defining the modern distribution of undercatch by gauges. Dr. Groisman of NCDC is apparently working on this and should be contacted. Changes in gauge deployment over the GPCP data record must be included in this study.*
3. Observation error characteristics
   - *Each input precipitation data set must be assigned comparable error estimates*
5. Future rain observing systems
   - *For the present, frozen/snowy areas lack useful microwave estimates.*
6. What satellite issues have been glossed over that must be confronted at fine scales?
   - *Parallax effects (and what's hidden behind a tall cloud), pixel overscans and gaps, surface type attribution, fall speeds, instantaneous 3-D structure, and 3-D radiative transfer must be confronted by the algorithm producers for best estimates at fine scales.*
7. How close are we to daily gauge estimates, if only by region, and how far back in time can they be constructed?
   - *CPC is doing daily global GTS precipitation analyses (from 1977 to the present in real time). There is not a uniform definition of the day boundary, but broad regions tend to have the same observing practice. The data set includes number of samples.*
   - *Daily raingauge analyses are being done in several regions, but this requires a large body of data that GPCC does not now access. GPCP should examine the institutional issue of how to access and manage daily gauge data and analyses.*
   - *Data producers must be informed that raingauge analyses always need the number-of-gauges field*

Analysis Issues

1a. What is the best approach in the recent/future era of plentiful satellite data?
   - *We are not yet in a position to identify a "best" approach. We need to identify the critical items for intercomparison. NB: The best approach might be obscured by simple mis-steps in implementation.*

1b. What is the best approach in the earlier era of limited satellite data?
   - *The 1979-1985 data record might be significantly improved by upgrading several early data sets: OLR, OPI, TOVS, MSU, and/or geo-IR.*
   - *There is an issue of attracting the attention of funders; we need to make a case.*

2. Are different analysis procedures needed for different spatial and temporal scales?
   - *Collaboration is needed among the gauge analysis groups to examine trade-offs for doing daily/hourly analysis.*

3. What analysis procedures should be used in complex terrain?
   - *Altitude and slope effects are clearly important in gauge analysis, but PRISM-like schemes are designed for monthly climatologies, not daily analysis based on sparse data.*
   - *Models and independent observations might provide useful approaches to the complex terrain issue, but research is needed to demonstrate reliable performance.*

6a. Since objectives analysis techniques best deal with unbiased input data, how can biases in the various input data be removed?
   - *Need to continue developing high-quality, unbiased reference sites across the range of climate regimes. We must continue to develop additional sites over ocean.*
- *We need research on the dominant bias fluctuations. As a first step, research should be done on creating a "bias index" to give users a first estimate of bias behavior.*

6b. Is bias removal best done during the retrieval process or during the analysis, or by a combination of both?
   - *Estimation groups should share reference data sets to ensure the best calibration/validation for each estimate. (This does answer the question- should we delete?*

7. What is the right calibration interval calibrating IR precipitation algorithms by microwave estimates?
   - *For microwave-IR, the stability and sensitivity of current schemes needs to be demonstrated at time intervals of monthly, pentad, daily or even microwave overpass by overpass. All these intervals which are used in IR-MW calibrations . sensitivity to time of day should be tested*

8. What should be the role of model-based estimates in developing an objective analysis of precipitation?
    - *A study should be carried out to determine whether model data be used to assist in the altitude and slope-aspect enhancement of precipitation. In order to address some opposition to mixing model outputs with observations The relative performance of the model compared to co-located observations should be researched as a basis for action. Users will continue to require a no-model analysis – the issue is whether a parallel observation+model analysis is sufficiently interesting to institute.*
9. How best to move away from the current assumption that at least some of the input data sets to the analysis are un-biased, e.g. gauge data?
    - *The goal is that all input data to a final precipitation estimate be biased corrected combination algorithm.*
10. How to establish physical consistency with other variables?
    - *Studies comparing data should be done, but after the first round we expect to learn about the errors in all the data sets, not just precipitation.*

Appendix III-2. Recommendations by each Working Group

Data Assimilation Working Group

Philippe Lopez, Peter Bauer, Frederic Chevallier, Sandra Dance, Arthur Hou, Per Kallberg, Masao Kanamitsu, Ko Koizumi, Bruce MacPherson, Emmanuel Moreau

I. Precipitation data ? NWP

The group expressed a general need for the validation of model precipitation by GPCP-type data products.

It was pointed out that at the current stage of the developments in various NWP-centers, the benefit of precipitation data assimilation is evident in both analyses and forecasts on the global as well as regional scale. While the assimilated information may not be retained over a long forecast period, there is an improvement of the atmospheric and surface analysis.

Both observations and validation (methodology) may provide information on the spatial characteristics of precipitation below the current NWP model grid-scale for the improvement of physical parameterizations and data assimilation due to the non-linear relationship between area-averaged products and area-averaged observations.

Almost the entire discussion focused on the problem of error definition / characterization:

1. In data assimilation, individual products from individual observational means are usually preferred because the definition of observation errors is facilitated. The exception would occur if an integrated/merged product could overcome the errors of the individual products in a better way.
2. For individual products, the error definition should follow the forward principle that is the estimation of error contributions from all contributing factors between the original observation and the final retrieval product. These contributions mainly originate from:
   - the instruments,
   - the involved physical models,
   - the assumptions on spatial representativeness,
   - the assumptions on temporal representativeness.
3. The error estimation has to include the spatio-temporal error correlation (i.e. error covariance and its dependence on state) as well as the error of rain detection.
4. In principle, data assimilation requires the elimination of systematic differences between observations and model background (on average), therefore both observation and model field biases are to be estimated. If the absolute bias cannot be determined, an uncertainty estimate should be provided along with the bias.
5. It was stressed that those parameters that determine both bias and error should be identified to allow a bias/error-prediction towards 'Gaussian' error statistics.
6. With respect to individual observations:
   Radar: The development/support of international radar networks is encouraged ensuring that the generation of a combined product is carried out at a central location to generate the most homogeneous/standardized product.
   Gauges: The role of gauges was identified as a calibrator for radar estimates rather than in data assimilation. In the future and for local applications, the assimilation of very dense gauge network observations in combined atmosphere-runoff models seems the represent the most likely development towards assimilation.
   Satellites: Apart from the comparison of rainfall products, satellite data provides large information content on precipitation-related physics and dynamics. Therefore, the indirect validation of NWP analyses with multi-spectral observations of radiation, humidity, clouds, precipitation, and soil moisture - in particular in radiance space - is recommended to further improve the moist model physics.

II. NWP ? Precipitation data

In addition to observation-only analyses that are required for model validation, data assimilation has the potential of providing a dynamically/physically consistent description of the hydrological cycle. This forms the basis for understanding the coupling of precipitation with the hydrological/energy cycle that cannot be obtained from QPE alone.

Given the accuracy of observation-only rain estimates the question arose whether the global user community needs the inclusion of NWP analyses of rainfall. Several areas were identified where the NWP analyses may complement stand-alone observational estimates:

- Higher latitudes and polar regions,
- Orographic precipitation,
- Precipitation over snow-covered surfaces,

- Snowfall.

In terms of methodology, physical algorithms applied to satellite data will more and more involve simplified dynamical cloud models (single-column) which need first-guess information on the atmospheric state and possibly variational retrieval methods (GPM era).

In principle, a global NWP model / data assimilation model offers many advantages over observation-only products; however, due to the restriction to nearly-linear physics in the vicinity of the model's first guess applied in current NWP systems, the quality of the first guess and the validity of the linearity assumption may cause problems. In certain cases, a well trained and non-linear algorithm may outperform the NWP analysis.

Recommendations:

Both streams observation-only and NWP-type analyses of precipitation are required.

Active collaboration between modeling/observation/validation groups is needed for a complete description of the analysis errors: biases (their uncertainties), error covariances, their state dependence, and methodologies for the description of their dependence on scales.

Observations/products are required on smaller scales (space/time) because data assimilation will increasingly employ time-series of data and focus on more regional applications.

Appendix III-3. Recommendations by each Working Group

Observations, Characteristics, Errors, and Validation Working Group

J. Turk, E. Foufoula-Georgiou, W. Krajewski, M. Serreze, A. Ghelli, E. Ebert, Y. Takayabu, A. Gruber, M. Salby, U. Schneider

1. Specific Recommendations on Additional/Improved Observations:

- Use data from **coastal radars** (e. g., Key West, Florida) to validate satellite **over-water** rainfall estimates and provide additional information on high resolution space-time characteristics. Use TRMM PR data as a "reference" for GPCP rainfall estimates over the ocean, then extend back in time (an engineering approach, but might improve the accuracy of the pre-TRMM product).

- Assess existing high latitude precipitation records not in current digital archives, and from research projects, in order to extend historical time series (e. g., Russian datasets, Greenland AWSs, SHEBA). Compare and explore new **high-latitude bias adjustments** being used in GPCP and in development at GPCC with those being performed in other groups.

- *Future*: **New EOS sensors** (e.g., AMSR) may have better sensitivity to solid precipitation for high latitude applications.

2. Specific Recommendations on Precipitation Characteristics:

- Consider **classifying the meteorological conditions**, based on something that is observable from satellite, such that the multi-scale rain structure (and error characteristics) can be deduced as a function of observed "storm type".

- **Grid cell spatial and temporal variability of intensity** could be computed from the original 3-hourly IR data that was used to build the GPCP product, along with other sources such as TRMM and GPM. This would enable GPCP monthly statistics to describe the **diurnal cycle** and characterize the rain type on a global scale.

- As GPCP doesn't yet have any **orographic correction**, consider going to the NCEP or ERA reanalyses to get low-level wind information to help make this adjustment.

3. Specific Recommendations on Validation:

- Invite participation among satellite estimation providers in **regional validation activities** over Australia and other domains

- Better define error characteristics of satellite precipitation retrievals over **high latitudes**, in light of degradation of gauge database since ~1990.

- *Future*: GPM physical validation efforts be coordinated with GPCP validation efforts, and vice-versa. For example, GPCP should make use of **special observation sites** (eg, future GPM supersites) in validating and classifying GPCP products by storm type.

4. Specific Recommendations on Error Analysis:

- Provide some **training or guidance** on "how to use error estimates", to encourage users of GPCP products to also use the accompanying error estimates.

- Strengthen research in estimating the errors associated with **radar rainfall** estimates, to be better able to use these radar rainfall estimates to validate high resolution satellite rainfall estimates. For example, **clusters of rain gauges** could be used to accurately measure the spatial correlation of rainfall at fine time and space scales.

- Develop **covariance models** for the individual components of the GPCP product (gauges, microwave estimates, IR estimates) to enable data assimilation techniques to be used to optimally combine these components.